UNIVERSIDAD AUTÓNOMA DE MADRID

FACULTAD DE CIENCIAS

DEPARTAMENTO DE BIOLOGÍA MOLECULAR

ANALYSIS OF A CELL MODEL OF NEURODEGENERATION INDUCED BY HERPES SIMPLEX VIRUS 1 AND OXIDATIVE STRESS. IMPLICATION OF THE LYSOSOMAL PATHWAY.

HENRIKE KRISTEN

June 2017

Thesis directors

Dr. María Jesús Bullido and Dr. Jesús Aldudo

Centro de Biología Molecular “Severo Ochoa”

Universidad Autónoma de Madrid

Biochemistry Kiel

Christian-Albrechts-University of Kiel

ACKNOWLEDGEMENTS

First, I would like to thank my thesis directors, Dr. María Jesús Bullido and Dr. Jesús Aldudo, for giving me the opportunity to work under their supervision. Since I entered the lab in 2011, all group members have become like a family to me. I feel very fortunate to have experienced such a great environment, both scientifically and personally.

I particularly thank Mariaje for her continued support and encouragement. She challenged me to think outside the box and to look critically at my work. I hugely appreciate her advice when preparing for conference presentations and her dedication of time and effort while writing the application project for the EMBO fellowship. These experiences helped me grow and built meaningful connections.

I would like to thank Jesús for teaching me most of the methods, how to design experiments and interpret data. Above all, for being available at all times and working next to me at the bench. He quickly became a partner to share interesting thoughts, experiments, and—not to forget—delicious olives. I am also grateful to him for all the proofreading he has done over the years.

A big thank you goes to Mary for being the good soul of the lab. I appreciate her contributions of time and her sharing of ideas and results.

Isabel, for everything!! She taught me cell culture skills and helped me out at any time. I can always count on her experience and expertise. Also, a special thanks to our friends Ángel and Angeles for being the best paddle team!

Patri deserves a big thank you from the whole team for filling up the stock. Personally, I am very glad that she has become my "partner in crime", she has always been there for me (and my scooter), and I am happy to call her a friend.

I would like to give special thanks to Dr. Ana Frank García and her team (especially Ángel Martín Montes) from the "Hospital Universitario La Paz" for the ongoing collaboration with our group that started long before I showed up. I personally worked with them in the joint project of iPS cell generation and deeply appreciate their dedication and enthusiasm towards this project and their work in general. I really enjoyed getting in contact with patients and hear first-hand about their motivation to participate in research.

I am especially grateful to Eva for preparing me (mentally and technically) to work with iPS cells. She has both listened to my questions and shared her expert knowledge with me. Her personal experience provided me with the necessary tips to successfully develop this part of my project.

I would like to thank Dr. Paul Saftig for giving me the opportunity of joining his team at the Biochemistry Institute of Kiel. Further, for his interest in our research project, the productive discussions and his interesting suggestions for future work, and not to forget, for kindly providing cell lines. A big thank you goes to his hugely collaborative team; especially André, Adriana, and Meryem. I gratefully acknowledge the collaboration of Dr. Fickenscher for providing the infection facilities, and Husam for showing me around and being available to help.

I would like to extend appreciation to the CBM staff that keep things running: Ángel from IT, Silvia and Berta from flow cytometry, all SMOC members, Juan for his help with preparation of media, as well as the cell culture team.

My thanks go to Mauro, Dani, Raquel (both of them) and Elena for their great company. Work, lunch and coffee breaks were so much more fun with them. They always had an open ear for my problems and helped me with motivation and/or tips and tricks.

Other great people I have had the pleasure to get to know over the years: Alba, Marta, Zaida, Adolfo, Alfonso, Curro, Javi, Fulvio, and Rafa.

Last but not least, there is Angie, who has become a true friend. Since she left it hasn't been the same. I am very thankful for all the good (and sad) moments we shared in and outside the CBM. I would also like to thank her for all the proofreading and her hugely helpful comments, personal advice for life and work, and for motivating me when I most need(ed) it.

I could continue this list endlessly, here just a thank you to all those who crossed my path and made my time during the PhD special.

CONTENTS

SUMMARY **1**
RESUMEN **5**
ABBREVIATIONS **9**
INTRODUCTION **15**
1. General aspects of Alzheimer's disease 17
2. Risk factors for AD 21
2.1. Genetic predisposition 21
2.2. Infectious hypothesis and AD 23
2.2.1. HSV-1 and AD 23
2.2.2. Interaction between HSV-1 and oxidative stress 25
3. The lysosomal pathway 27
3.1. Endocytic pathway 28
3.2. Autophagy 29
3.3. Lysosomal alterations and neurodegeneration 30
OBJECTIVES **33**
MATERIALS & METHODS **37**
1. Cell lines and cell culture conditions 39
2. Infection conditions and induction of oxidative stress 39
3. Treatments 40
4. Generation of cell lines with stable gene-silencing of LAMP2 40
5. Analysis of cell viability 40
6. Immunoblot 41
7. Immunocytochemistry 41
8. Antibodies 42
8.1. Primary antibodies 42
8.2. Secondary antibodies 42
9. Viral DNA quantification by real-time quantitative polymerase chain reaction (qPCR) 43
10. Quantification of mRNA by reverse transcription followed by real-time PCR (RT-qPCR) 43
11. Measurement of secreted Aβ 44
12. Quantification of lysosomal cellular content 44
12.1. Flow cytometry 44
12.2. Fluorogenic enzyme assay 44
13. Assessment of lysosomal enzyme activity 45
13.1. Measurement of cathepsin activities 45
13.2. Measurement of β-hexosaminidase activity 45
14. EGF receptor degradation assay 45
15. Partial purification of lysosomes 46

16. Cholesterol quantification 46
17. Filipin labelling of membrane cholesterol 46
18. Expression microarrays: Gene quantification and functional annotations....47
18.1. RNA extraction and hybridization to the arrays 47
18.2. Data analysis 47
18.3. Functional enrichment of differentially expressed genes by GeneCodis and IPA ...47
19. Genetic association study....48
19.1. Study subjects 48
19.2. Genotyping....48
19.3. SNP selection 48
20. Generation of induced pluripotent stem cells (iPSCs) 50
20.1. Cell culture media 50
20.1.1. Fibroblast medium 50
20.1.2. MEFs medium....50
20.1.3. iPSC medium 50
20.2. Establishing primary cell cultures from patient biopsies 50
20.3. Generation of a stock of irradiated mouse embryonic fibroblasts 50
20.4. Sendai viral transduction of fibroblasts and generation of iPSCs....51
21. Characterization of iPSC lines 51
21.1. Alkaline phosphatase staining....51
21.2. TRA1-60 live staining....52
21.3. Immunofluorescence analysis 52
21.4. RT-qPCR analysis....53
22. Statistical analysis 53
RESULTS....55
1. Differential gene expression studies after X-XOD treatment in cell models of sporadic and familial AD suggest alterations of the lysosomal pathway 57
1.1. Quality control of samples 58
1.2. Microarray gene expression studies of our cell models....59
1.3. Validation of microarray results by RT-qPCR 61
2. HSV-1 infection and OS alter the lysosomal pathway in SK-N-MC cells 63
2.1. HSV-1 and OS increase lysosomal content 63
2.2. HSV-1 and OS reduce the activity of lysosomal enzymes 65
2.3. HSV-1 and OS alter endocytosis-mediated lysosomal degradation of the EGF receptor 68
2.4. HSV-1 infection and OS increase intracellular cholesterol levels....71
3. Role of LAMP2 in the AD-like neurodegeneration events induced by HSV-1 and OS.....73
3.1. *LAMP2* polymorphisms are associated with sporadic AD....73

3.2. Generation of SK-N-MC cell lines with a stable knockdown for LAMP2 75
3.3. LAMP2 deficiency does not affect cell viability after X-XOD treatment 77
3.4. LAMP2 deficiency decreases efficiency of HSV-1 infection 78
3.5. Effect of LAMP2 deficiency on lysosomal activity 82
3.6. Effect of LAMP2 deficiency on AD-like neurodegeneration markers 84
3.6.1. Analysis of tau phosphorylation 84
3.6.2. Analysis of Aβ levels 85
3.6.3. Analysis of LC3 levels 87
4. Generation of induced pluripotent stem cells 88
4.1. Establishing primary cell cultures from patient biopsies 89
4.2. Generation of iPSCs 90
5. Characterization of iPSC lines 92
5.1. Alkaline phosphatase and TRA1-60 staining 92
5.2. Analysis of the expression of pluripotency markers in iPSC lines 93
DISCUSSION 97
1. Identification of the lysosomal pathway as involved in SAD 99
2. Alterations of lysosomal function induced by HSV-1 and OS 101
3. Role of LAMP2 in AD-like neurodegeneration induced by HSV-1 and OS 106
4. Generation of patient-specific iPSCs 111
CONCLUSIONS 113
CONCLUSIONES 117
REFERENCES 121
ANNEX I 143

FIGURE INDEX:

Figure 1. Schematic diagram of the canonical APP processing. 18
Figure 2. Genetics of Alzheimer's disease. 22
Figure 3. HSV-1 access route to the CNS. 24
Figure 4. Schematic representation of the endocytic pathway. 29
Figure 5. Schematic representation of the autophagic process. 30
Figure 6. Work scheme overview of microarray analysis. 57
Figure 7. Validation of apoptosis and HSV-1 infection. 58
Figure 8. Genes modulated by differential gene expression analyses. 60
Figure 9. Genes showing altered expression in the KEGG pathway 4142: Lysosome. 61
Figure 10. Validation of expression microarray data for the genes of the lysosomal pathway. 62
Figure 11. HSV-1 infection and OS increase the protein levels of endo-lysosomal markers. 63
Figure 12. HSV-1 infection increases cellular lysosomal content. 64
Figure 13. HSV-1 infection increases cellular lysosomal content. 65
Figure 14. HSV-1 and OS induce a reduction of lysosomal enzyme activity. 66
Figure 15. Effect of lower HSV-1 dose on lysosomal content and cathepsin activities. 67
Figure 16. HSV-1 and OS impair EGFR lysosomal degradation. 69
Figure 17. HSV-1 and OS impair EGFR lysosomal degradation. 70
Figure 18. Internalized EGFR colocalizes with late endosomal markers in HSV-1 infected cells. 71
Figure 19. Effect of HSV-1 infection and OS on cholesterol levels and its cellular localization. 73
Figure 20. Analysis of LAMP2 expression in SK-N-MC cells transfected with shRNA clones against LAMP2. 76
Figure 21. Analysis of LAMP2 protein and mRNA levels of murine cell lines. 77
Figure 22. LAMP2 deficiency does not affect cell viability of cells exposed to oxidative stress. 77
Figure 23. Effect of LAMP2 deficiency on HSV-1 infection in N2a cells. 78
Figure 24. Effect of LAMP2 deficiency on HSV-1 infection in MEF cells. 79
Figure 25. Analysis of infected cells by immunofluorescence experiments 79
Figure 26. LAMP2 deficiency and OS reduce HSV-1 infection in N2a cells. 81
Figure 27. LAMP2 deficiency and OS reduce HSV-1 infection in MEF cells. 82
Figure 28. Effect of LAMP2 deficiency on activity of lysosomal hydrolases. 83
Figure 29. Effect of LAMP2 deficiency on tau phosphorylation site thr205. 84
Figure 30. Effect of LAMP2-deficiency on tau phosphorylation site thr205. 85
Figure 31. Effect of LAMP2 deficiency on Aβ42 accumulation. 86
Figure 32. Effect of LAMP2 deficiency on Aβ secretion. 87
Figure 33. Effect of LAMP2 deficiency on LC3-II levels. 88
Figure 34. Overview of processing and growth of human dermal fibroblasts. 90

Figure 35. Sendaiviral transduction of fibroblasts and generation of iPSCs. 91
Figure 36. iPSC morphology of mature colonies. 91
Figure 37. Alkaline phosphatase (AP) and TRA1-60 live staining of iPSC lines. 92
Figure 38. Morphology of partially differentiated iPSC colonies. 93
Figure 39. Analysis of the expression of pluripotency markers in iPSC lines. 94

TABLE INDEX:

Table 1. Mission control shRNA DNA clone sequences. 40
Table 2. Primary antibodies used in this work. 42
Table 3. Specific primers and TaqMan assays for real-time PCR. 43
Table 4. Basic characteristics of the SNPs analysed in the genetic association study. 49
Table 5. CytoTune 2.0 reprogramming vectors. 51
Table 6. Primary and secondary antibodies used for immunocytochemistry of iPSC colonies. 52
Table 7. Human iPSC real-time PCR primers. 53
Table 8. Allele frequencies of the studied SNPs in the AD-case/control sample. 74
Table 9. AD risk associated with LAMP2 SNPs in the sample stratified by gender and *APOE* genotype. 74

SUMMARY

Alzheimer's disease (AD), the single most common cause of dementia, is characterized by massive neuronal damage leading to cerebral atrophy and the loss of cognitive function. Most AD cases (>95%) are sporadic. Sporadic AD is a highly complex disease for which neither the causal agent(s) nor the molecular mechanisms behind are well known. Among the environmental risk factors, persistent brain infections, particularly those induced by Herpes simplex virus type 1 (HSV-1), seem to play a key role in AD pathogenesis. Another factor is oxidative stress (OS), intimately linked to aging and, therefore, thought to be crucial to the onset and development of the disease. Our group works with both factors to simulate the sporadic form of AD *in vitro*. The objective of the present study was the identification of genes and pathways associated with AD to provide novel diagnostic tools predicting the risk and/or the progression of the symptoms, and to establish possible therapeutic targets for the disease. Gene expression studies of the human neuroblastoma cell line SK-N-MC have identified a set of OS-regulated genes in infected cells and in cells harbouring APP with the Swedish mutation (APP_{swe}), a cell model of familial AD. Analysis of these genes revealed that the main pathway altered was the lysosomal system suggesting that the interaction of OS with both HSV-1 and APP_{swe} affects lysosomal function. These data support earlier findings and those of other authors highlighting the role of lysosomal pathway in early stages of AD neurodegeneration. To strengthen this hypothesis, we focused on the lysosomal pathway in our cell models and found that HSV-1 infection and OS led to an increase of lysosomal content, decreased activity of several lysosomal hydrolases, inhibition of the endocytosis-mediated degradation of the EGF receptor, and accumulation of intracellular cholesterol. Taken together, these results confirm that the lysosomal pathway is severely impaired. The lysosomal-associated membrane protein 2 (*LAMP2*) gene was one of the most strongly modulated ones in the differential expression analysis. In addition, LAMP2 has been functionally involved in the export of cholesterol out of lysosomes and in the final stages of autophagy. Both processes are essential for lysosome function and have been reported to be deeply altered in AD. All these evidences point to LAMP2 as a strong candidate to mediate the lysosomal alterations observed in our models. Indeed, the case/control studies revealed *LAMP2* genetic variants to be associated with AD risk suggesting that *LAMP2* is involved in the disease. To study the role of this candidate in the neurodegenerative events induced by HSV-1, human neuroblastoma cell lines with a stable knockdown for LAMP2 were generated in-house and two additional murine LAMP2-deficient cell lines—MEFs and N2a—were used. LAMP2 deficiency induced a less effective HSV-1 infection in both cell lines suggesting a functional role of LAMP2 in viral cycle. Preliminary results indicate that the absence of LAMP2 does not affect HSV-1-induced neurodegenerative events like tau phosphorylation, accumulation of intracellular Aβ42 and inhibition of Aβ secretion. In conclusion, the results of the current project point to alterations in the lysosomal pathway as a potential common pathogenic mechanism underlying the different forms of AD (familial and sporadic) and suggest that pharmacological modulation of this pathway might be beneficial for AD.

RESUMEN

La enfermedad de Alzheimer (EA) es la causa más común de demencia y se caracteriza por un masivo daño neuronal que conduce a la atrofia cerebral y a la pérdida de funciones cognitivas. En la gran mayoría de los casos (>95%), la EA constituye una enfermedad compleja cuya causa y mecanismos moleculares aún se desconocen. Entre los factores de riesgo ambientales, las infecciones cerebrales, y en particular la infección por el virus herpes simplex 1 (HSV-1), desempeñan un papel clave en la patogénesis. Otro factor clave en el desarrollo de la enfermedad es el estrés oxidativo (EO) asociado al envejecimiento. Nuestro grupo trabaja con ambos factores para simular la forma esporádica de la EA *in vitro*. El objetivo del presente estudio fue la identificación de genes y rutas asociados a la EA que pudiesen integrarse en procedimientos diagnósticos útiles para evaluar el riesgo o el curso clínico probable de la enfermedad, o constituir dianas terapéuticas potenciales. Mediante estudios de expresión génica en la línea celular de neuroblastoma humano SK-N-MC, hemos identificado un conjunto de genes cuya expresión se regula por EO tanto en células infectadas como en células portadoras de la mutación APP_{swe}, un modelo celular de la EA familiar. El análisis de los genes modulados reveló que el sistema lisosomal es la principal ruta alterada sugiriendo que la interacción del EO con HSV-1 y con la mutación APP_{swe} modifica la función lisosomal, y apoya datos de otros autores sobre la implicación de esta vía en las primeras etapas de la neurodegeneración. Para confirmar la hipótesis, hemos analizado la vía lisosomal demostrando que el HSV-1 y el EO producen un aumento en la cantidad de lisosomas, una inhibición de la actividad de varias hidrolasas lisosomales y de la degradación del receptor de EGF mediada por endocitosis, y una acumulación intracelular de colesterol. En conjunto, estos resultados indican que la funcionalidad de la vía lisosomal está afectada. El gen lisosomal *LAMP2* fue uno de los más modulados en el análisis de expresión diferencial. Además, LAMP2 está implicado en las etapas finales de la autofagia y en el transporte de colesterol fuera del compartimento lisosomal. Ambos procesos son esenciales para la función lisosomal y están fuertemente alterados en la EA. Todas estas evidencias apuntan a LAMP2 como un posible candidato para mediar las alteraciones lisosomales de nuestros modelos. Además, los estudios caso/control mostraron variantes genéticas de *LAMP2* asociadas con riesgo de EA, sugiriendo su implicación en la enfermedad. Para estudiar su participación en la neurodegeneración inducida por HSV-1, hemos generado varias líneas celulares SK-N-MC con una inhibición estable de la expresión de LAMP2. Además, hemos analizado líneas celulares murinas—MEFs y N2a—deficientes en LAMP2. La ausencia de LAMP2 indujo una inhibición de la infección sugiriendo que ejerce un papel funcional en el ciclo viral. Resultados preliminares indican que la ausencia de LAMP2 no afecta a los marcadores de neurodegeneración inducidos por HSV-1, como son la fosforilación de tau, la acumulación intracelular de Aβ42 y la inhibición de la secreción de Aβ. En conclusión, los resultados del presente trabajo apuntan a alteraciones en la función lisosomal como posible mecanismo patogénico común de las formas monogénica y esporádica de la EA y sugieren que la modulación farmacológica de esta vía podría ser beneficiosa para la enfermedad.

ABBREVIATIONS

27-OHC 27-hydroxycholesterol
ABCA7 ..... ATP-binding cassette transporter A7
ACV ..... Acyclovir
AD ..... Alzheimer's disease
AICD ..... APP intracellular domain
AMC 7-amino-4-methylcoumarin
AP ..... Alkaline phosphatase
APLP1 ..... APP-like protein 1
APLP2 ..... APP-like protein 2
APOE ..... Apolipoprotein E
APP ..... Amyloid precursor protein
ATCC ..... American Type Culture Collection
Aβ ..... β-amyloid
Baf A1 ..... Bafilomycin A1
BCA ..... Bicinchoninic acid
BCIP ..... Bromochloroindolyl phosphate
bFGF ..... Basic fibroblast growth factor
BIN1 ..... Bridging integrator 1
C ..... Control
CaMKII ..... Calcium and calmodulin-dependent protein kinase II
CD2AP ..... CD2-associated protein
CDK5 ..... Cyclin-dependent protein kinase 5
cDNA ..... Complementary DNA
CLEAR ..... Coordinated lysosomal expression and regulation
CLU ..... Clusterin
CMA ..... Chaperone-mediated autophagy
CMV ..... Cytomegalovirus
CNS ..... Central nervous system
Co-IP ..... Co-immunoprecipitation
CSF ..... Cerebrospinal fluid
CTF ..... C-terminal fragment
CTS ..... Cathepsin
Dapi ..... 4',6-diamidino-2-phenylindole
DMEM ..... Dulbecco's modified Eagle medium
DSHB ..... Developmental Studies Hybridoma Bank
EADI ..... European Alzheimer's Disease Initiative
EBSS ..... Earle's balanced salt solution
EBV ..... Epstein Barr Virus
EEA1 ..... Early endosome antigen 1
EGF ..... Epidermal growth factor
EGFR ..... Epidermal growth factor receptor
ELISA ..... Enzyme-linked immunosorbent assay
ELMO ..... Estudio Longitudinal Multicéntrico y Observacional
ER ..... Endoplasmic reticulum
FAD ..... Familial AD
FBS ..... Fetal bovine serum
FC ..... Fold change
FCS ..... Fetal calf serum

FTDP-17 ..... Frontotemporal dementia and parkinsonism linked to chromosome 17
GeneCodis ..... Gene annotations co-occurrence discovery
GERAD ..... Genetic and Environmental Risk in Alzheimer's Disease
GSK3 ..... Glycogen synthase kinase 3
GWAS ..... Genome-wide association studies
h ..... Hours
H_2O_2 ..... Hydrogen peroxide
HDF ..... Human dermal fibroblast
HDL ..... High-density lipoprotein
HHV6 ..... Human herpes virus 6
HIV ..... Human immunodeficiency virus
HMGCR ..... 3-hydroxy-3-methylglutaryl-CoA reductase
HP-β-cyclodextrin 2-hydroxypropyl-beta-cyclodextrin
HRP ..... Horseradish peroxidase
HSA ..... Human serum albumin
HSV-1 ..... Herpes simplex virus type 1
ILV ..... Intraluminal vesicle
IMDM ..... Iscove's Modified Dulbecco's Medium
iNOS ..... Induced nitric oxide synthase
IPA ..... Ingenuity Pathway Analysis
iPSC ..... Induced pluripotent stem cells
ISCBI ..... International Stem Cell Banking Initiative
LAMP ..... Lysosome-associated membrane protein
LC3 ..... Microtubule-associated protein light chain 3
LDL ..... Low-density lipoprotein
LIMP ..... Lysosomal integral membrane protein
LSD ..... Lysosomal storage disease
LSG ..... LysoSensor® Green DND-189
LTR ..... LysoTracker® Red DND-99
M6P ..... Mannose 6-phosphate
MAF ..... Minor allele frequency
MAP ..... Microtubule-associated protein
MAPT ..... Microtubule-associated protein tau
MEF ..... Mouse embryonic fibroblast
MEM ..... Minimal Eagle's medium
Min ..... Minutes
Moi ..... Multiplicity of infection
mTOR ..... Mammalian target of rapamycin
MTT ..... 3-(4,5-dimethyl-thiazol-2-yl)-2,5-diphenyl tetrazolium bromide
MVBs ..... Multivesicular bodies
MβCD ..... Methyl-β-cycodextrin
N_2 ..... Nitrogen
NA ..... Not applicable
NaCl ..... Sodium chloride
NBT ..... Nitro blue tetrazolium
NCL ..... Neuronal ceroid lipofuscinosis
ND ..... Not detected

ND ..... Not determined
NEAA ..... Non-essential amino acid
NFT ..... Neurofibrillary tangle
NH_4Cl ..... Ammonium chloride
NMDA ..... N-methyl-D-aspartate
NPC1 ..... Niemann-Pick type C disease
ns ..... Non significant
ON ..... Overnight
OR ..... Odds ratio
P ..... Patient
p-tau ..... Hyperphosphorylated tau
PARP ..... Poly ADP-ribose polymerase
PBS ..... Phosphate-buffered saline
PCR ..... Polymerase chain reaction
PFU ..... Plaque forming units
PHF ..... Paired helical filaments
PKA ..... Protein kinase A
PLA ..... Proximity ligation assay
PLD3 ..... Phospholipase D3
PNS ..... Peripheral nervous system
PP ..... Protein phosphatase
PSEN ..... Presenilin
RIPA ..... Radioimmunoprecipitation assay
ROS ..... Reactive oxygen species
RQ ..... Relative quantity
RT ..... Room temperature
RT-PCR ..... Reverse transcription polymerase chain reaction
SAD ..... Sporadic AD
SD ..... Standard deviation
SDS ..... Sodium deoxycholate sulphate
SEM ..... Standard error of the mean
SeV ..... Sendai virus
shRNA ..... Short hairpin RNA
SNP ..... Single nucleotide polymorphism
SNV ..... Single nucleotide variant
SORL1 ..... Sortilin-related receptor 1
SP ..... Senile plaque
TBS ..... Tris-buffered saline
TFEB ..... Transcription factor EB
TGN ..... Trans-Golgi-network
TNFα ..... Tumor necrosis factor α
TREM2 ..... Triggering receptor expressed on myeloid cells 2
V ..... Vacuolar
WT ..... Wildtype
X-XOD ..... Xanthine-xanthine oxidase
β-ME ..... Beta-mercaptoethanol

INTRODUCTION

1. General aspects of Alzheimer's disease

Alzheimer's disease (AD), the most common cause of dementia, is characterized by an irreversible progression of neuronal death, memory loss, as well as general cognitive decline. The disease is divided into two subtypes based on the genetic background: familial early-onset AD (FAD) and sporadic late-onset AD (SAD). 99% of all cases demonstrate the sporadic form: a complex interaction of genetic and environmental factors. Among the non-genetic risk factors, age is the most important one. AD incidence increases exponentially with ages from 65 to 90 years and doubles approximately every 5 years (Jorm et al., 1998). Further, other non-genetic factors for AD are female gender (Vina et al., 2010), oxidative stress (Markesbery et al., 1999; Smith et al., 2000) and lipid alterations (Bjorkhem, 2006; Grimm et al., 2013). Growing evidence points to chronic or latent infections of the central nervous system (CNS) as a major player in the pathogenesis of AD (Harris et al., 2015; Itzhaki et al., 2016).

In 1906, Alois Alzheimer described for the first time the neuropathological lesions he observed in a brain autopsy of a patient with early-onset dementia, which are considered until today the two pathological hallmarks of AD. He observed the presence of "striking changes in neurofibrils" and the distribution of "minute military foci caused by the deposition of a special substance". Today, these features are known as neurofibrillary tangles (NFTs) and senile plaques (SPs), respectively. SPs are extracellular aggregates of β-amyloid peptide (Aβ), a proteolytic product of the amyloid precursor protein (APP). NFTs are intracellular and are composed mainly by hyperphosphorylated microtubule-associated protein tau (MAPT).

The human *APP* gene was first identified in 1987 (Kang et al., 1987) and belongs, together with the APP-like protein 1 (*APLP1*) and 2 (*APLP2*), to the APP protein family in mammals. All three are type I transmembrane proteins with a single membrane-spinning domain, a large extracellular N-terminal region and a short cytoplasmic C-terminal tail (De Strooper et al., 2000). Although they undergo similar processing, only APP contains the sequence encoding the Aβ domain. *APP* is localized on chromosome 21 and alternative splicing of exons 7 and 8 gives rise to three major isoforms: APP695, APP751 and APP770 (containing 695, 751, and 770 amino acids, respectively) (Kitaguchi et al., 1988). APP751 and APP770 are ubiquitously expressed (Schmechel et al., 1988), whereas APP695 is predominantly expressed in neurons (Tanaka et al., 1988).

A role of APP in transmembrane transduction, cell adhesion, calcium metabolism, neurite outgrowth, and synaptogenesis has been reported (Muller et al., 2017). APP is localized on the plasma membrane, but also in membranes of the endoplasmic reticulum (ER), Golgi, trans-Golgi-network (TGN), lysosomes, endosomes, and mitochondria (Zhang et al., 2011).

APP is mainly processed in the canonical pathway, which includes the amyloidogenic and non-amyloidogenic route (Figure 1) (Zhang et al., 2011). The latter is more prevalent and excludes

the generation of Aβ. Here, APP is first cleaved by the α-secretase within the Aβ-domain, which results in a large N-terminal ectodomain (sAPPα) and the membrane-remaining C-terminal fragment (α-CTF), which is subsequently cleaved by the γ-secretase. This second cleavage produces the short peptide P3 and the APP intracellular domain fragment (AICD or γ-CTF). In contrast, the amyloidogenic pathway leads to the production of Aβ because of the sequential cleavage of the β- and γ-secretase. In a first step, the β-secretase cleaves APP in the N-terminal end of the Aβ domain to generate sAPPβ and the 99 amino acid long membrane-bound C-terminal fragment (β-CTF). Further processing of β-CTF causes Aβ and γ-CTF-formation. This final step can produce Aβ peptides of different length, between 39 and 42 amino acids. The non-canonical processing routes have been described more recently and new secretases and corresponding proteolytic fragments have been identified, with probably more to be discovered (Muller et al., 2017).

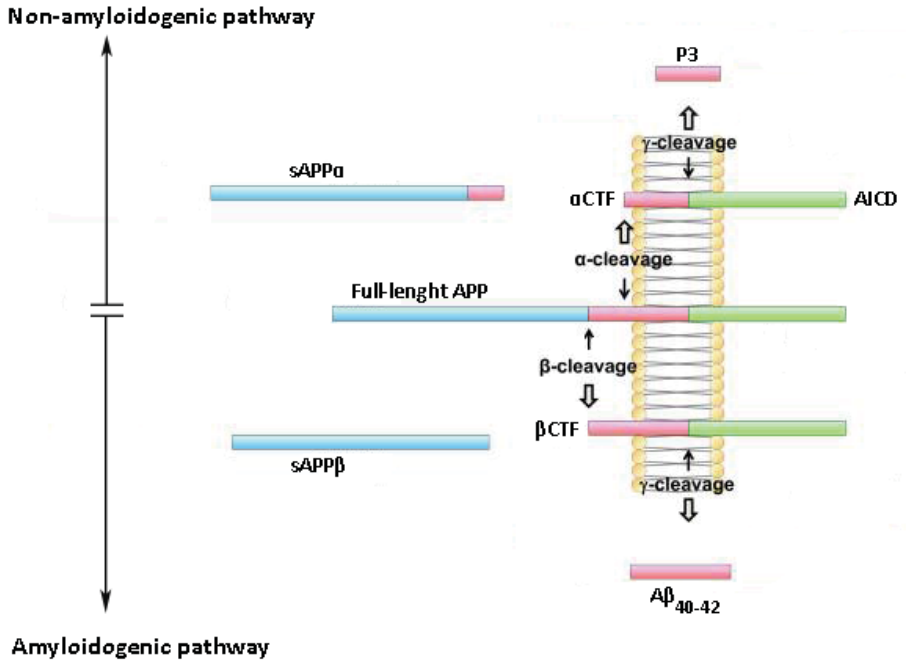

Figure 1. Schematic diagram of the canonical APP processing.
Image modified from Zhang et al., 2011.

The generation of Aβ takes place in different cellular organelles including plasma membrane, ER, Golgi/TGN, lysosomes, and endosomes. The Aβ40 isoform is the most abundant (80-90%), whereas Aβ42 is more hydrophobic and fibrillogenic (LaFerla et al., 2007). Aβ peptides not only differ in length, additional heterogeneity is added by modifications through aminopeptidases, glutaminylcyclases, and other modifications that might contribute to Aβ neurotoxicity (De Strooper, 2010). Monomeric Aβ peptides form low molecular oligomers (dimer/trimer) and then soluble high molecular aggregates. Those finally build spherical oligomers composed of 12-24 monomers, which prolong to form protofibrils and become insoluble fibrils (Glabe, 2008).

The amyloid hypothesis, which has been the predominant framework for AD research, postulates that the accumulation of Aβ acts as the root cause of AD and initiates its pathogenesis (Selkoe et al., 2016). For a long time, it has been believed that insoluble extracellular fibrils (classical amyloid plaques) were the most neurotoxic. However, they are also present in the brain of non-demented individuals and do not correlate with deterioration of cognitive function (Aizenstein et al., 2008). Clinical trials that removed plaques failed to reverse the damage or stop disease progression (Cappai et al., 2008; Hardy, 2009). Focus switched then to soluble Aβ aggregates as the primary toxic species. Indeed, those are better correlated with disease severity (Tomic et al., 2009). How exactly Aβ oligomers mediate neurotoxicity is still unknown. Several studies propose the interaction of soluble extracellular Aβ with receptors of the cell surface as causative for neuronal dysfunction and neurodegeneration. Aβ oligomers caused functional disruption of the N-methyl-D-aspartate (NMDA) receptor by inducing its endocytosis and repressing NMDA-evoked currents in neurons (Snyder et al., 2005). Interaction of Aβ with nerve growth factor receptor induces neuronal death (Yamamoto et al., 2007) through the p75 neurothrophin receptor—a member of the tumor necrosis factor receptor superfamily (Sotthibundhu et al., 2008). Another mechanism by which Aβ might induce neurodegeneration is the ability of this peptide to integrate into membranes to form membrane channels. These channels permit influx of some ions—including calcium—leading to the disruption of calcium homeostasis (Kawahara et al., 2000), increased reactive oxygen species (ROS) formation (Yatin et al., 1998) and tau phosphorylation (Takashima et al., 1993). In contrast, others say that amyloid oligomers cause membrane permeabilization by affecting the lipid bilayer conductance (Kayed et al., 2004).

Numerous authors suggest that intracellular accumulation of Aβ is an even earlier event preceding the formation of extracellular deposits of Aβ (LaFerla et al., 2007). In this sense, intracellular Aβ may contribute to AD pathology through the inhibition of mitochondrial enzymes causing a reduction in oxygen consumption (Caspersen et al., 2005), as well as mediating the inhibition of proteasome function (Almeida et al., 2006). Furthermore, intraneuronal Aβ peptides cause synaptic dysfunction and memory impairment (Billings et al., 2005; Oddo et al., 2003). Other studies report Aβ toxicity trough the inhibition of cell redox activity (Shearman et al., 1994), induction of apoptosis and activation of caspases (Lustbader et al., 2004), as well as the possible contribution to tau phosphorylation and paired helical filament (PHF) formation (Lewis et al., 2001; Zheng et al., 2002).

The second neuropathologic hallmark of AD are NFTs, composed of abnormally hyperphosphorylated tau (p-tau) proteins that aggregate into PHFs. Tau belongs to a family of phosphoproteins—the so-called microtubule-associated proteins (MAPs). Tau and two other proteins—MAP1 and MAP2—are the major MAPs expressed in mature neurons. For long, the only known functions were the promotion of the assembly of tubulin into microtubules and the

stabilisation of their structure (Weingarten et al., 1975). However, tau has been proposed to be a key regulator of axonal transport and signalling cascades, cellular responses to heat shock, and adult neurogenesis (Morris et al., 2011). Tau function is mainly regulated by the degree of phosphorylation, however tau can also receive many other posttranslational modifications, such as glycosylation, ubiquitination, glycation, nitration and truncation (Avila et al., 2004). The human tau gene (*MAPT*) is localized on chromosome 17 and contains 16 exons. Alternative splicing of exon 2, 3, and 10 generates six different isoforms ranging from 48 to 68 kDa in molecular weight.

Tau contains 85 putative phosphorylation sites (Goedert et al., 1989) that can be phosphorylated by several kinases. Among them, the cyclin-dependent protein kinase 5 (CDK5), glycogen synthase kinase 3 (GSK3), protein kinase A (PKA), calcium and calmodulin-dependent protein kinase II (CaMKII), mitogen activated protein kinase ERK 1/2, and stress-activated protein kinases have mostly been implicated in the hyperphosphorylation of tau. The contrary event—dephosphorylation—is managed by the activity of phosphoseryl/phosphothreonyl protein phosphatases (PP). PP2A is the major enzyme involved in dephosphorylation of tau in the brain (Gong et al., 2000).

In AD, 40 phosphorylation sites have been reported (Hanger et al., 2009; Wang et al., 2008) including mainly serine/threonine residues and only two tyrosine residues. P-tau might result from upregulation of tau kinases and/or downregulation of phosphatases (Buee et al., 2000; Trojanowski et al., 1995). Indeed, PP2A activity is reduced in selected areas of AD brains (Vogelsberg-Ragaglia et al., 2001). All six tau isoforms are abnormally hyperphosphorylated and aggregate into PHFs leading to NFTs, neuropil threads, and plaque dystrophic neurites in the brain of AD cases (Grundke-Iqbal et al., 1986; Iqbal et al., 2009). In contrast to SPs, the density of NFTs has been correlated with disease progression (Arriagada et al., 1992; Giannakopoulos et al., 2003). Neurofibrillary degeneration has been observed not only in brains of AD patients, but also in a group of several other neurodegenerative diseases, called tauopaties. This group of diseases include frontotemporal dementia and parkinsonism linked to chromosome 17 (FTDP-17), progressive supranuclear palsy and corticobasal dementia.

The phosphorylation level of tau affects the interaction of tau with microtubules and other proteins, and its tendency to form aggregates. In AD, p-tau loses its affinity to microtubules and leads to the formation of NFTs (Avila, 2000). P-tau sequesters normal tau (Alonso et al., 1996; Alonso et al., 1994), MAP1 and MAP2, thereby further enhancing its toxic effects (Alonso et al., 1997). Such breakdown of the microtubule network might affect other subcellular structures such as mitochondria or lysosomes, and further promote tau pathology.

2. Risk factors for AD

2.1. Genetic predisposition

Genetic researchers first could identify the 3 genes associated with FAD: *APP*, Presenilin 1 (*PSEN1*) and Presenilin 2 (*PSEN2*). Mutations and duplications of these genes cause autosomal-dominant FAD with a penetrance of almost a 100%. *PSEN1* is the most commonly involved gene, with 221 pathogenic mutations reported in the Alzforum database (www.alzforum.org/mutations). Those account for about 80% autosomal dominant FAD cases, mutations in *APP* for about 15% and *PSEN2* for 5%. What all these mutations have in common is that they increase the aggregation of the Aβ peptide by increased production or production of a more aggregation-prone form of the peptide (Rogaeva, 2002). Although these genes are known to cause FAD, there are additional variants in *APP*, *PSEN1*, *PSEN2* and *ADAM10*—the major α-secretase involved in proteolysis of the APP ectodomain—that alter the risk in SAD cases (Cruchaga et al., 2012).

After the discovery of *APP*, *PSEN1* and *PSEN2*, genetic studies aimed to identify genes causing the more frequent late-onset form of the disease. In this way, already twenty-five years ago, Apolipoprotein E (*APOE*) was discovered as a genetic risk factor for SAD (Corder et al., 1993). The *APOE* gene is located at chromosome 19q13.2 and encodes a highly pleiotropic glycoprotein (Siest et al., 1995). There are three alleles (ε2, ε3, and ε4) for the *APOE* gene, and risk of AD and early age of onset is associated with *APOE-ε4*, whereas the *ε2* allele is associated with protection and delayed age of onset (Corder et al., 1994). Still, the combinations of these four genes (*APP*, *PSEN1*, *PSEN2* and *APOE*) might explain 30-50% of inheritability. Advances in genomic technologies and the advent of genome-wide association studies (GWAS) have allowed the identification of novel genetic associations. Consortia like the Genetic and Environmental Risk in Alzheimer's Disease (GERAD) and the European Alzheimer's Disease Initiative (EADI) were able to identify genome-wide significant associations with single nucleotide polymorphisms (SNPs) in more than twenty loci besides *APOE* (Lambert et al., 2009; Lambert et al., 2013; Lambert et al., 2011). However, most of these loci present common variants with a small individual effect on risk (Figure 2), but still have helped create a broader picture of the processes and pathways involved. It has been estimated that they only modify disease risk by 0.10 to 0.15-fold, whereas the presence of *APOE-ε4* results in an almost 4-fold increase (Bertram et al., 2010). Interestingly, these variants can be clustered into three pathways, namely lipid metabolism, immune response, and endocytosis (International Genomics of Alzheimer's Disease, 2015; Karch et al., 2015).

New approaches are necessary in order to identify new candidates with higher risk. Recently, whole-exome sequencing and whole-genome sequencing strategies discovered rare coding variants of two AD-linked genes. The variants in the triggering receptor expressed on myeloid cells 2 (*TREM2*) (p.R47H) and phospholipase D3 (*PLD3*) (V232M) genes appear to confer

a higher risk for AD than other genes identified by GWAS (Cruchaga et al., 2014; Guerreiro et al., 2013). Despite all efforts, we are still under pressure to explain the missing inheritability, which in part might be explained by epistasis, rare variants, and somatic mutations (Karch et al., 2015).

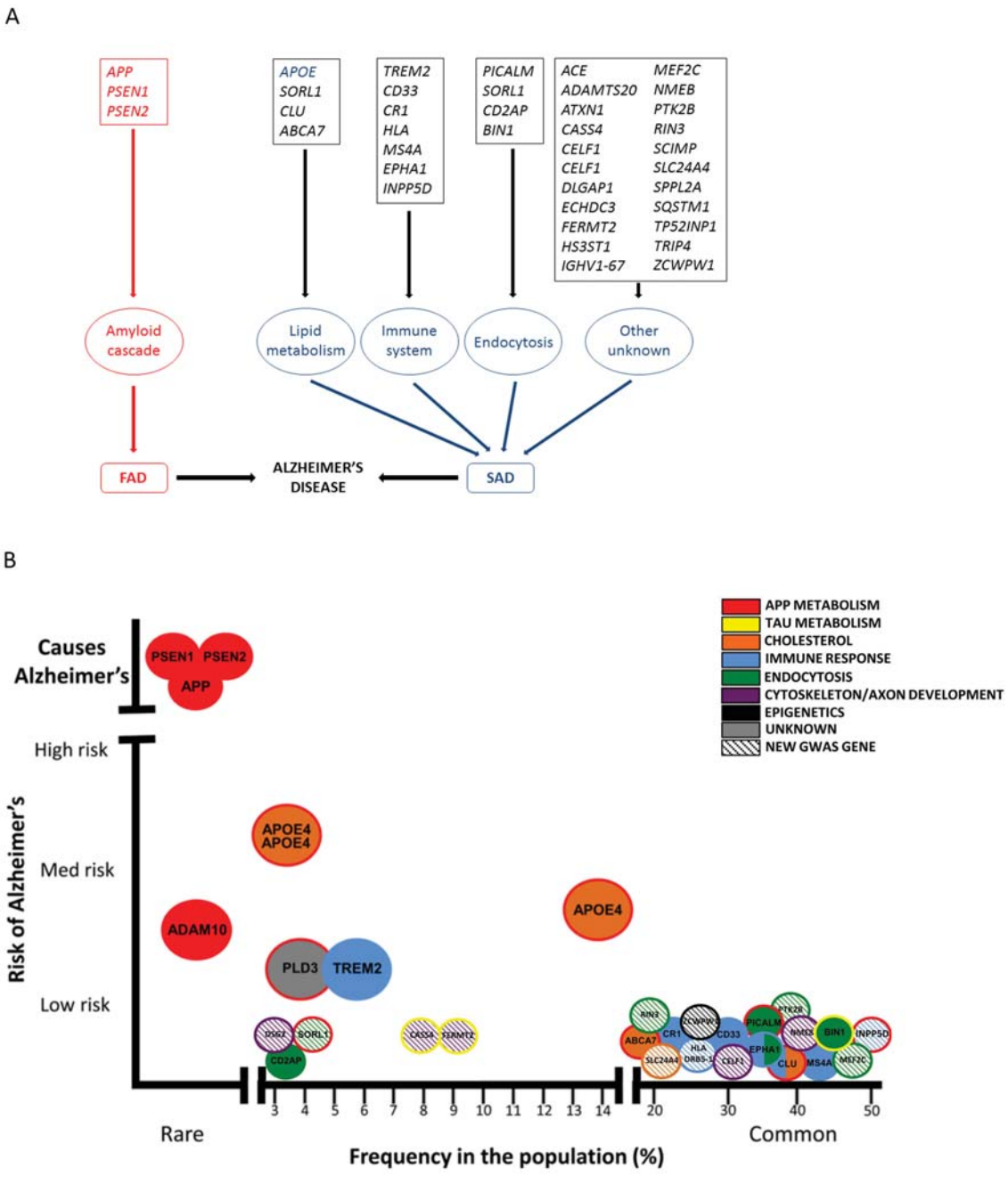

Figure 2. Genetics of Alzheimer's disease.
(A) Genetic risk factors for AD and their implication in lipid metabolism, immune system, and endocytosis. (B) Rare and common variants contribute to AD risk. Image from Karch et al., 2015.

2.2. Infectious hypothesis and AD

Growing evidence support that chronic or latent infection of the CNS might be implicated in the etiology of AD (Miklossy, 2011). The idea of the so-called pathogen/infectious hypothesis came up in the 1960s and has gained support since then. First evidence came from the fact that several microbes can access the CNS, remain there in latent form by evading the host immune response, and that they are highly prevalent in the AD brain (Harris et al., 2015). Among them, bacteria like *Chlamydia pneumonia* (Gerard et al., 2006), *Helicobacter pylori* (Kountouras et al., 2007) and several types of spirochaete (Miklossy, 2011), and herpes viruses such as Epstein Barr Virus (EBV), Herpes simplex virus type 1 (HSV-1), Cytomegalovirus (CMV), and Human herpes virus 6 (HHV6), have been associated with AD (Harris et al., 2015). Two recent studies reported the presence of fungal infections in the brain of AD patients (Alonso et al., 2014; Pisa et al., 2015). The hypothesis states that in combination with genetic risk factors, these pathogens participate in the generation of the Aβ peptide, tau hyperphosphorylation and inflammation. Of all studied pathogens in relation with AD, HSV-1 has emerged as a major factor in the etiology of the disease (Itzhaki, 2014).

2.2.1. HSV-1 and AD

HSV-1 belongs to the alphaherpesvirus subfamily. Other members of this group are the closely related HSV-2 and Varicella zoster virus (Steiner et al., 2007). HSV-1 is a ubiquitous neurotropic virus, with a worldwide seroprevalence of more than 80% in adults. The virion of all alphaherpesviruses consists of four components: (1) an electron-dense core containing lineal viral DNA of approximately 152 kDa, (2) the capsid, an icosadeltahedral structure that surrounds the core composed of 6 structural proteins, (3) the surrounding tegument, a protein layer composed of 22 viral proteins and (4) an envelope (Owen et al., 2015). The envelope is derived from cellular membranes and includes viral glycoproteins, which are important for the virus adsorption to the cell surface, receptor recognition and membrane fusion to enable viral entry into the host cell (Fields et al., 1996).

HSV-1 usually enters orofacial mucosal epithelia cells where productive infection takes place (Figure 3). From there, the virus can spread to neurons of the trigeminal ganglia innervating the epithelium where it can establish lifelong latency (Kennedy et al., 2015; Nicoll et al., 2012). After primary infection, the virus can replicate or stay latent in the neuron cell body until reactivation by diverse stimuli (like stress and immunosuppression). When reactivated, the virus travels back to the primary site of infection where it causes the so-called cold sores (herpes labialis). Infected peripheral nervous system (PNS) neurons are in direct synaptic contact with CNS neurons providing a direct route of spread from the periphery (Koyuncu et al., 2013). Once in the CNS, the virus can stay latent until periodical reactivation, which could cause neuronal damage.

Acute HSV-1 infection is known to cause different neurological diseases, like herpes keratitis (Rowe et al., 2013) or encephalitis (Bradshaw et al., 2016), and mounting evidence links it to AD.

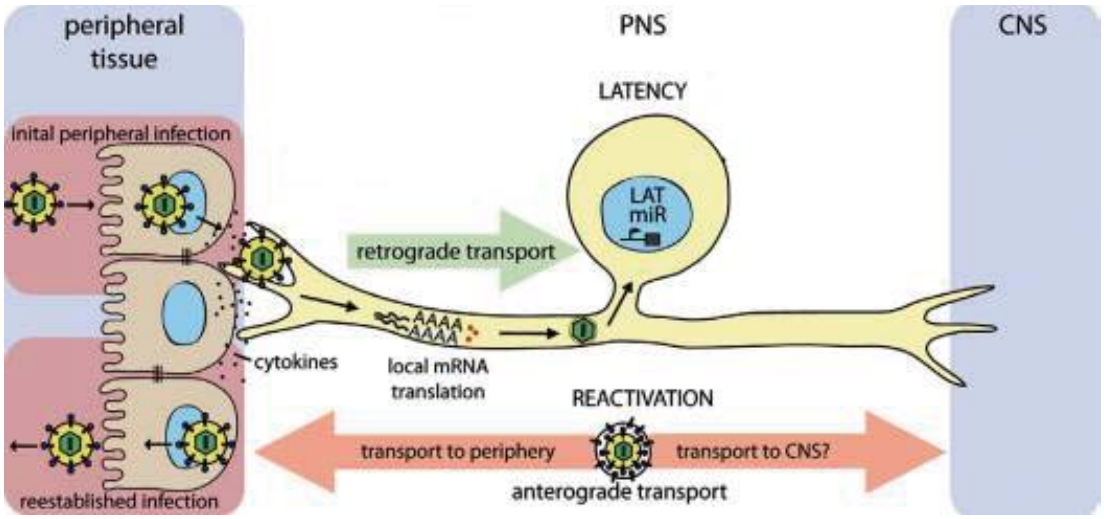

Figure 3. HSV-1 access route to the CNS.
Epithelial cells of the orofacial mucosa are initially infected with HSV-1. The virus enters sensory neurons by fusion with the plasma membrane or via endocytosis. Once inside the sensory process, viral particles undergo long-distance retrograde transport to the neuronal cell body, where the virus replicates or becomes latent. When the HSV-1 genome reactivates, newly synthesized virions travel anterograde back to the primary site of infection causing recurrent herpes labialis and/or access the CNS. Image modified from Koyuncu et al., 2013.

Brain autopsies showed that latent HSV-1 is present in a high proportion of SAD and normal elderly individuals, and that it was found in the areas most affected by AD, namely temporal and frontal cortices and hippocampus (Jamieson et al., 1991). Furthermore, the viral DNA seems to colocalize with SPs suggesting an active role of the virus in their generation (Wozniak et al., 2009). In contrast, no viral DNA has been found in younger brains (Wozniak et al., 2005), suggesting that HSV-1 reaches the CNS at older age when the immune system declines. Evidence from epidemiological studies postulate that in synergy with the possession of the *APOE-ε4* allele, HSV-1 infection represents a risk factor for AD (Itzhaki et al., 1997), even though neither of the two factors alone is necessary nor sufficient for the development of the disease. In this sense, using mice models, our group previously showed that the *ApoE* dose and genotype determine the viral load in the CNS. The viral neuroinvasion was reduced in animals lacking the *ApoE* gene compared to wildtype animals and a direct correlation between HSV-1 concentration and ApoE allelic dose was detected (Burgos et al., 2002). In posterior reports, we then showed that during both acute and latent infection, *ApoE-ε4* was more efficient than *ApoE-ε3* in promoting viral colonisation of the brain (Burgos et al., 2003; Burgos et al., 2006). Besides *APOE*, many genes are thought to interact with some aspect of HSV-1 infection. Indeed, GWAS identified a set of genes associated with SAD which may affect the individual susceptibility to HSV-1 infection (Porcellini et al., 2010).

These genes could constitute in a genetic fingerprint modulating the individual's susceptibility to HSV-1 infection thereby causing neuronal loss, inflammation and Aβ deposition (Licastro et al., 2011; Porcellini et al., 2010). Letenneur and colleagues studied the presence of HSV IgG (a marker of primary infection) and IgM antibodies (a marker of HSV reactivation) in the serum of AD patients and controls. They found out that the reactivation of HSV is highly correlated with the progression of the disease (Letenneur et al., 2008). These results were recently confirmed by Lövheim's group in an independent study (Lovheim et al., 2014). Finally, several researchers, including our group, linked HSV-1 to the main neuropathological hallmarks of AD in neuronal and animal models of HSV-1 infection: infection leads to an accumulation of intracellular Aβ (Santana et al., 2012; Wozniak et al., 2007), autophagic vesicles (Itzhaki et al., 2008; Santana et al., 2012) and hyperphosphorylated tau protein (Alvarez et al., 2012; Wozniak et al., 2009).

Under these circumstances it is not surprising that researchers study the effect of anti-viral treatments in relation with AD (Itzhaki et al., 2012). In cell culture experiments, the use of acyclovir (ACV), an inhibitor of viral replication, reduced the amount of HSV-1, Aβ formation and tau hyperphosphorylation (Wozniak et al., 2011). Valacyclovir, the ACV's biodrug, is already being tested in clinical trials for its use in multiple sclerosis with promising results (Friedman et al., 2005), although it has not been tested in AD patients so far. These preliminary results indicate that antiviral treatment might stop or slow down the disease progression especially in AD patients who are *APOE-ε4* carriers. In this context, a large group of researchers and clinicians gathered together recently to express their concern about the fact that—despite all evidence—the infectious hypothesis still is not fully accepted and no effort is made to initiate antiviral/antimicrobial clinical studies in relation to AD (Itzhaki et al., 2016).

2.2.2. Interaction between HSV-1 and oxidative stress

Oxidative stress contributes to neuronal damage and has been associated with neuronal cell death in certain neurodegenerative diseases such as AD (Andersen, 2004; Nunomura et al., 2006). Although the most important non-genetic risk factor for AD is aging, various studies report the presence of oxidative stress in the brains and peripheral tissues of patients with AD and animal models (Gibson et al., 2005). Oxidative stress results from an imbalance in prooxidant/antioxidant homeostasis leading to the generation of toxic ROS. Under normal conditions, ROS are produced as a consequence of cellular processes and their amount is controlled by antioxidants such as glutathione peroxidase and catalase and by non-enzymatic antioxidant molecules such as glutathione, vitamin E, ascorbic acid and carotenoids (Su et al., 2008). In relation with AD, an increase of OS markers, including RNA/DNA damage and lipid peroxidation, have been reported in AD brains and animal models of the disease (Gabbita et al., 1998; Nunomura et al., 1999; Williams et al., 2006). Several studies reported increased activity of the major antioxidant enzymes in cortex and hippocampus of AD patients (Pappolla et al., 1992; Zemlan et al., 1989).

The high oxygen consumption of the human brain makes this organ especially susceptible to oxidative stress (Shulman et al., 2004). Since aging is associated with increased ROS production and decreased ROS clearance, in age-related neurodegenerative diseases—like AD—oxidative stress is not only an early event but also would play an important role in initiating the disease through activation of cell signalling pathways leading to apoptosis and neuroinflammation (Cai et al., 2011). On the other hand, oxidative stress contributes to Aβ generation and NFTs by different mechanisms (reviewed in Cai et al., 2011).

Our group has also found several evidence linking OS to alterations characteristic of AD. Using the free radical-generating system xanthine-xanthine oxidase (X-XOD) to induce mild oxidative stress in neuronal cell models, as it might occur during normal aging, we showed that OS alters cholesterol biosynthesis—one of the earliest events observed in AD patients (Recuero et al., 2009). We then reported that the X-XOD system is able to modify the metabolism/processing of APP (Recuero et al., 2010) through the autophagy-lysosome and ubiquitin-proteasome pathway (Recuero et al., 2013). In combination with HSV-1, we showed that OS enhances the intracellular accumulation of Aβ mediated by HSV-1 infection, and further decreased its secretion to the extracellular medium. Furthermore, OS potentiates the accumulation of immature autophagic compartments and the inhibition of the autophagic flux induced by HSV-1. At the same time, OS reduced the efficiency of HSV-1 infection (Santana et al., 2013).

Other authors also reported association between acute and latent HSV-1 infection of the CNS and oxidative damage (Milatovic et al., 2002; Valyi-Nagy et al., 2000). HSV-1 has been described to induce the peroxidation of lipids (Palu et al., 1994). During acute infection, HSV-1 provokes encephalitis in mice accompanied by severe inflammation and elevated levels of F2-isoprostanes and F4-neuroprostanes—two markers of oxidative damage (Milatovic et al., 2002). Latent HSV-1 infection induces oxidative damage of RNA and DNA molecules in infected areas of the murine brain (Valyi-Nagy et al., 2000). On the other hand, latent infection of HSV-1 in murine models is also associated with persistent and chronic inflammation in the brain, and with high levels of proinflammatory cytokines such as the tumor necrosis factor α (TNFα) and increased activity of induced nitric oxide synthase (iNOS). These factors may play an important role in preventing the reactivation of HSV-1 (Koprowski et al., 1993; Marques et al., 2008; Meyding-Lamade et al., 1998). Both TNFα and nitric oxide have antiviral activities but can directly generate potent free radicals or ROS-mediated oxidative damage through different cell signalling pathways. Therefore, the host's immune and inflammatory response plays an important role in the generation of oxidative damage in the brain during HSV-1 infection (Valyi-Nagy et al., 2005). In conclusion, although few reports exist on the interplay of OS and HSV-1 infection, the results suggest that OS may promote the neurodegenerative events associated to HSV-1 infection.

3. The lysosomal pathway

Lysosomes were first described in 1955 by Christian de Duve and thought to be just the cellular waste bags. They are the major digestive compartments within cells and are involved in multiple functions like the degradation and recycling of intra- and extracellular material, cholesterol homeostasis and cell death signalling (Appelqvist et al., 2013). Lysosomes have an acidic lumen, limited by a 7-10 nm thick phospholipid bilayer membrane, and contain several types of hydrolases for the degradation of substrates. There are 25 lysosomal membrane proteins (Lubke et al., 2009) being the lysosome-associated membrane protein (LAMP) 1 and LAMP2, lysosomal integral membrane protein (LIMP) 2, and LIMP1 (also known as CD63) the most abundant ones (Eskelinen et al., 2003). Because the low lysosomal pH provides optimal conditions for hydrolase activity, those proteins are protected from cleavage by dense glycosylation. Besides being a mechanical border, the lysosomal membrane has many other features, like the maintenance of the pH gradient between lysosomal lumen and cytoplasm, the mediation of fusion with endosomes or other organelles, and the selective transport of material into and/or out of the lysosome (Eskelinen et al., 2003; Saftig et al., 2009).

Inside the lysosome reside more than 60 different soluble hydrolases, including sulphatases, glycosidases, peptidases, phosphatases, lipases and nucleases, most of them only active at acidic pH. The best-studied hydrolases are the cathepsins (CTSs). They are categorised in three groups based on the amino acid at their active site: serine, cysteine, and aspartic CTSs. Aspartic CTSs include CTS D and E, cysteine CTSs include CTS B, C, F, H, K, L, O, S, V, X and W, whereas CTS A and G belong to the serine CTSs (Turk et al., 2012).

Lysosomal hydrolases are synthesized in the ER as immature and enzymatically inactive precursors. They are then transported in vesicles from the ER through the Golgi to the TGN and from there to the lysosome. To be targeted to lysosomes, a mannose 6-phosphate (M6P) tag is added in the Golgi complex (Rohrer et al., 2001). This signal is recognised by diverse M6P receptors in the TGN (Braulke et al., 2009; Ghosh et al., 2003). There, clathrin-coated vesicles were formed containing the receptor-ligand complexes. These vesicles move towards the cell periphery and fuse with endosomes. Inside the endosome, the hydrolases were dissociated from the receptors because of the low pH (around pH 6) and the receptors will be transported back to the TGN(Braulke et al., 2009). The constant trafficking of material from the TGN to the endosomes and back is an important feature for the maintenance of lysosomal intactness, acidity, and perinuclear localization (Bucci et al., 2000). The decreasing intraluminal pH during endosomal maturation initiates hydrolase activity and digestion of endocytosed material. However, only after fusion with lysosomes, the hydrolases have reached their final destination with maximal proteolytic activity.

A constant lysosomal pH between 4.8-5.2 is guaranteed by the action of an ATP-dependent proton pump—the vacuolar (V)-ATPase (Toei et al., 2010). V-ATPases are multi-subunit protein complexes consisting of a membrane-associated V0 complex that serves as a transmembrane pore for protons, and a soluble cytosolic V1 complex. Beside the maintenance of lysosomal pH, the V-ATPase also regulates vesicle fusion and is located to several membranes including lysosomes, endosomes, Golgi-derived vesicles and sometimes even to the plasma membrane (Yamamoto et al., 1998; Yoshimori et al., 1991). Several potent and selective inhibitors have been identified over the years to interfere with this tightly regulated network. Ammonium chloride or chloroquine are lysosomotropic weak bases, which elevate the pH by entering the acidic compartment in their unprotonated form and titrating the pH upward (Ohkuma et al., 1978). Bafilomycin A1, in contrast, is a specific V-ATPase inhibitor (Bowman et al., 1988).

There are two routes by which material for degradation reaches the lysosome: (i) extracellular material and parts of the plasma membrane reach the lysosome by endocytosis, whereas (ii) intracellular material is transported to the lysosome through autophagy.

3.1. Endocytic pathway

Endocytosis is a process by which cells internalize the plasma membrane along with cell surface receptors and soluble molecules (Maxfield et al., 2004). As a first step, the material to be ingested is progressively enclosed by parts of the plasma membrane, which invaginates and then pinches off to form an endocytic vesicle. These vesicles then fuse with early endosomes, the first sorting station of endocytosis. From there, the majority of the cargo is recycled back to the plasma membrane via recycling endosomes. Every hour, 50% of the surface area of the plasma membrane is cycled in and out of a typical mammalian cell (Steinman et al., 1983). Otherwise, cargo will be retained in the early endosomes, which mature into late endosomes—the second sorting station. During maturation several events take place, amongst other things the formation of intraluminal vesicles (ILVs) from the limiting membrane. The presence of many ILVs inside the late endosomes (often up to >30) got them the name of multivesicular bodies (MVBs) (Piper et al., 2007). Further, the decrease in luminal pH is taking place during this transformation from early (pH 6.8-5.9) to late endosomes (pH 6.0-4.9). The continuous transformation, fusion and fission of these organelles make their identification with molecular markers difficult. The early endosomal antigen 1 (EEA1) is widely accepted as marker for early endosomes (Mu et al., 1995). Late endosomes differ from lysosomes by the presence/absence of M6P receptors, respectively (Brown et al., 1986).

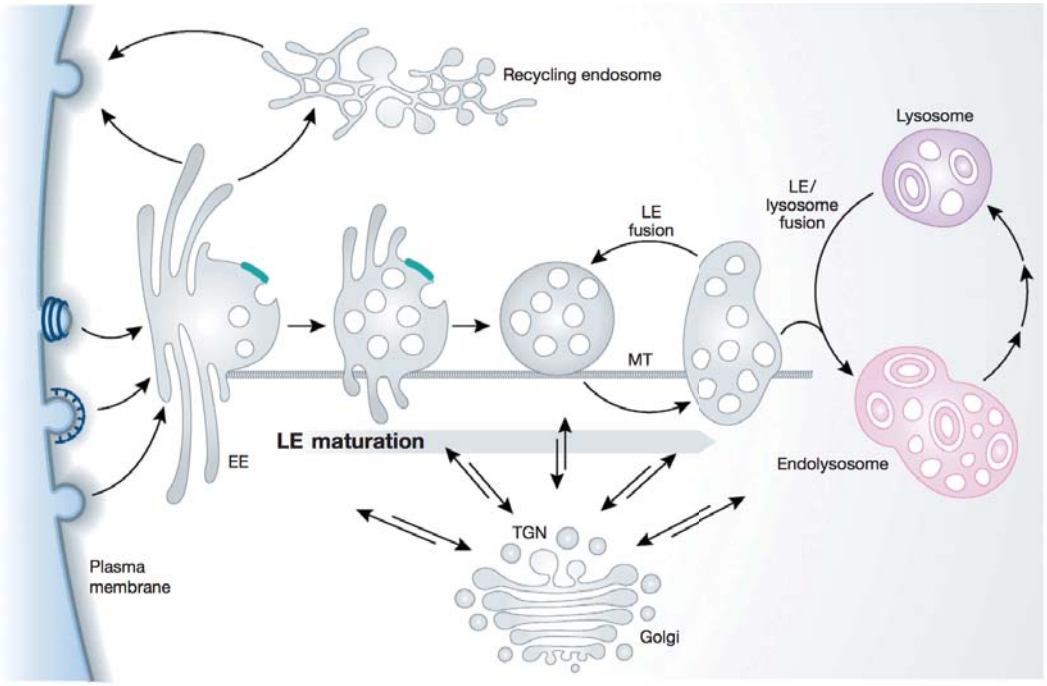

Figure 4. Schematic representation of the endocytic pathway.
Primary endocytic vesicles were formed at the plasma membrane and deliver their cargo to early endosomes where some material will be recycled back to the plasma membrane (directly or via recycling endosomes). Maturation from early endosomes (EE) to late endosomes (LE) takes place. Endosomes receive newly synthesized hydrolases and membrane compounds from the trans-Golgi-network (TGN), grow in size and acquire more intraluminal vesicles. Fusion with lysosomes forms hybrid organelles, endolysosomes, where degradation of the cargo takes place. Image from Huotari et al., 2011.

3.2. Autophagy

Autophagy is the process by which cells digest their own cytoplasm to provide material for new synthesis. There exist three forms of autophagy in the cell: chaperone-mediated autophagy (CMA), microautophagy, and macroautophagy. CMA, as indicated by its name, includes the recognition of the substrates via the action of chaperones and the lysosomal receptor LAMP2A (Kaushik et al., 2012). The direct engulfment of small cytoplasmic material by the lysosomal membrane is called microautophagy (Li et al., 2012). The principal form of autophagy, though, is macroautophagy, herein referred to as autophagy.

Autophagy begins with the formation of a double-layered isolation membrane (also called phagophore) that engulfs and sequesters cytoplasmic material in its interior. The elongation of this phagophore assures the formation of a double-membraned structure, the so-called autophagosome (Nakamura et al., 2017). The most characterized protein associated with autophagosomes is the lipidated form of microtubule-associated protein light chain 3 (LC3-II). The conversion of LC3-I (the non-lipidated form) to LC3-II is the main marker for monitoring autophagic flux (Klionsky et al., 2016). The autophagosome subsequently might fuse with endosomes or directly with lysosomes

for the degradation and recycling of their cargo. In this way, the degraded products are released into the cytoplasm to newly synthesize macromolecules or serve as energy source. There is always a basal activity of autophagy present to maintain cellular homeostasis acting as an essential mechanism of quality control for cellular structures. However, autophagy can be activated through diverse stimuli, like stress, low nutrient levels or viral infections, participating in multiple processes such as cell differentiation, innate and adaptive immunity and anti-tumoral and anti-aging mechanisms (Yin et al., 2016). In this scenario, the coordinated lysosomal expression and regulation (CLEAR) gene network gets activated through the inhibition of the mammalian target of rapamycin (mTOR) signalling—the main regulatory pathway of the autophagic process. Inhibition of mTOR dephosphorylates the master regulator of the CLEAR network—the transcription factor EB (TFEB) (Settembre et al., 2013). This induces its nuclear translocation, where TFEB activates gene transcription of more than 500 targets involved in lysosome biogenesis and autophagy.

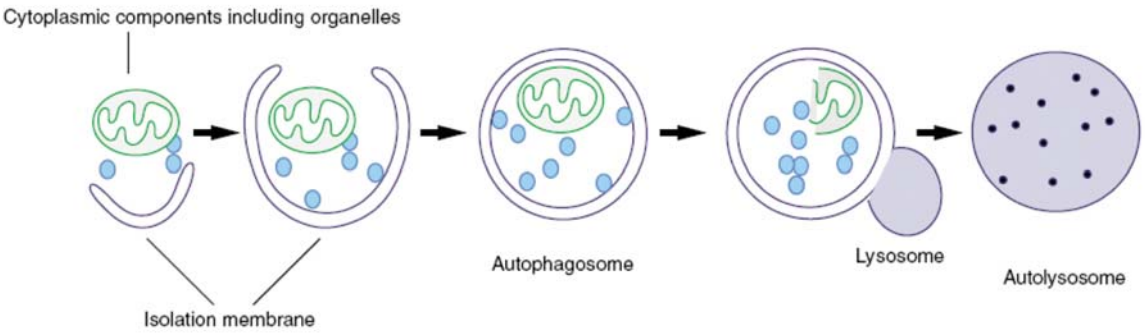

Figure 5. Schematic representation of the autophagic process.
Autophagy begins with the formation of an isolation membrane (phagophore). This membrane elongates thereby engulfing cytoplasm or selected material until a double-membraned structure is formed—the autophagosome. The final step includes fusion with hydrolase-containing lysosomes for the degradation of the cargo. Image modified from Komatsu et al., 2007.

3.3. Lysosomal alterations and neurodegeneration

Neurons especially rely on functional lysosomal degradation (endocytic and autophagic pathways) since they live extremely long without cell division. It is therefore not surprising that defects in autophagy and endocytosis are relevant to neurodegenerative diseases, in particular to AD (Whyte et al., 2017). Indeed, altered endocytosis is one of the earliest neuropathologic features observed in AD preceding Aβ accumulation (Cataldo et al., 2000). The presence of autophagic vesicles was detected in dystrophic neurites of cortex and hippocampus in brains of transgenic mice expressing human APP (Yu et al., 2005). These vesicles contained APP, different Aβ peptides, and β- and γ-secretases necessary for their generation (Yu et al., 2004). In this sense, autophagic activation significantly increases Aβ production in mouse fibroblasts (Yu et al., 2005) and in rat

neurons (LeBlanc et al., 1996). The generated Aβ is targeted to the lysosome for degradation by cathepsins. Thus, efficient autophagy plays a protective role against Aβ-induced neurotoxicity in human neuroblastoma cells (Hung et al., 2009). Further evidence came from the discovery of genetic risk factors and their molecular mechanisms. FAD-causing mutations in *PSEN1* severely compromise autophagy-mediated recycling of proteins, affecting autophagy-dependent processes such as APP processing and Aβ accumulation (Nixon, 2006). Finally, several studies point to lysosomal acidification defects in different AD models causing a failure in lysosomal proteolysis (Avrahami et al., 2013; Nixon et al., 2011; Torres et al., 2012).

Support also comes from knowledge about lysosomal storage diseases (LSDs). LSDs are a family of disorders that result from recessively inherited gene mutations that perturb lysosomal homeostasis. Age of onset and clinical features vary, depending on the nature of accumulating substrate and the cell types affected. Common to all LSD though is the initial accumulation of specific macromolecules or monomeric compounds inside organelles of the endosomal-autophagic-lysosomal system (Platt et al., 2012). Most of LSDs result from decreased activity of acidic hydrolases, but few are also caused by defects in lysosomal membrane proteins or non-enzymatic soluble proteins (Saftig et al., 2009). Almost all LSDs present pathology of the CNS, and in some cases neurodegeneration occurs in multiple brain regions (thalamus, cortex, hippocampus, and cerebellum). For example, *CTS D* deficiency causes neuronal ceroid lipofuscinosis—a severe neurodegenerative disorder (Siintola et al., 2006). Niemann-Pick type C disease (NPC) is provoked by alterations of cholesterol trafficking and other lipids by the defective function/absence of either two endosomal proteins—NPC1 or NPC2. This leads to an accumulation of autophagic vesicles and finally neuronal death. Interestingly, NPC patients show typical AD lesions like NFTs, intracellular Aβ42 accumulation and endosome deficits (Malnar et al., 2014). Indeed, LSD and AD display strong phenotypic overlap, including neuronal accumulation of autophagic or lysosomal vesicles, dystrophic axons, ectopic dentrites, cognitive deficits, and neurodegeneration. Many researchers claim that AD should be included in the group of LSDs due to these similarities (Nixon, 2005; Wolfe et al., 2013).

One of the mechanisms that might explain lysosomal dysfunction causing neurodegeneration is the alteration of cholesterol homeostasis. This disturbance is one of the earliest and most important aspects in AD pathology. Our group previously reported that OS induces cholesterol biosynthesis in neuroblastoma cells, and that polymorphisms in the 3-hydroxy-3-methylglutaryl-CoA reductase (*HMGCR*)—a key gene in cholesterol metabolism—are associated with AD risk (Recuero et al., 2009).

Epidemiological evidence suggests a link between serum cholesterol levels and AD development. It has been proposed that cholesterol-lowering drugs, such as statins, might present potential therapeutic effectiveness for AD. This topic is highly controversial since several reports

claim that statins reduce the risk of AD (Jick et al., 2000), whereas others fail to reproduce those indicating a neutral or even negative relationship (Zandi et al., 2005). Of special interest are the high levels of side-chain oxidized oxysterols, like 27-hydroxycholesterol (27-OHC), observed in brains of SAD patients. In contrast to cholesterol, 27-OHC is able to cross the blood brain barrier. This fact support the theory that hypercholesterolemia might be associated with AD risk (Bjorkhem, 2013). Accordingly, studies with AD patient-derived fibroblasts and peripheral blood mononuclear cells confirmed the presence of lipid alterations in those cells (Pani et al., 2009; Pani et al., 2009). Increased neuronal cholesterol levels also affect APP processing, Aβ generation and tau phosphorylation (Burg et al., 2013; Ghribi et al., 2006).

APOE—the strongest genetic risk factor for SAD—encodes a highly pleiotropic glycoprotein involved in the transport of cholesterol and other lipids in the periphery and brain. In the CNS, APOE plays important roles not only in cholesterol transport but also neuroplasticity and neuroinflammation (Mahley et al., 2000). As mentioned previously, *APOE* generates 3 isoforms, which regulate in a different manner aggregation, capture and degradation of the Aβ peptide. The *APOE-ε4* allele, which is associated with high low-density lipoprotein (LDL) and low high-density lipoprotein (HDL) levels in plasma, increases plaque formation in AD patients (Kok et al., 2009). This might be due to their differential affinity to the LDL receptor thereby increasing cholesterol in plasma and brain. Other SAD-associated genes have been identified in large GWAS studies, including clusterin (*CLU*), ATP-binding cassette transporter A7 (*ABCA7*), and sortilin-related receptor 1 (*SORL1*) (Karch et al., 2015). They all affect lipid metabolism though highlighting the involvement of this mechanism in AD pathology.

OBJECTIVES

Oxidative stress and infection of the brain with HSV-1 have been proposed to be important factors in the pathogenesis of sporadic AD. Although this form of the disease is multifactorial and environmental factors are determining, there is no doubt that the genetic predisposition plays an important role. To investigate the relationships between both risk factors and to identify genes and pathways associated with AD, an analysis of differential expression by microarrays has been performed in a neuronal cell model of HSV-1 infection in the presence of oxidative stress. The following objectives were proposed:

1. Analysis of differently expressed genes via whole genome microarrays and identification of modulated pathways in the cell model of infection and oxidative stress.
2. Analysis of functional alterations of the pathways identified by the gene expression analysis in the cell model of infection and oxidative stress.
3. Study of the genetic association of selected candidate genes from microarray data with AD in case/control samples.
4. Study of the role of the candidate genes in the neurodegenerative events induced by HSV-1 and oxidative stress.
5. Development of patient-derived induced pluripotent stem cells for validating the genes/pathways identified in the gene expression studies in a more physiological cell model.

MATERIALS & METHODS

1. Cell lines and cell culture conditions

The human neuroblastoma cell line SK-N-MC used in this work was purchased from the American Type Culture Collection (ATCC) (No. HTB-10). SK-N-MC cells with a stable knockdown of LAMP2 were produced in-house as described in section 4. SK-N-MC cells stably transfected with human wildtype (wt) APP695 (SK-APP) or mutant APP695 harbouring the Swedish mutation (K670N/M671L) (SK-APP_{Swe}) were prepared in-house by M Recuero and commercialised by NeuronBio. All SK-N-MC cells were grown as monolayers in minimal Eagle's medium (MEM) supplemented with 10% heat-inactivated fetal calf serum (FCS), 1 mM sodium pyruvate, non-essential amino acids (NEAAs), 2 mM glutamine, and 50 µg/mL gentamycin.

The African green monkey epithelial kidney cell line Vero (ATCC No. CCL-81) and the human epithelial adenocarcinoma cell line HeLa (ATCC No. CCL-2) were passaged in Dulbecco's modified Eagle medium (DMEM) supplemented with 10% FCS, 1 mM sodium pyruvate, NEAAs, 2 mM glutamine and 50 µg/mL gentamycin.

The murine neuroblastoma N2a cell lines (wt and with a stable knockdown of LAMP2) were kindly provided by P. Saftig (Rothaug et al., 2015). N2a cells were cultured in DMEM supplemented with 10% FCS, 1 mM sodium pyruvate, NEAAs, 2mM glutamine and 50 µg/mL gentamycin. To the N2a LAMP2-deficient cells, 400 µg/mL G418 (Invivogen) was added to the media. Wt and LAMP2-deficient murine embryonic fibroblast (MEF) cells were also kindly provided by P. Saftig (Eskelinen et al., 2004). MEFs were cultured in DMEM-low glucose (1 g/L) supplemented with 10% FCS, 1 mM sodium pyruvate, NEAAs, 2 mM glutamine and 50 µg/mL gentamycin.

All cells were grown at 37ºC in a 5% CO_2 atmosphere.

2. Infection conditions and induction of oxidative stress

The wt HSV-1 strain KOS 1.1 was cultivated, propagated and titered on a monolayer of Vero cells following described methods (Carrascosa et al., 1982) and stored at -70°C. For infection experiments, cells were seeded in complete media at 70-80% confluency and exposed to HSV-1 at 37°C for 1 h. Mock infections were performed using a virus-free suspension. In order to remove unbound virus, the medium was changed and cells were incubated in complete medium at 37ºC. Time and multiplicity of infection (expressed in plaque forming units per cell [pfu/cell]) are as indicated in each experiment. The infectious titers of HSV-1 were determined by plaque assays with Vero cells as previously described (Santana et al., 2012). Induction of oxidative stress was performed through addition of xanthine (10 µM)-xanthine oxidase (50 mU/mL) (X-XOD) to fresh medium. Exposure times are indicated in each experiment. In samples exposed to oxidative stress and HSV-1, X-XOD was added after the virus adsorption and maintained until the end of infection.

3. Treatments

Epidermal growth factor (EGF; 40 ng/mL) was purchased from Calbiochem. Xanthine oxidase (50 mU/mL) was purchased from Roche. Heparin (10 µg/mL), bafilomycin A1 (100 nm), and xanthine (10 µM) were purchased from Sigma. 4',6-diamidino-2-phenylindole (Dapi; 5 µg/mL) and ammonium chloride (NH_4Cl; 20 mM) were obtained from Merck. For nutrient starvation, culture medium was exchanged for Earle's balanced salt solution (EBSS).

4. Generation of cell lines with stable gene-silencing of LAMP2

For the generation of cell lines with a stable knockdown of LAMP2, cells were transfected with short hairpin RNA (shRNA) clones specific to LAMP2 and with a scrambled control shRNA clone (Mission control shRNA library from Sigma; listed in Table 1). The five specific shRNA clones are validated and reach more than 90% knockdown. Transfections were performed with Lipofectamine 2000 reagent according to the manufacturer's recommendations (Life Technologies). Briefly, SK-N-MC cells were cultured in 6 well plates until 70% confluency and then transfected by the mixture of 0.5 µg DNA and 2 µL Lipofectamine transfection reagent, both diluted in Opti-MEM medium. The mixture was incubated for 5 min at room temperature (RT) to form DNA-lipid complexes and was then added to the cells. 48 h after transfection, cells were trypsinized and re-plated at low densities (dilutions 1:50, 1:500, 1:5,000) in P100 dishes with the selection antibiotic puromycin at a final concentration of 0.25 µg/mL (the effective concentration was previously determined in a dose-response experiment with SK-N-MC cells and puromycin concentrations between 0 and 10 µg/mL). Medium supplemented with puromycin was replaced every 2-3 days. Clones were picked manually and expanded until enough cells were available for generating a frozen stock and for isolating total RNA and protein extracts for analysis. Finally, clones with a low expression of LAMP2 were selected for further analyses.

Table 1. Mission control shRNA DNA clone sequences.

Item number	Insert sequence/vector	No.
TRCN0000029259	**CCGG**GCCATCAGAATTCCATTGAAT**CTCGAG**ATTCAATGGAATTCTGATGGC**TTTTT**	1
TRCN0000029260	**CCGG**GAAGTGAACATCAGCATGTAT**CTCGAG**ATACATGCTGATGTTCACTTC**TTTTT**	2
TRCN0000029261	**CCGG**CCAAGGCAGCATCTACTTATT**CTCGAG**AATAAGTAGATGCTGCCTTGG**TTTTT**	3
TRCN0000029262	**CCGG**GTACGCTATGAAACTACAAAT**CTCGAG**ATTTGTAGTTTCATAGCGTAC**TTTTT**	4
TRCN0000029263	**CCGG**CTGGAGCATTTCAGATAAATA**CTCGAG**TATTTATCTGAAATGCTCCAG**TTTTT**	5
SHC005	**CCGG**TACAACAGCCACAACGTCTAT**CTCGAG**ATAGACGTTGTGGCTGTTGTA**TTTTT**	6

5. Analysis of cell viability

The extent of cell injury was evaluated using the 3-(4,5-dimethyl-thiazol-2-yl)-2,5-diphenyl tetrazolium bromide (MTT; Sigma) assay (Hansen et al., 1989). Briefly, cells were seeded in 96 well plates, and 2 h before the end of treatment incubated with 0.5 mg/mL MTT at 37ºC. The

MTT/formazan released from the cells during overnight (ON) incubation at 37ºC with 100 µL extraction buffer (20% sodium dodecyl sulphate [SDS], 50% formamide adjusted to pH 4.7 with 0.02% acetic acid and 0.025 N HCl) was determined. Optical densities were measured at 550 nm using a microplate reader (Bio-Rad, Model 680).

6. Immunoblot

Cells were harvested and lysed in RIPA buffer (50 mM Tris-HCl pH 7.5, 1% Triton X-100, 150 mM NaCl, 1 mM EDTA and 0.1% sodium deoxycholate) containing a protease inhibitor cocktail (Complete Mini, Roche). For tau analysis a phosphatase inhibitor cocktail (PhosSTOP, Roche) was also added. Cell lysates were incubated at 4°C for 30 min and centrifuged at 13,000*g* for 15 min at 4ºC. The protein concentration of the lysates was quantified by the bicinchoninic acid assay (BCA) according to the manufacturer's instructions (Pierce). Cell lysates were mixed with Laemmli loading buffer (25 mM Tris-HCl pH 6.3, 10% glycerol, 2% SDS, 5% beta-mercaptoethanol [β-ME], and 0.01% bromophenol blue) and incubated at 100°C for 4 min. Protein separation was performed using Laemmli discontinuous SDS-polyacrylamide gel electrophoresis with variable acrylamide concentrations of the resolving gel based on the molecular weight of the protein of interest. To define the size of the proteins separated by electrophoresis the molecular weight markers Precision Plus Protein Standards Dual Color (Bio-Rad; 250, 150, 100, 75, 50, 37, 25, 20, 15 and 10 kDa) were loaded. Gels were then transferred by semi-dry (30 min at RT) or wet transfer (ON at 4ºC) to a nitrocellulose membrane with a pore-size of 0.45 µm (Bio-Rad). Total protein stain with Ponceau S was performed to check for transfer efficiency. Membranes were subsequently blocked ON at 4ºC in 3% BSA and 0.2% Tween-20 in phosphate-buffered saline (PBS) and incubated with the primary antibody diluted in PBS, 1% BSA and 0.1% Tween-20. After washing in PBS, 0.05% Tween-20, the blots were incubated with the corresponding horseradish peroxidase (HRP)-coupled secondary antibodies. Alternatively, blots were blocked 1 h at RT in 5% milk and 0.1% Tween-20 in tris-buffered saline (TBS) and incubated with the primary and secondary antibody diluted in TBS, 5% milk and 0.1% Tween-20. All used antibodies and their dilutions are listed in Table 2. Immunodetection was performed using ECL™ Western blotting Detection Reagents according to manufacturer's instructions (GE Healthcare Life Sciences). To quantify the intensity of protein band, densitometric analysis was performed using the Quantity One® Software (Bio-Rad).

7. Immunocytochemistry

Cells grown on coverslips were fixed with 4% formaldehyde for 10 min at RT and washed 3 times with PBS for 5 min. Fixed cells were then permeabilized and blocked ON at 4ºC with a blocking solution containing 0.2% Triton X-100 and 2% horse serum in PBS (pH 7.4), followed by incubation with the corresponding primary antibody (Table 2) for 90 min at RT diluted in blocking

solution. After 3 washing steps in blocking solution for 5 min at RT, cells were incubated with Alexa Fluor-coupled secondary antibodies for 90 min at RT and protected from light. Cells were counterstained with Dapi (5 µg/mL) in PBS for 10 min at RT to visualize the nuclei, followed by 3 more washing steps in PBS. Afterwards, coverslips were washed in water and dehydrated in 100% EtOH. Finally, coverslips were mounted with Mowiol mounting medium (Sigma) on a microscope slide.

Cells were examined using an Axiovert200 or LSM710 confocal microscope (both from Zeiss) and a 63x oil-immersion objective controlled by MetaMorph® 7.10 (Molecular Devices) and ZEN 2010 software (Carl Zeiss Microscopy GmbH), respectively. Images were processed using Adobe Photoshop CS4.

8. Antibodies

8.1. Primary antibodies

All primary antibodies and their dilution factors used are listed in Table 2.

Table 2. Primary antibodies used in this work.

Antigen	Clonality	Host	Dilution		Reference
			WB	IF	
Aβ42	monoclonal	rabbit		1:200	ThermoFisher (H31L21)
c-myc	monoclonal	mouse	1:1,000		Roche (clone 9E10)
CD222	monoclonal	mouse		1:100	BioLegend (315902)
CD63	monoclonal	mouse		1:100	DSHB (H5C6)
EEA1	monoclonal	mouse		1:100	BD Biosciences (610457)
EGFR	monoclonal	mouse	1:500	1:200	Santa Cruz (sc-101)
EGFR	polyclonal	rabbit	1:500	1:100	Santa Cruz (sc-03)
GAPDH	polyclonal	rabbit	1:5,000		Santa cruz (sc-25778)
gC	monoclonal	mouse	1:3,000		Abcam (ab6509)
Human LAMP1	monoclonal	mouse	1:1,000	1:50	DSHB (H4A3)
Murine LAMP1	monoclonal	rat	1:1,000		DSHB (1D4B)
Human LAMP2	monoclonal	mouse	1:1,000	1:50	DSHB (H4B4)
Murine LAMP2	monoclonal	rat	1:1,000	1:400	DSHB (ABL-93)
LC3	polyclonal	rabbit	1:1,000	1:100	MBL (PD014)
p85	monoclonal	mouse	1:1,000		Santa Cruz (sc-56196)
Phospho-tau (thr205)	polyclonal	rabbit	1:1,000	1:50	ThermoFisher (44-738G)
Rab7	monoclonal	rabbit	1:1,000	1:100	Cell Signaling Technology (9367)
Tubulin	monoclonal	mouse	1:20,000		Sigma (clone B-5-1-2)
β-actin	polyclonal	rabbit	1:2,000		Sigma (A2066)

8.2. Secondary antibodies

The secondary antibodies used for immunostaining were HRP-coupled antibodies (Vector; dilution 1:50,000), or antibodies labelled with Alexa Fluor 488 or 555 dyes (Invitrogen; dilution 1:1,000).

9. Viral DNA quantification by real-time quantitative polymerase chain reaction (qPCR)

DNA was extracted using the QIAamp® DNA Mini Kit (QIAGEN) as previously described (Burgos et al., 2006). The concentration of viral DNA was then quantified by qPCR with an ABI Prism 7900HT SD® system (Applied Biosystems) using a custom designed TaqMan probe specific for the *US12* viral gene (5'-AGGCGGCCAGAACC-3'). Viral DNA content was then normalized in terms of human genomic DNA, quantified with a predesigned TaqMan probe specific for the *18S* gene (Applied Biosystems). The quantification results were represented as viral DNA copy numbers per ng of genomic DNA.

10. Quantification of mRNA by reverse transcription followed by real-time PCR (RT-qPCR)

Total RNA was purified with the High Pure RNA Isolation kit according to the manufacturer's instructions (Roche). To determine the RNA quantity, samples were analysed with a NanoDrop® ND-1000 (NanoDrop Technologies). Complementary DNA (cDNA) was obtained from 0.5 μg of RNA by reverse transcription using the High Capacity RNA to cDNA Archive Kit (Applied Biosystems). Real-time PCR was carried out with an ABI Prism 7900HT SD® (Applied Biosystems) using TaqMan assays (in individual or in array format) or specific primers for the genes listed in Table 3. The target-specific primer sequences were designed by using the ProbeFinder Assay Design Software (Roche). Samples were normalized with respect to the value obtained for the *18S* or *GAPDH* gene due to its constant expression.

Table 3. Specific primers and TaqMan assays for real-time PCR.

Gene	Primer	Sequence (5'-3')
Human LAMP2	forward	GCTCGTTCTGGTCTGCCTA
	reverse	TGTCAAATTAAGTTCCAATGCATAA
Human LAMP2B	forward	AAGGGTTCAGCCTTTCAATG
	reverse	CAACTATAATTGGGATTAGAATGGTGT
Murine LAMP2	forward	TGCAGAATGGGAGATGAATTT
	reverse	GGCACTATTCCGGTCATCC

Gene	TaqMan assay ID
18S	Hs99999901_s1
GAPDH	Hs02758991_g1
ATP6AP1	Hs00184593_m1
ATP6V1H	Hs00977530_m1
CTSB	Hs00947433_m1
CTSF	Hs00186901_m1
LAMP2	Hs00174474_m1
LIPA	Hs01548815_m1
NPC1	Hs00264835_m1
NPC2	Hs00197565_m1
CHMP6	Hs00226234_m1

Gene	TaqMan assay ID
GGA2	Hs00370910_m1
GGA3	Hs01597827_m1
MAP1LC3B	Hs00797944_s1
RAB33A	Hs00191243_m1
SNAPIN	Hs00276176_m1
STX18	Hs01099207_m1
UBQLN1	Hs00923840_m1
VAMP3	Hs00922166_m1
VAMP7	Hs00194568_m1
VAMP8	Hs00186809_m1
VTI1B	Hs00762282_s1

11. Measurement of secreted Aβ

For secreted Aβ analysis, conditioned media of N2a and MEF cells were collected and centrifuged at 1,000*g* for 10 min. Viral particles of supernatants were inactivated by ultraviolet irradiation. Because of the lower Aβ levels in conditioned media of MEF cells, those were stored at -80°C and concentrated 5-fold by lyophilization. The media was then assayed for murine Aβ40 and Aβ42 using commercial sandwich enzyme-linked immunosorbent assay (ELISA) kits according to the manufacturer's instructions (WAKO). Briefly, media was added to ELISA plates pre-coated with monoclonal antibodies specific for the murine Aβ (the capture antibody), followed by an antibody specific for the amino acid sequence (amino acids 1-40 or 1-42) of Aβ (the detection antibody) labelled with HRP. The detection antibody bound was quantified measuring the absorbance at 450 nm within 30 min of the completion of the procedure. Values were normalized with the Aβ standard curve and expressed in pg/mL.

12. Quantification of lysosomal cellular content

12.1. Flow cytometry

Lysosomal burden was evaluated using the acidotropic probe LysoSensor® Green DND-189 (LSG; Molecular Probes). This probe freely passes through cell membranes and typically concentrates in acidic organelles. 1 h before the end of treatments, cells were loaded with 0.1 µM LSG for 1 h at 37°C in culture medium. Cells were then washed with PBS and fixed with 2% formaldehyde. After washing twice with PBS, cells were subjected to flow cytometry analysis by counting 10,000 events with a FACS Calibur flow cytometer (BD Biosciences). LSG fluorescence intensity was recorded in the FL-1 channel (530/30 nm) with the CellQuest Pro software (BD Biosciences). Data were analysed using the FlowJo® software.

12.2. Fluorogenic enzyme assay

Lysosomal burden was also evaluated using the acidotropic probe Lysotracker® Red DND-99 (LTR; Molecular Probes). 1 h before the end of treatments, cells were loaded with 1 µM LTR for 1 h at 37°C in culture medium and were then washed with PBS. Cells were lysed with RIPA buffer for 30 min at 4ºC and the lysates were centrifuged at 13,000*g* for 10 min. The protein concentration of the lysates was quantified by the BCA method and the fluorescence of 50 µg of total protein was recorded using a FLUOstar® OPTIMA microplate reader (BMG LABTECH) with excitation at 560 nm and emission at 590 nm.

13. Assessment of lysosomal enzyme activity

13.1. Measurement of cathepsin activities

The enzymatic activity of several cathepsins (CTSs) was determined as previously described with minor modifications (Porter et al., 2013). Briefly, 25-75 µg of protein from cell lysates were incubated for 30 and 60 min in the presence of the following fluorogenic substrates (all from Enzo Life Sciences): Z-VVR-AMC (most sensitive substrate for CTS S; 20 µM), Z-GPR-AMC (specific for CTS K; 20 µM), Z-RR-AMC (specific for CTS B; 20 µM) and CTS D and E fluorogenic substrate (10 µM). These synthetic substrates have a 7-amino-4-methylcoumarin (AMC) tag next to the cleavage site. While attached to the substrates, its fluorescence is quenched. Cleavage of the AMC peptide generates strongly fluorescent AMC that can be monitored fluorimetrically. The fluorescence of AMC released as a result of proteolytic activity was quantified with a microplate reader (Tecan Trading AG) with excitation at 360 nm and emission at 430 nm (Z-VVR-AMC, Z-GPR-AMC and Z-RR-AMC) or with excitation at 320 nm and emission at 400 nm (CTS D and E fluorogenic substrate).

13.2. Measurement of β-hexosaminidase activity

As a substrate for β-hexosaminidase activity, the artificial, chromogenic substrate 4-nitrophenyl-N-acetyl-β-D-glucosaminide was used (Sigma). Briefly, 10 µL of protein lysates were incubated for 60 min with 10 mM substrate in 100 µL assay buffer (0.2 M trisodium citrate pH 4.6, 0.4% BSA, and 0.08% sodium azide) at 37°C. Hydrolysis was stopped by adding 0.5 mL of 0.4 M glycine solution (pH 10.4). Samples were then centrifuged at 16,000*g* for 10 min at RT. The proteolysis of the substrate leads to the generation of 4-nitrophenol, which was determined spectrophotometrically by measuring the absorbance at 405 nm with a microplate reader (Synergy HT from BioTEK). Specific enzymatic activity is expressed as nmol of released 4-nitrophenol per hour and mg protein.

14. EGF receptor degradation assay

HeLa cells were cultured in serum free medium for at least 6 h before the treatments with HSV-1 and X-XOD. After HSV-1 adsorption/X-XOD addition, cells were incubated with medium containing 2% FCS. To stimulate EGF receptor (EGFR) endocytosis, EGF (40 ng/mL) was added at the times indicated in each experiment. Cells were collected at various time points and levels of EGFR analysed by Western blot (see section 6) or immunofluorescence (section 7). For EGFR experiments in SK-N-MC, cells were first transfected with a myc-tagged EGFR expression plasmid (pEGFR-c-myc) using the JetPEI DNA transfection reagent according to the manufacturer's recommendations (Polyplus transfections). Briefly, cells were cultured in P100 dishes until 70% confluency and then transfected by the mixture of 15 µg DNA and 30 µL JetPEI transfection

reagent, both diluted in 150 mM NaCl. The JetPEI/DNA mix was incubated for 25 min at RT and then added dropwise to the dishes with fresh medium. After 24 h, the cells were trypsinized and seeded in 24 well plates for EGF treatment and HSV-1 infection as previously described. After the treatments, levels of EGFR-c-myc in cell lysates were analysed by Western blot using an antibody specific for the myc epitope.

15. Partial purification of lysosomes

The partial purification of lysosomes was performed as previously described with minor modifications (Avrahami et al., 2013). Briefly, cells were washed once in PBS, collected with wash buffer (125 mM KCl, 30 mM Tris pH 7.5, 5 mM MgOAc, 1 mM β-ME) and centrifuged at 800*g* for 5 min. Cells were resuspended in hypotonic buffer (10 mM KCl, 30 mM Tris pH 7.5, 5 mM MgOAc, 1 mM β-ME, protease inhibitor cocktail) and broken with a 23G needle by 15 strokes (fraction F0: total cellular lysate). Homogenates were centrifuged at 1,000*g* for 5 min to precipitate nuclei. The supernatants (nuclei-free lysate: fraction F2) were again centrifuged at 100,000*g* for 1 h at 4ºC. The supernatant was stored (cytosolic fraction F3) and the pellet (membrane fraction including lysosomes: fraction F4) was lysed in RIPA buffer containing protease and phosphatase inhibitors. Protein concentration of the lysates was quantified by the BCA method.

16. Cholesterol quantification

The levels of cellular cholesterol were quantified enzymatically using the Amplex Red Cholesterol Assay kit following the manufacturer's instructions (Invitrogen). This method is based on enzyme-coupled reactions that allow detection of both—free and esterified—cholesterol. In our experiments only free cholesterol was measured (lack of cholesterol esterase in the reaction mix). Free cholesterol is oxidized by the enzyme cholesterol oxidase generating hydrogen peroxide (H_2O_2) and the corresponding ketone product. H_2O_2 is detected by the 10-acetyl-3,7-dihydroxyphenoxazine (Amplex Red reagent). In the presence of HRP, H_2O_2 reacts with Amplex Red to produce the fluorescent compound resorufin, which can then be quantified. To perform the assay, 10 µg of total cell lysates or 5 µg of partially purified lysosome fractions were diluted in Reaction Buffer and incubated with Amplex Red working solution (Amplex Red reagent/HRP/cholesterol oxidase) for 30 min at 37°C. Fluorescence values at an excitation wavelength of 570 nm and an emission wavelength of 585 nm were measured with a microplate reader, normalized to control samples and expressed in percentages.

17. Filipin labelling of membrane cholesterol

To monitor cholesterol by fluorescence microscopy, cells were fixed with 4% formaldehyde, washed with PBS and incubated for 1 h with filipin (50 µg/mL)—a fluorescent

polyene antibiotic that binds free cholesterol. Cells were washed again with PBS and mounted with Mowiol mounting medium on microscope coverslips. Images were taken using an Axiovert200 microscope (Zeiss) with a 63x oil-immersion objective and processed with Adobe Photoshop CS4.

18. Expression microarrays: Gene quantification and functional annotations

18.1. RNA extraction and hybridization to the arrays

Total RNA of SK-N-MC cells was obtained using a commercial kit (High Pure RNA isolation kit from Roche). RNA was then sent to a platform associated with the National Center of Genotyping (GENOMA ESPAÑA) in the Centro de Investigaciones Cardiovasculares (CNIC). Samples were hybridized to a Whole Human Genome Microarray 4x44K (G4112F from Agilent Technologies). Arrays were scanned at 5 μM resolution on an Agilent DNA Microarray scanner (G2565BA from Agilent Technologies) using the default settings for 4x44K format one-color assays. Provided Images were analysed using Feature Extraction software v10.7 (Agilent Technologies).

18.2. Data analysis

Raw signals were thresholded to 1 and quantiles normalization (Bolstad et al., 2003) was performed using the software GeneSpring v11. Data were considered in the log2 scale. Default flags were considered as absent, except saturated points that were flagged as marginal. The following filters were applied: (I) Expression: Genes with at least all replicates in 1 out of 6 conditions of all the samples within the accepted intensity range were retained, (II) Flags: Genes with at least all replicates in 1 out of 6 conditions with the reliable values (Present and Marginal Flags) were retained, and (III) Error: Only those genes that change across the experiment, i.e. with coefficient of variation >1% across all samples were retained. For statistical analysis the limma package (Bioconductor) for differential gene expression was used (Smyth, 2004). It calculates moderated t-statistics, adding to the error term some information on the variance of all genes, solving the typical microarray problem of small size. Those probes with a corrected p-value <0.05 were considered as differentially expressed.

18.3. Functional enrichment of differentially expressed genes by GeneCodis and IPA

Genes that were differentially expressed were uploaded to bioinformatic tools for posterior data mining. Gene annotations co-occurrence discovery (GeneCodis; genecodis.cnb.csic.es) and Ingenuity Pathway Analysis (IPA; Ingenuity® Systems, www.ingenuity.com) were used to identify pathways and functions significantly over- or underrepresented in the gene lists compared with the whole human genome.

19. Genetic association study

19.1. Study subjects

The study sample included 587 patients with sporadic AD (mean age at onset 73 ± 8 years; range 55-109 years; 65% women) who met NINCDS/ADRDA criteria for probable AD (McKhann et al., 1984). All AD cases were defined as sporadic because their family history did not mention any first-degree relative with dementia. AD patients were recruited from the Departments of Neurology of the Hospital La Paz (Madrid, Spain), ISCIII Collection (C.0002965) and the Hospital Marques de Valdecilla (Santander, Spain). Control subjects were 615 unrelated individuals (mean age at examination 77 years ± 9.6 years; range 55-104 years; 67% women). These subjects were free of significant illness and had Mini Mental State Examination scores of 27 or more. The controls arose from the same base population as the cases and both groups were of Caucasian origin. All subjects gave their informed consent to be included in the study, which was approved by the Ethics Committees of the participating institutions.

19.2. Genotyping

Genotyping was performed with predesigned assays (TaqMan SNPs OpenArrays; Applied Biosystems) according to manufacturer instructions and genotypes were assigned with the TaqMan Genotyper Software (Applied Biosystems). Genotypes and allele distributions were compared using the $\chi 2$ test (crude analysis) and in logistic regression models adjusting for age at AD onset, gender and *APOE* genotype. SPSS v.19.0 software was used for all statistical analyses.

19.3. SNP selection

TagSNPs were selected to cover 80% of the variability of the genes of interest (*LAMP2*, *NPC1* and *CTSF*) in the CEU population (Utah residents with Northern and Western European ancestry) included in the HapMap project. The tagSNPs representative of each haplotype block were chosen based on genotyping probe availability (TaqMan assays from Applied Biosystems), minor allele frequency (MAF>5%), linkage disequilibrium (r^2>0.8) and, when possible, predicted functional effect. The SNPinfo tool (https://snpinfo.niehs.nih.gov/cgi-bin/snpinfo/snptag.cgi) was used for the selection. For the *LAMP2* gene, an additional SNP in the promoter region (rs42901) was included based on its potential effect on the binding of transcription factors, although it was represented in the Yoruba but not in the CEU population.

At the end of this work, the tagSNPs originally chosen from the HapMap CEU population were restudied in the Iberian population included in the 1000 Genomes project located in the ENSEMBL server (human genome version GRCh37.p13) (http://www.ensembl.org/Homo_sapiens/Info/Index?db=core). We found no major differences in the haplotype architecture

between the Iberian and CEU populations indicating that the selected tagSNPs were actually valid for our study sample. However, some exceptions were found, like stronger linkage disequilibrium between the LAMP2 SNPs rs7889047 and rs42892 in the Iberian (pairwise r^2 0.62) compared to the CEU population (r^2 0.35), illustrating the possibility that genetic background of AD varies among populations.

Table 4. Basic characteristics of the SNPs analysed in the genetic association study.

Gene Symbol[1] ENSEMBL Gene Code Chromosome	dbSNP ID[2]	Assay ID[3]	Haplotype block[4]	No. of SNPs in the block[5]	MAF in 1000 Genomes[6]
LAMP2 ENSG00000005893 Chr. X	rs7889047	C__34815961_10	1	14	0.37 (0.41)
	rs2283738	C__15959427_10	1	14	0.38 (0.47)
	rs42892	C___2543545_10	2*	9	0.29 (0.45)
	rs42894	C___2256955_10	3**	4	0.21 (0.47)
	rs42901	C___2543554_10	4	1	0.30 (0.50)
CTSF ENSG00000174080 Chr.11	rs4576	C___9575148_10	1	4	0.25 (0.50)
	rs572846	C____926303_10	2	7	0.41 (0.47)
	rs77760653	C_105393089_10	4	nd	0.07 (0.10)
	rs2242663	C__16174621_10	3	1	0.21 (0.80)
NPC1 ENSG00000141458 Chr. 18	rs1805082	C___7490135_10	1	23	0.49 (0.47)
	rs1788799	C___7490119_10	2	8	0.17 (0.35)
	rs1620047	C___7490067_10	3	6	0.44 (0.50)
MAP1LC3B ENSG00000140941 Chr. 16	rs11117269	C___2849677_10	NA	NA	0.16 (0.50)
SORL1 ENSG00000137642 Chr. 11	rs668387	C____638456_10	NA	NA	0.42 (0.73)
	rs12364988	C__31696838_10	NA	NA	0.44 (0.50)
UBC ENSG00000150991 Chr. 12	rs13624	C__11348775_20	NA	NA	0.49 (1.00)

1. Official Gene symbol and Code of the gene (ENSEMBL, human genome version hGCR37.p13).
2, 3. Identification of the SNPs in the dbSNP database (2) and corresponding TaqMan genotyping assay code in Applied Biosystems (3).
4. Haplotype blocks were defined with a pairwise r^2 cut-off of 0.8 in the CEU population.
5. Number of SNPs with a minor allele frequency (MAF) higher than 0.05 in the haplotype block.
6. Frequency of the minor allele (MAF) in the 1000 Genomes project (human genome version GRCh37.p13). The mean and, in parenthesis, the maximum MAF for the different populations included in the project.
*partially linked to block 1 and ** to block 4 in Iberian population (r^2 0.63 and r^2 0.56, respectively).
NA: not applicable; nd: not determined

20. Generation of induced pluripotent stem cells (iPSCs)

Procedures for sample collection and iPSC line generation were approved by the Institutional Ethics Committee (Hospital Universitario La Paz and Universidad Autónoma de Madrid) and informed consent was obtained from the patients.

20.1. Cell culture media

20.1.1. Fibroblast medium

DMEM supplemented with 10% fetal bovine serum (FBS) HyClone, 2 mM GlutaMAX, 50 mg/mL gentamycin, and 0.1 mM NEAAs. Media was stored at 4ºC in the dark and used within 1 month.

20.1.2. MEFs medium

Iscove's Modified Dulbecco's Medium (IMDM) supplemented with 10% FCS, 2 mM glutamine and 50 mg/mL gentamycin. Media was stored at 4ºC in the dark and used within 1 month.

20.1.3. iPSC medium

KnockOut DMEM supplemented with 10% KnockOut Serum Replacement, 0.5% human serum albumin (HSA), 2 mM GlutaMAX, 50 mg/mL gentamycin, 0.1 mM of each NEAA, 55 µM β-ME, 100 µg/mL basic fibroblast growth factor (bFGF). Medium was filtered through a 0.22 µM filter, stored at 4ºC in the dark and used for up to 1 week.

20.2. Establishing primary cell cultures from patient biopsies

A 6 mm skin punch biopsy was obtained by a trained physician from the inner side of the forearm from an AD patient and an age-matched control. The skin specimens were placed in a 50 mL conical tube containing ~25 mL of sterile complete fibroblast media at RT for shipment to the laboratory and stored ON. Within 24 h, the biopsy specimens were cut using sterile forceps and scissors into 20-30 pieces of ~1-3 mm size. The pieces were then transferred onto the surface of a T25 flask and incubated with complete fibroblast media at 37ºC, 5% CO_2 for 14 days. Medium was changed twice a week. After 21-28 days, human dermal fibroblasts (HDFs) were passaged and frozen at passage 2 in freezing media (90% FCS, 10% DMSO) ON at -80ºC using a cryo 1ºC-freezing container, before transferring the frozen vials to liquid N_2 for long-term storage.

20.3. Generation of a stock of irradiated mouse embryonic fibroblasts

MEF cells from 12 x P150 dishes were harvested and centrifuged at 800*g* for 5 min at RT. The cells were then resuspended in fresh MEF medium and irradiated at 80 Grays. Subsequently,

irradiated cells were centrifuged at 800*g* for 5 min at RT and frozen in freezing media as previously described.

20.4. Sendai viral transduction of fibroblasts and generation of iPSCs

HDFs were collected and cultured from a patient and an age-matched control as described previously in section 20.2. iPSCs were generated using integration-free CytoTune®-iPS 2.0 Sendai Reprogramming Kit including Sendai virus particles expressing the four Yamanaka factors OCT4, SOX2, KLF4, and cMYC according to the manufacturer's protocol (Invitrogen). Briefly, 2.5 x 10^5 HDFs were plated onto one well of a 6 well plate. In a single reprogramming experiment each of the Sendai viruses was used to transduce the cells (Table 5) (KOS Moi=5, cMYC Moi=5, KLF4 Moi=3). Seven days after transduction, cells were plated in P100 dishes onto irradiated MEF feeder cells, and fed with iPSC medium. 2-3 weeks post-transduction the colonies were selected by its morphology and TRA1-60 live staining and picked for expansion into individual iPSC lines. Once a week, each iPSC line was mechanically passaged using a Stripper micropipette (Origio) with 150 μm capillaries (Genetics).

Table 5. CytoTune 2.0 reprogramming vectors.

CytoTune Sendai vector	Factor	GenBank ID	Moi
KOS	human KLF4 human OCT3/4 human SOX2	BC029923.1 NM_002701.4 NM_003106.2	5
hcMYC	human cMYC	K02276.1	5
hKLF4	human KLF4	BC029923.1	3

21. Characterization of iPSC lines

21.1. Alkaline phosphatase staining

This assay is based on the reaction of two components—bromochloroindolyl phosphate (BCIP) and nitro blue tetrazolium (NBT). In the presence of alkaline phosphatase (AP) a bluish-purple product is produced. For AP staining, cells must be fixed and cannot be maintained in culture afterwards. Therefore, during weekly splitting, a few iPSC colonies (3-4) were seeded in 6 well plates on irradiated MEFs and grown for approximately 5-6 days. Phase contrast images of the colonies were taken before the staining. Then, cells were fixed for 2 min with formalin at RT and washed twice with PBS. To heat-inactivate endogenous AP from MEFs, cells were incubated with pre-warmed PBS for 20 min at 64ºC. Then, AP staining was performed with Alkaline Phosphatase Blue Membrane Substrate Solution according to manufacturer's instructions (Sigma). Cells were washed again to eliminate remaining AP staining solution, and phase contrast images of the same iPSC colonies were taken with a standard microscope (magnification: 4x or 10x).

21.2. TRA1-60 live staining

To select colonies expressing TRA1-60, primary (anti-TRA1-60, 1:300) and secondary (anti-mouse IgM Alexa Fluor 555, 1:200) antibodies diluted in iPSC media were added to the cells (3 mL per 100 mm dish) and incubated for 1 h at 37ºC. To remove any unbound antibodies, cells were washed once with PBS and incubated with fresh media for 15 min at 37ºC. Cells were then visualized under a standard fluorescent microscope. TRA1-60 positive colonies were selected for expansion.

21.3. Immunofluorescence analysis

To confirm the pluripotency of iPSC colonies by immunostaining, 3-4 colonies were seeded on irradiated MEFs in each well of a chambered coverslip (Ibidi). After 7 days, colonies were fixed in 4% formaldehyde for 30 min, permeabilized and blocked with buffer containing 0.3% Triton X-100 and 3% donkey serum in PBS for 1 h. Cells were then incubated with the appropriate primary antibodies listed in Table 6. Then, incubation with the appropriate Alexa Fluor 488-, 555- or 647-labeled secondary antibodies (dilution 1:200) was performed for 2 h. Nuclei were counterstained with Dapi. Images were taken with a 25x oil-immersion objective using a Zeiss LSM 710 confocal microscope.

Table 6. Primary and secondary antibodies used for immunocytochemistry of iPSC colonies.

Primary Antibody	Host	Dilution	Source	Reference
NANOG	goat	1:25	R&D	AF1997
OCT4	mouse	1:60	Santa Cruz	sc-5279
SOX2	rabbit	1:100	Thermo Scientific	PA1-16968
SSEA3	rat	1:15	DSHB	MC-631
SSEA4	mouse	1:15	DSHB	MC-813-70
TRA1-60	mouse	1:200	Millipore	MAB4360
TRA1-81	mouse	1:200	Millipore	MAB4381

Secondary Antibody	Host	Dilution	Source	Reference
Cy3 IgG	mouse	1:200	ThermoFischer	A31572
Cy2 IgM	rat	1:200	Life Technologies	A21212
Cy2 IgG	rabbit	1:200	ThermoFischer	A21206
Cy5 IgM	mouse	1:200	Life Technologies	A21238
Cy5 IgG	goat	1:200	ThermoFischer	A21447
Cy3 IgM	mouse	1:200	Jackson ImmunoResearch Laboratories	715-165-140

21.4. RT-qPCR analysis

Total RNA was isolated using TRIZOL reagent and was then sent to the Genomic Unit of the Fundación Parque Científico from Madrid. Briefly, 250 ng of RNA was used to synthesize cDNA using the High capacity RNA to cDNA kit (Applied Biosystems). Each cDNA sample was amplified using SYBR Green Mix on the thermocycler LightCycler 480 (Roche). Primer sequences are shown in Table 7. All the expression values were normalized to the *GAPDH* housekeeping gene.

Table 7. Human iPSC real-time PCR primers.

Oligo name	Primer	Sequence (5'-3')	Marker
OCT4	forward	GGAGGAAGCTGACAACAATGAAA	Undifferentiated ES cell
	reverse	GGCCTGCACGAGGGTTT	
SOX2	forward	TGCGAGCGCTGCACAT	Undifferentiated ES cell
	reverse	TCATGAGCGTCTTGGTTTTCC	
NANOG	forward	ACAACTGGCCGAAGAATAGCA	Undifferentiated ES cell
	reverse	GGTTCCCAGTCGGGTTCAC	
CRIPTO	forward	CGGAACTGTGAGCACGATGT	Undifferentiated ES cell
	reverse	GGGCAGCCAGGTGTCATG	
REX1	forward	CCTGCAGGCGGAAATAGAAC	Undifferentiated ES cell
	reverse	GCACACATAGCCATCACATAAGG	
KLF4	forward	CGAACCCACACAGGTGAGAA	Undifferentiated ES cell
	reverse	GAGCGGGCGAATTTCCAT	
CMYC	forward	AGGGTCAAGTTGGACAGTGTCA	Undifferentiated ES cell
	reverse	TGGTGCATTTTCGGTTGTTG	
TBX5	forward	ATGTCAAGAATGCAAAGTAAAGAATATCC	Cardiomyocyte markers
	reverse	GACTCGCTGCTGAAAGGACTGT	
MEF2C	forward	CTGGCAACAGCAACACCTACA	Cardiomyocyte markers
	reverse	GCTAGTGCAAGCTCCCAACTG	
FOXA2	forward	CTGAAGCCGGAACACCACTAC	Endoderm
	reverse	CGAGGACATGAGGTTGTTGATG	
HNF4	forward	CTGCAGGCTCAAGAAATGCTT	Mesoderm
	reverse	TCATTCTGGACGGCTTCCTT	
SOX17	forward	TGGCGCAGCAGAATCCA	Endoderm
	reverse	CCACGACTTGCCCAGCAT	
TUBB3	forward	GGCCAAGTTCTGGGAAGTCA	Ectoderm
	reverse	CGAGTCGCCCACGTAGTTG	
PAX6	forward	GCTTCACCATGGCAAATAACC	Ectoderm
	reverse	GGCAGCATGCAGGAGTATGA	
GAPDH	forward	GCACCGTCAAGGCTGAGAAC	Housekeeping
	reverse	AGGGATCTCGCTCCTGGAA	

22. Statistical analysis

Graph values are expressed as mean ± standard error of the mean (SEM) or standard deviation (SD). Unless otherwise indicated in specific experiments, differences between groups were analysed using the 2-tailed Student *t* test. Significance was recorded as *$p<0.05$; **$p<0.01$; ***$p<0.001$.

RESULTS

1. Differential gene expression studies after X-XOD treatment in cell models of sporadic and familial AD suggest alterations of the lysosomal pathway

Chronic infections of the CNS and oxidative stress associated with aging are important factors in the pathogenesis of AD (Harris et al., 2015; Persson et al., 2014). Herpes viruses are pathogens with high prevalence in the population and HSV-1 infection has been associated with SAD (Itzhaki, 2014). To study the impact of HSV-1 infection and oxidative stress on gene expression and identify putative genes or/and pathways associated with AD pathogenesis, a microarray analysis was performed in human neuroblastoma cells. To mimic the situation of endogenous infection in AD brains, a cell model of HSV-1 infection at a low viral dose in the presence of mild oxidative stress was developed. SK-N-MC cells were infected with HSV-1 for 24 and 36 hours in the presence and absence of oxidative stress induced by X-XOD. Thus, four conditions were finally established: untreated cells (mock), cells subjected to oxidative stress (X-XOD), cells infected with HSV-1 at a moi of 0.1 pfu/cell (HSV-1) and cells infected with HSV-1 and subjected to oxidative stress (HSV-1+X-XOD) (Figure 6). The microarray analysis of a monogenic cell model for FAD (SK-APP_{Swe}) exposed to OS for 24 and 36 hours was also included. This model was generated in-house and consists of SK-N-MC cells stably transfected with human APP695 harbouring a double mutation (K670N/M671L) known as the Swedish mutation. The name makes reference to its identification in two large Swedish families with early-onset FAD (Mullan et al., 1992).

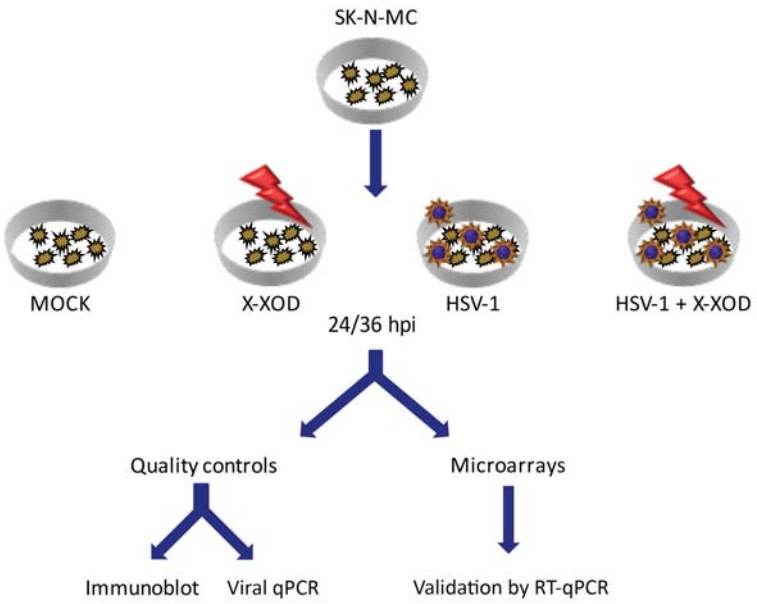

Figure 6. Work scheme overview of microarray analysis.
SK-N-MC cells were infected with HSV-1 at a moi of 0.1 pfu/cell for 24 or 36 hours in the presence or absence of X-XOD. Samples were then prepared for quality control assays and microarray analysis. Some of the microarray data were afterwards validated by RT-qPCR.

1.1. Quality control of samples

Before the samples were processed for microarray analysis their quality must be confirmed. To ensure correct HSV-1 infection and X-XOD treatment, cells were harvested and samples prepared for two different quality control assays: (1) Immunoblot of viral and apoptosis-associated proteins and (2) viral qPCR. For each time point, at least three independent experiments were performed.

The X-XOD system represents a free radical-generating system inducing apoptotic cell death and was first described in cerebellar granule neuronal cultures via ROS production (Fatokun et al., 2007). Our laboratory established a model of mild oxidative stress induced by X-XOD in human neuroblastoma cells which was used in this work (Recuero et al., 2009). To validate the apoptosis induced by X-XOD, Western blot analyses with the anti-p85 antibody were performed. Cleavage of poly ADP-ribose polymerase (PARP) by caspases is a fairly early event in apoptosis and the level of p85 fragment is a common apoptotic marker. As shown in Figure 7A lower panel, p85 was not detected in mock (24 hpi) and slightly increased in X-XOD (24 hpi), mock (36 hpi) and HSV-1 infected cells (24 and 36 hpi) indicating a low level of apoptosis in these conditions. However, oxidative stress induced a strong increase of p85 levels after 36 hours of X-XOD treatment indicating an induction of apoptosis at this time-point. The simultaneous infection with HSV-1 did not show any influence on the amount of p85 at 24 hpi but p85 levels were reduced compared to that observed in X-XOD treated cells at 36 hpi. These data are in agreement with the capacity of HSV-1 to block the apoptotic process induced by different stimuli (Aubert et al., 2001; Jerome et al., 2001). The results confirm an efficient induction of apoptosis by the X-XOD system.

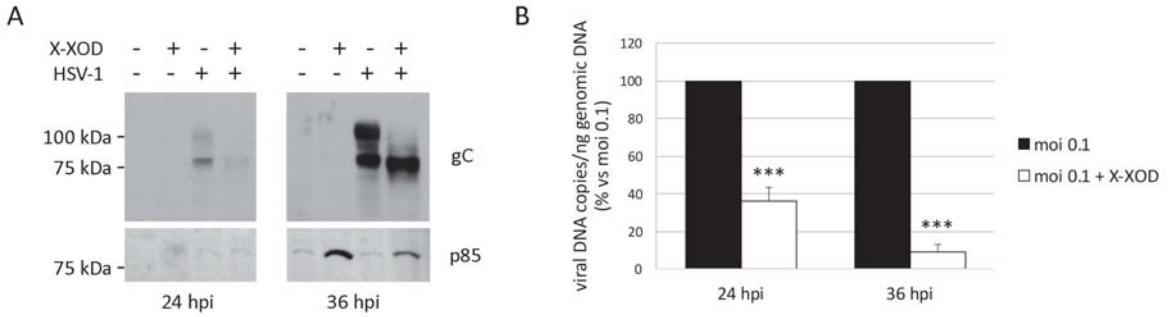

Figure 7. Validation of apoptosis and HSV-1 infection.
Cells were infected with HSV-1 at a moi of 0.1 pfu/cell for 24 and 36 hours in the presence and absence of X-XOD. (A) Western blot analysis was performed to quantify the amount of the p85 fragment. HSV-1 infection was detected by Western blot using an anti-gC antibody. The blots are representative of three independent experiments. (B) Efficiency of HSV-1 infection was quantified by qPCR. The mean ± SEM of 3 independent experiments are shown (***p<0.001).

To check the efficiency of HSV-1 infection, the level of the late viral glycoprotein gC was monitored. Western blots were performed using the anti-gC antibody. Figure 7 shows that all mock and X-XOD samples were virus-free, whereas HSV-1 infected cell lysates presented a pattern of bands corresponding to the differently glycosylated gC. The gC levels were dependent on time of infection. When the cells additionally were exposed to X-XOD a strong decrease of the gC levels was observed, particularly the highly glycosylated forms of the protein (Figure 7A upper panel).

Another method to confirm the efficiency of HSV-1 infection is the quantification of viral DNA by qPCR. As expected, non-infected samples (mock and X-XOD) did not contain any viral DNA. HSV-1 infected cells for 24 and 36 hours presented high amounts of viral DNA (absolute values: $2.15x10^5$ [24 hpi] and $1.52x10^6$ [36 hpi] viral DNA copies per ng genomic DNA). X-XOD treatment significantly reduced the levels of viral DNA at both time points (24 hpi: 63% of reduction; 36 hpi: 91% of reduction [mean of three independent experiments]) (Figure 7B). This interaction between HSV-1 infection and OS has been extensively studied in SK-N-MC cells by our group showing that OS inhibits the generation of infectious viral particles and protects against cell death induced by the virus (Santana et al., 2013).

Taken together, these results showed that HSV-1 infection and X-XOD treatment were efficient, all mock and X-XOD treated samples were virus-free and OS interacts with HSV-1 infection causing a strong inhibition of infection revealed by a diminution of viral protein and viral DNA levels. Thus, the samples obtained are adequate to perform differential gene expression analysis by microarrays.

1.2. Microarray gene expression studies of our cell models

Total RNAs from the samples were obtained and the gene expression was analysed by microarrays covering the whole human genome. Compared to uninfected cells, 833 genes were modulated by OS in the infection cell model (HSV-1) and 158 genes in the monogenic cell model ($SK\text{-}APP_{Swe}$) at 24 hpi (Figure 8) but not in the respective controls. In order to identify a common pathogenic mechanism for both models—sporadic and familial AD—the focus was set on those genes regulated by OS in the infection and monogenic cell models. This approach let to a list of 68 differently expressed genes using a p-value cut-off of 0.05 (for complete list of genes see Annex I).

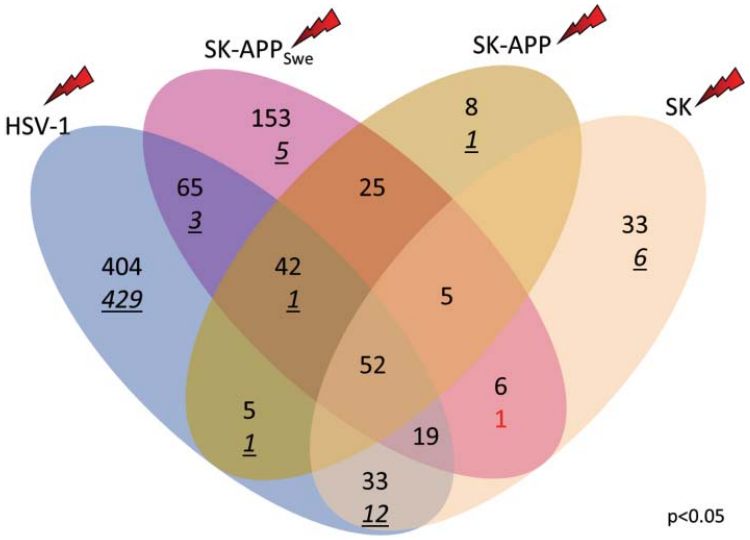

Figure 8. Genes modulated by differential gene expression analyses.
Venn diagram showing the number of genes differently expressed by OS in each condition at 24 hours post-treatment. SK: Parental SK-N-MC cells; HSV-1: SK-N-MC cells infected with HSV-1 at 0.1 pfu/cell; SK-APP$_{Swe}$: SK-N-MC cells stably transfected with the 695 isoform of human APP carrying the Swedish mutation; SK-APP: SK-N-MC cells stably transfected with the wild type 695 isoform of human APP. Number of upregulated genes is written in bold and downregulated ones underlined. The figure shows the amount of genes that are exclusively regulated by one condition or shared by two or all conditions. Red lightning symbol stands for OS (X-XOD treatment). 0: upregulated; *0*: downregulated; **0**: contraregulated.

In the list of genes modulated by OS, 65 genes were found to be significantly overexpressed (fold change [FC]>1.5) and 3 significantly repressed (FC<0.67). To study the pathways associated with differently expressed genes the Gene Annotations Co-occurrence Discovery (GeneCodis) software was used (Carmona-Saez et al., 2007; Nogales-Cadenas et al., 2009; Tabas-Madrid et al., 2012). Significant enrichment of the Kyoto Encyclopedia of Genes and Genomes (KEGG) pathway 04142: "Lysosome", in the list of overexpressed genes was noted (Figure 9). Five genes of those 68, namely cathepsin F (*CTSF*); lipase A, lysosomal acid, cholesterol esterase (*LIPA*); ATPase, H+ transporting, lysosomal accessory protein 1 (*ATP6AP1*); Niemann-Pick disease, type C1 (*NPC1*); and lysosomal-associated membrane protein 2 (*LAMP2*), were annotated to the lysosomal pathway.

To confirm the results obtained from GeneCodis, the same gene list was analysed with another software. Running the core analysis of the Ingenuity Pathway Analysis (IPA) software, we obtained as the top annotated Diseases & Functions the "lysosomal storage disease", and then "metabolism of sterols" (with a p-value of 1,42E-05 and 4,78E-05, respectively). These results reproduce the findings obtained with the GeneCodis analysis identifying the lysosome as the main altered pathway and further indicating an alteration of lipid metabolism.

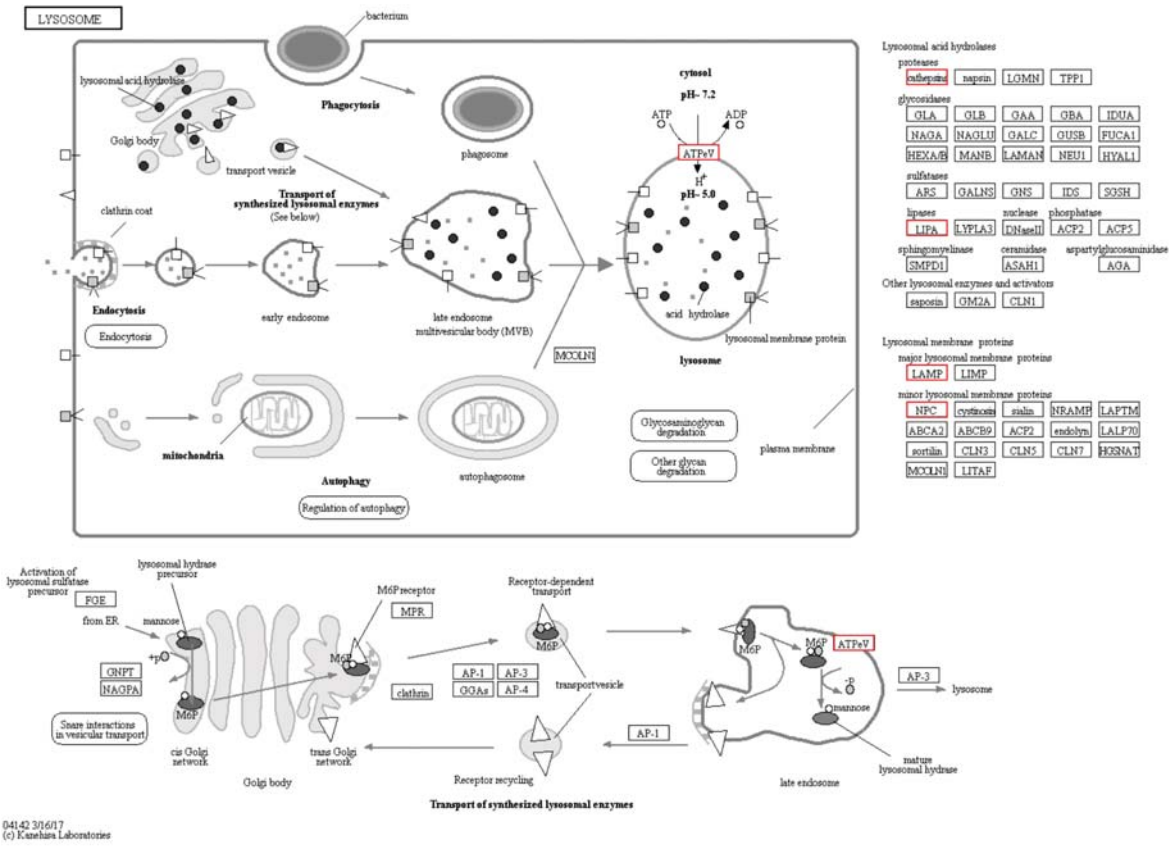

Figure 9. Genes showing altered expression in the KEGG pathway 4142: Lysosome.
Gene enrichment analyses of microarray expression data revealed significant annotation of OS-modulated genes in the infection and monogenic cell models to the lysosomal pathway. The annotated genes from our dataset are highlighted in red: the two lysosomal hydrolases cathepsin F (*CTS F*) and lipase A, lysosomal acid, cholesterol esterase (*LIPA*); the major lysosomal membrane protein *LAMP2*; the subunit of the V-ATPase: ATPase, H+ transporting, lysosomal accessory protein 1 (*ATP6AP1*); and the minor lysosomal membrane protein Niemann-Pick disease, type C1 (*NPC1*). Image from www.genome.jp.

1.3. Validation of microarray results by RT-qPCR

To confirm the microarray data, an independent gene expression profiling method is required. Quality control is crucial and diverse confirmation methods such as RT-PCR, northern blot, or *in situ* hybridization are valid depending on the type of experiment. RT-PCR is the method of choice for most researchers because of its high sensitivity. Briefly, SK-N-MC cells were grown on P100 plates and the same conditions as in microarray analysis were established: mock cells, cells treated with X-XOD, cells infected with HSV-1 and cells infected with HSV-1 and treated with X-XOD (Figure 6). We decided to analyse the expression of 20 selected genes because of their functional involvement in two KEGG pathways associated with the lysosome: (i) the lysosomal pathway (KEGG no. 4142; Figure 9) and (ii) the SNARE interactions in vesicular transport pathway (KEGG no. 4130). The expression values obtained for the genes of the lysosomal pathway at 24 and 36 hours modulated by either one of the conditions alone or in combination are shown in Figure 10. All 5 genes annotated to the lysosomal pathway showed the

same direction in expression levels as the microarray results. As can be observed in the figure, all the genes—except CTSB—were upregulated by X-XOD treatment in infected and uninfected cells, suggesting that the lysosomal pathway was mainly regulated by OS in our cells. However, gene expression continued growing at 36 h compared with 24 h in non-infected cells, whereas this increase did not appear in infected cells, suggesting that HSV-1 and OS actually interact in the regulation of the lysosomal pathway. These results pushed our interest to perform a functional analysis of this pathway in our cell model of neurodegeneration.

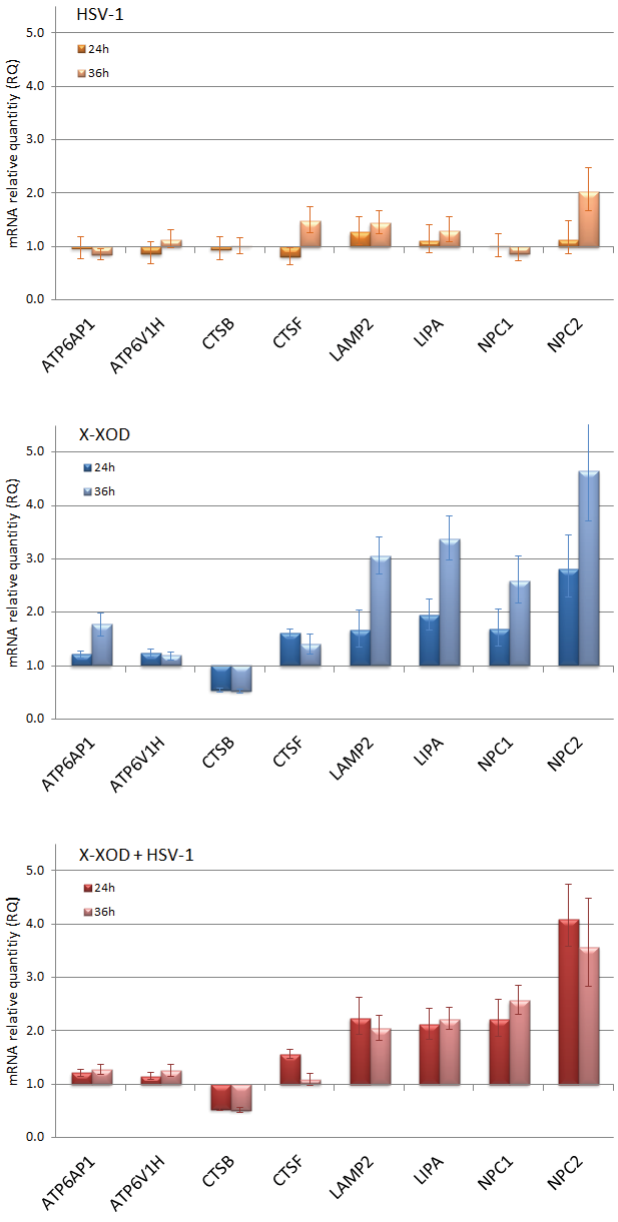

Figure 10. Validation of expression microarray data for the genes of the lysosomal pathway.
SK-N-MC cells were infected with HSV-1 at a moi of 0.1 pfu/cell for 24 and 36 hours in the presence and absence of X-XOD. The mRNA transcribed from each gene was quantified by RT-qPCR as described in Methods, and normalized in terms of the GAPDH mRNA levels. The relative quantity with respect to control cultures was determined by the $\Delta\Delta C_t$ method using the RQ manager 1.2.1. software (Applied Biosystems). Error bars represent the 95% confidence interval.

2. HSV-1 infection and OS alter the lysosomal pathway in SK-N-MC cells

Gene expression microarray data of oxidative stress treated samples in two cell models (infection and monogenic model) revealed a significant annotation of the lysosomal pathway. Therefore, we decided to study different aspects of this pathway in our cell models with the aim of investigating possible alterations induced by HSV-1 and OS. Previous work by our group reported that the highest effect on neurodegenerative events provoked by HSV-1 and OS is achieved with a moi of 10 pfu/cell for 18 hours. These conditions ensure that almost all cells are infected and are therefore set as the standard ones in the following experiments.

2.1. HSV-1 and OS increase lysosomal content

In this first part, we evaluated the effect of HSV-1 and OS on lysosomal content. SK-N-MC cells were exposed to HSV-1 and OS and the samples analysed by Western blot using specific antibodies for several markers of the endo-lysosomal system. Rab7 and LAMP1 and 2 are known as specific markers for late endosomes and lysosomes, respectively. HSV-1 infection and OS increased the amount of Rab7, LAMP1 and LAMP2 proteins compared to untreated cells. However, the combination of both treatments showed no synergistic effect (Figure 11).

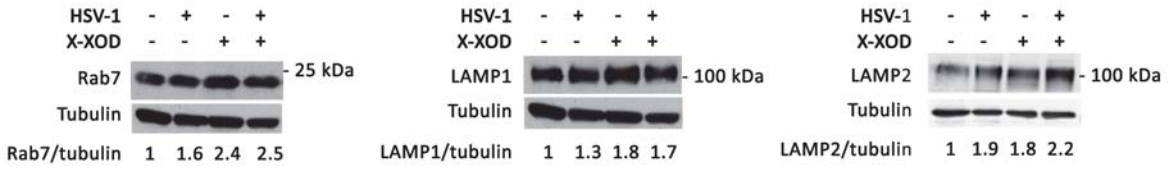

Figure 11. HSV-1 infection and OS increase the protein levels of endo-lysosomal markers.
Western blot analysis, using specific antibodies for Rab7, LAMP1 and LAMP2 proteins, of SK-N-MC cells infected with HSV-1 at a moi of 10 pfu/cell for 18 hours in the absence or presence of X-XOD. A representative experiment of four performed is shown. As a control for equal loading tubulin blots are also shown. The ratios of protein of interest to tubulin are presented below each blot.

Next, we decided to measure the effect of HSV-1 and OS on cellular lysosomal content with lysosomotropic dyes. These probes selectively accumulate in cellular compartments with low internal pH. LysoSensor Green DND 189 (LSG) is a pH sensitive probe that exhibits an increase or decrease in fluorescence intensity upon intracellular acidification or alkalinisation, respectively. LSG quantification by flow cytometry showed a significant increase of fluorescence intensity in HSV-1 infected cells (Figure 12A and B), whereas OS had no effect on LSG fluorescence. The use of the lysosomal inhibitor ammonium chloride—a weak base that alkalinizes the lysosome—and nutrient starvation—as a positive control to increase lysosomal content—confirmed the specificity of the assay (Figure 12C). These first results indicate that HSV-1 infection leads to an increased number of lysosomes.

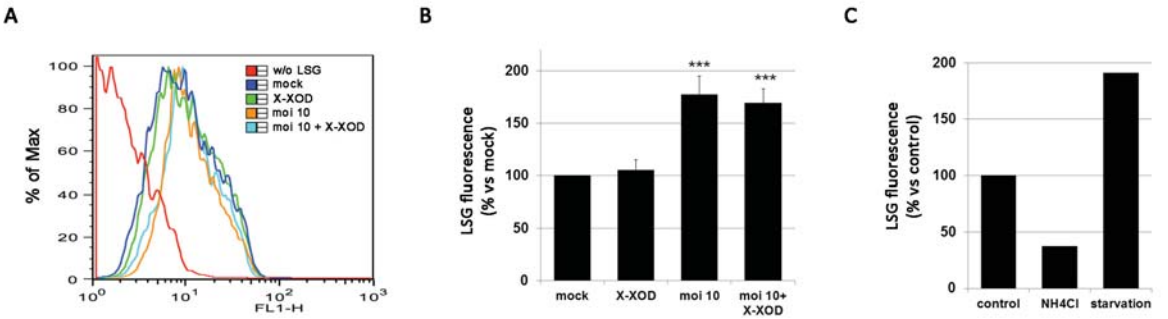

Figure 12. HSV-1 infection increases cellular lysosomal content.
SK-N-MC cells were infected at a moi of 10 pfu/cell for 18 hours in the presence or absence of X-XOD. One hour before the end of the treatments, cells were loaded with LysoSensor Green DND 189 (LSG). Fluorescence was quantified by flow cytometry in the green (FL-1 channel). (A) Representative image by flow cytometry of LSG staining. (B) Fluorescence measurements of LSG intensity. Graphs represent the mean ± SEM of five experiments and are represented in percentage with respect to mock cells (***p<0.001). (C) To validate the assay, cells were exposed to ammonium chloride (NH_4Cl) and nutrient starvation and LSG fluorescence was quantified.

To confirm the increase of the lysosomal burden in infected cells, we measured the fluorescence of LysoTracker Red (LTR) with a microplate reader. As LSG, LTR is a lysosomotropic dye, however its fluorescence is independent of pH. As shown in Figure 13A, HSV-1 infection significantly increased the LTR intensity, confirming the increment of cellular lysosomal content provoked by the virus. In contrast with LSG data, cultures subjected to OS also showed a strong and significant increase in LTR fluorescence indicating that OS enhances the lysosomal burden but could be affecting the lysosome acidity. We did not observe a synergistic effect when cells were cultivated in the presence of both factors. Again, bafilomycin A1—a specific V-ATPase inhibitor that increases lysosomal pH—and nutrient starvation—to increase lysosomal content—were used to confirm the specificity of the assay (Figure 13B). Taken together, these results suggest that HSV-1 infection and OS lead to an increase of lysosomal content in SK-N-MC cells. In addition, these results are consistent with the microarray data indicating that the increase of the expression of lysosomal genes induced by HSV-1 and OS is translated into an increment of endo-lysosomal protein levels and lysosomal burden.

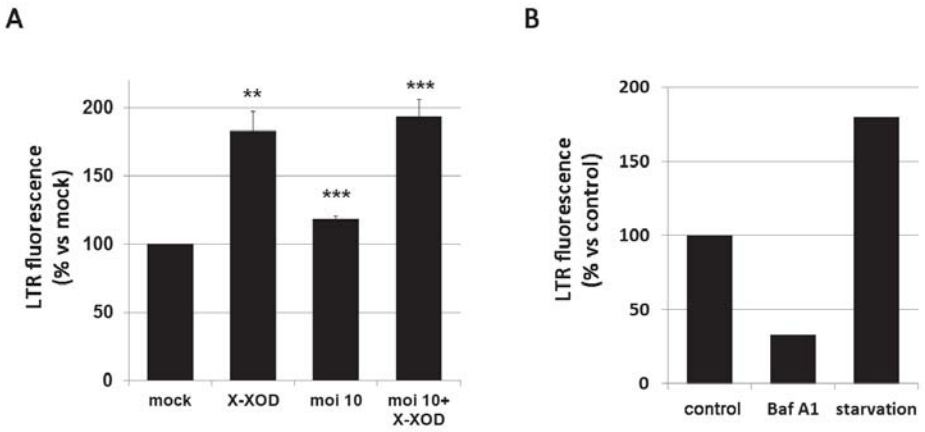

Figure 13. HSV-1 infection increases cellular lysosomal content.
SK-N-MC cells were infected at a moi of 10 pfu/cell for 18 hours in the presence or absence of X-XOD. One hour before the end of the treatments cells were loaded with LysoTracker Red (LTR). (A) LTR fluorescence was recorded with a microplate reader. Graphs represent the percentage compared with untreated cells. Data are the mean ± SEM, n=5 (**p<0.01, ***p<0.001). (B) To validate the assay, cells were exposed to bafilomycin A1 (Baf A1) or nutrient starvation.

2.2. HSV-1 and OS reduce the activity of lysosomal enzymes

Given the increased lysosomal burden observed in HSV-1 infected cells, we then evaluated the lysosomal activity. With this aim, the enzymatic activity of several lysosomal CTSs was quantified. CTSs are abundant lysosomal endopeptidases that catalyse the hydrolysis of a variety of substrates. CTS D and E are aspartic proteases whereas CTS B, K and S are cysteine proteases. In these studies, fluorogenic substrates specific for each of these CTSs were used. As shown in Figure 14, infection with HSV-1 reduced the activity of all studied CTS. Cultures treated with OS showed reduced activity in mock and HSV-1 infected samples. The reduction of activity provoked by OS is stronger than that observed in infected cells. No synergistic effect was seen with the combined treatment.

To confirm the lysosomal dysfunction induced by HSV-1 and OS, the activity of β-hexosaminidase—another lysosomal hydrolase—was assessed. Consistent with the results obtained with CTSs, HSV-1 infection reduced its activity in a dose-dependent manner, just as X-XOD treatment minimized its activity to a minimum (in mock and HSV-1 infected cells) (Figure 14B). These results revealed severely altered proteolytic activity of lysosomes in HSV-1 infected and OS treated SK-N-MC cells.

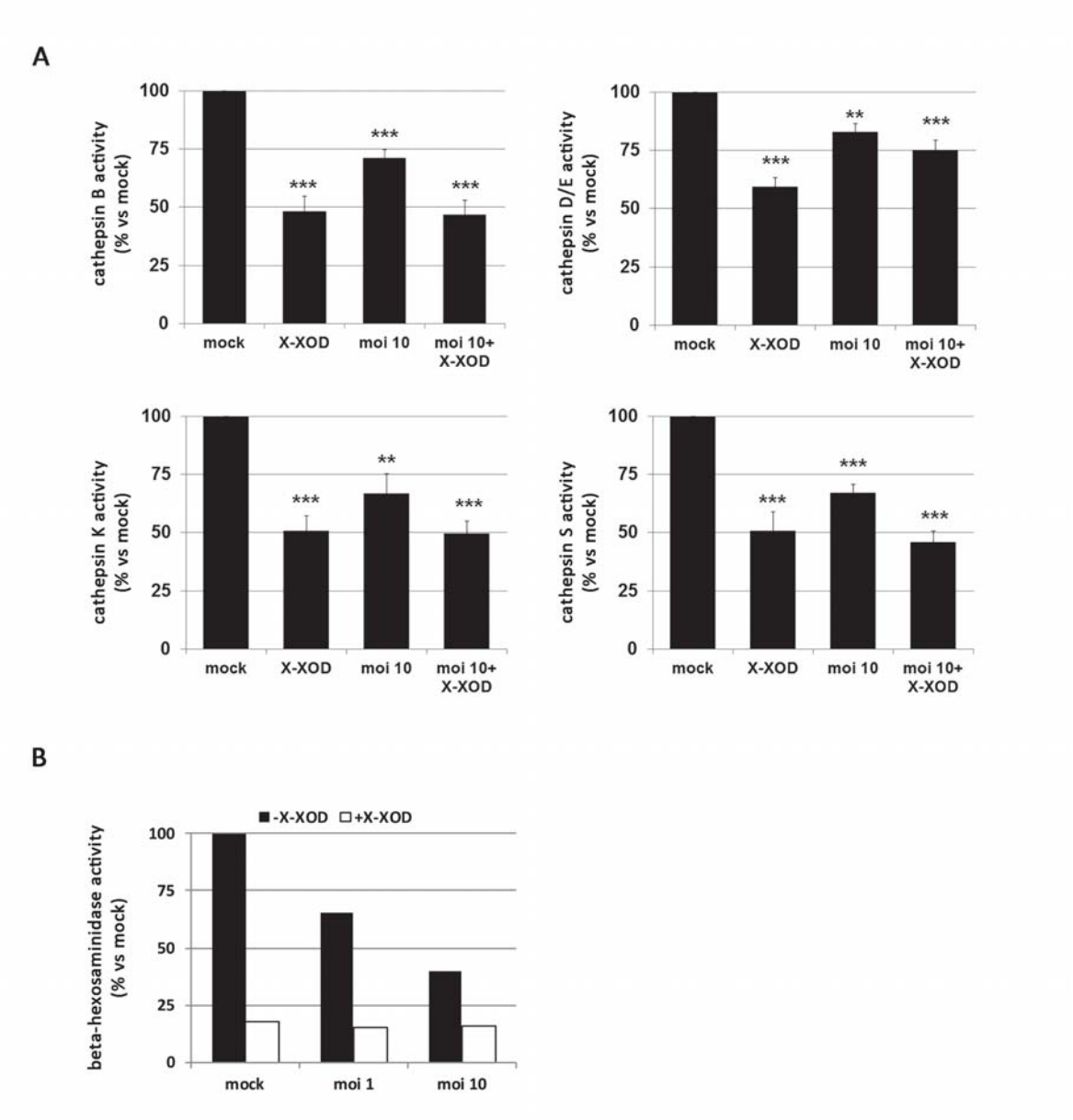

Figure 14. HSV-1 and OS induce a reduction of lysosomal enzyme activity.
(A) SK-N-MC cells were exposed to HSV-1 (moi 10) and X-XOD for 18 hours. The relative enzymatic activities (compared with mock cells) of cathepsins B, D/E, K and S were quantified and normalized by the protein content of the lysates. Data are the mean ± SEM of at least four experiments (**p<0.01, ***p<0.001). (B) SK-N-MC cells were HSV-1 infected (moi 1 and moi 10) for 18 hours in the presence/absence of X-XOD. The relative enzymatic activity with respect to mock cells of the lysosomal hydrolase β-hexosaminidase was determined in a representative experiment of two performed.

For the microarray analysis, SK-N-MC cells were infected with a lower dose of HSV-1 (moi of 0.1 pfu/cell for 24 and 36 hours) in the presence of a mild oxidative stress to mimic more likely the physiological conditions of natural infection. These analyses revealed that the main pathway altered was the lysosomal system. To confirm that the impairment of lysosomal function also takes place in cells treated at the same conditions as of microarray experiments, the amount

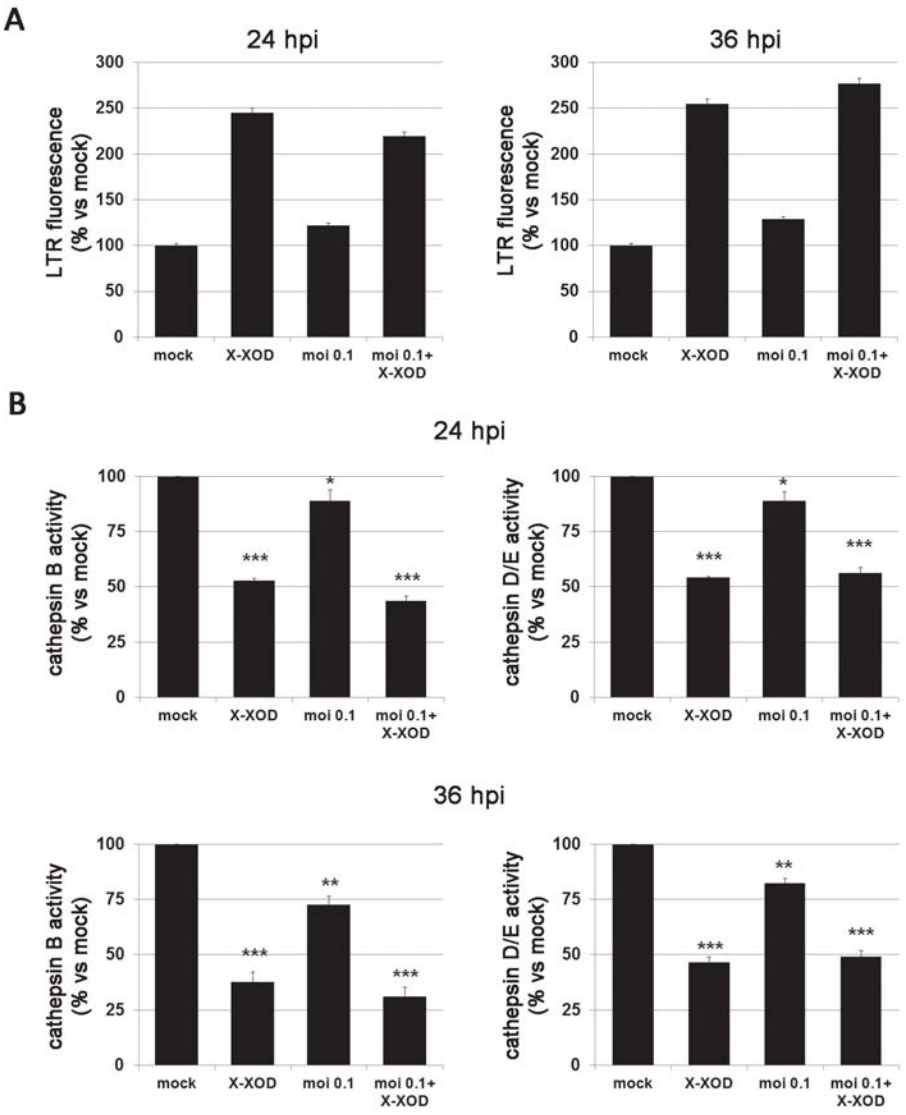

Figure 15. Effect of lower HSV-1 dose on lysosomal content and cathepsin activities.
SK-N-MC cells were treated with X-XOD and infected with HSV-1 at a moi of 0.1 pfu/cell for 24 or 36 hours. (A) LysoTracker Red (LTR) fluorescence was quantified using a microplate reader. Graphs represent the mean ± SD of a representative experiment performed in triplicate and data are expressed as the percentage with respect to untreated cells (mock). (B) The relative enzymatic activities (compared with mock cells) of cathepsins B and D/E were quantified and normalized by the protein content of the lysates. Data are the mean ± SEM of three experiments (*p<0.05, **p<0.01, ***p<0.001).

and functionality of lysosomes were determined. In these conditions, a marked increase of the lysosomal content—revealed by an increase of the LTR fluorescence (Figure 15A)—and a significant reduction of the activity of cathepsins B and D/E (Figure 15B) were observed in cells exposed to HSV-1 and OS both at 24 and 36 hours of treatment.

2.3. HSV-1 and OS alter endocytosis-mediated lysosomal degradation of the EGF receptor

Potential alterations in lysosomal activity can also be measured monitoring the dynamics of the EGF receptor (EGFR). There are at least eight ligands of EGFR (Henriksen et al., 2013). Upon EGF binding, activated EGFR is rapidly internalized through endocytosis (Madshus et al., 2009). After internalization to early endosomes, ligand-receptor complexes are either kept in endosomes to mature into late endosomes and posterior degradation in lysosomes, or recycled back from early endosomes to the plasma membrane. This decision is partly determined by the ligand. EGF has been described to drive the receptor mainly toward degradation in lysosomes (Henriksen et al., 2013) and is therefore used as a ligand in our experiments. Given the fact that SK-N-MC cells lack the endogenous EGFR (van Weering et al., 1995), SK-N-MC cells were transient transfected with an expression plasmid of EGFR tagged to cmyc (pEGFR-c-myc). In mock cells, the stimulation of EGFR degradation by EGF addition was not observed, the EGFR-c-myc protein levels stayed constant even after 5 hours of EGF treatment. However, HSV-1 infected cells showed an increasing level of EGFR over time (Figure 16A) suggesting a failure in EGFR degradation. Nevertheless, the lack of EGFR degradation in mock cells might be a consequence of the plasmid overexpression, and the experiments with SK-N-MC cells were not continued. Instead, we decided to use HeLa cells, which express endogenous EGFR, for the experiments regarding EGFR.

To measure EGFR degradation, Western blot analyses using the anti-EGFR antibody were performed (Figure 16B). In mock cells, 1 hour after EGF stimulation, there was a decrease of 20% in the EGFR levels. After 3 hours, 75% reduction of EGFR was already observed which was maintained at 5 hours of EGF stimulation indicating the internalization and degradation of the receptor induced by EGF. In contrast, cells exposed to OS or HSV-1 infection showed an inhibition of EGFR degradation indicating an alteration of its lysosomal degradation by both treatments. In the absence of EGF, the amount of EGFR protein did not change at all time-points in either of the conditions (data not shown).

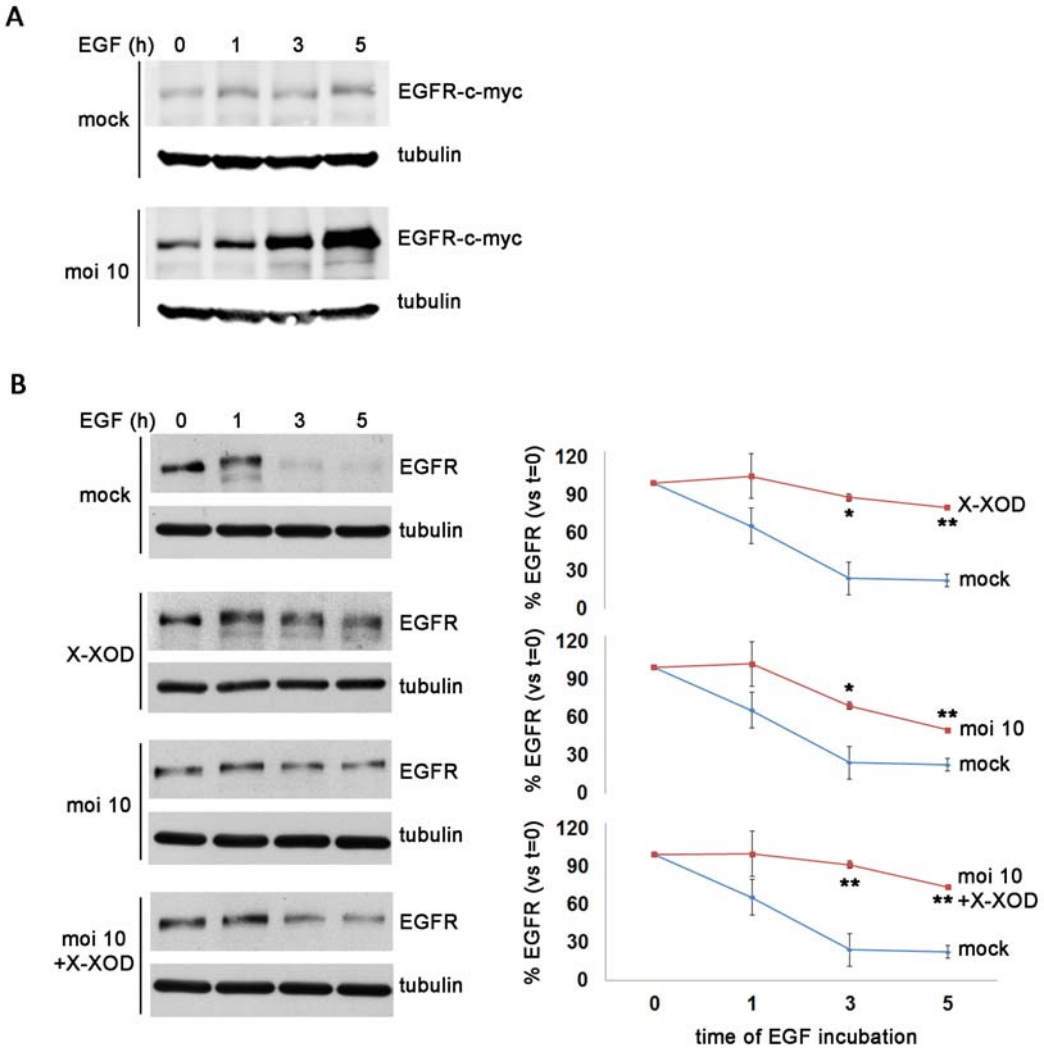

Figure 16. HSV-1 and OS impair EGFR lysosomal degradation.
HeLa or SK-N-MC cells were treated with HSV-1 (moi 10) and X-XOD (only HeLa) for 13 hours and then EGFR degradation was determined by stimulating the cells with 40 ng/mL EGF for the indicated times to induce EGFR internalization. (A) SK-N-MC cells were previously transfected with pEGFR-c-myc and then exposed to HSV-1. The image shows a representative blot using anti-c-myc and anti-tubulin antibodies. (B) Western blot analysis of HeLa cells with anti-EGFR and anti-tubulin antibodies. EGFR degradation was determined by quantifying the amount of remaining EGFR by densitometric analysis and normalized by tubulin amount. Graphical data represent the mean ± SEM of three experiments and are expressed as the percentage of the EGFR amount present at time t=0 (100%) (*p<0.05, **p<0.01).

These results were confirmed by immunofluorescence experiments. In non-treated HeLa cells, EGFR was mainly localized to the plasma membrane and, after EGF addition, was internalized and rapidly degraded. In contrast, HSV-1 and OS induced a strong increase of EGFR intracellular staining (Figure 17), suggesting a defect of EGF-induced EGFR degradation caused by both treatments.

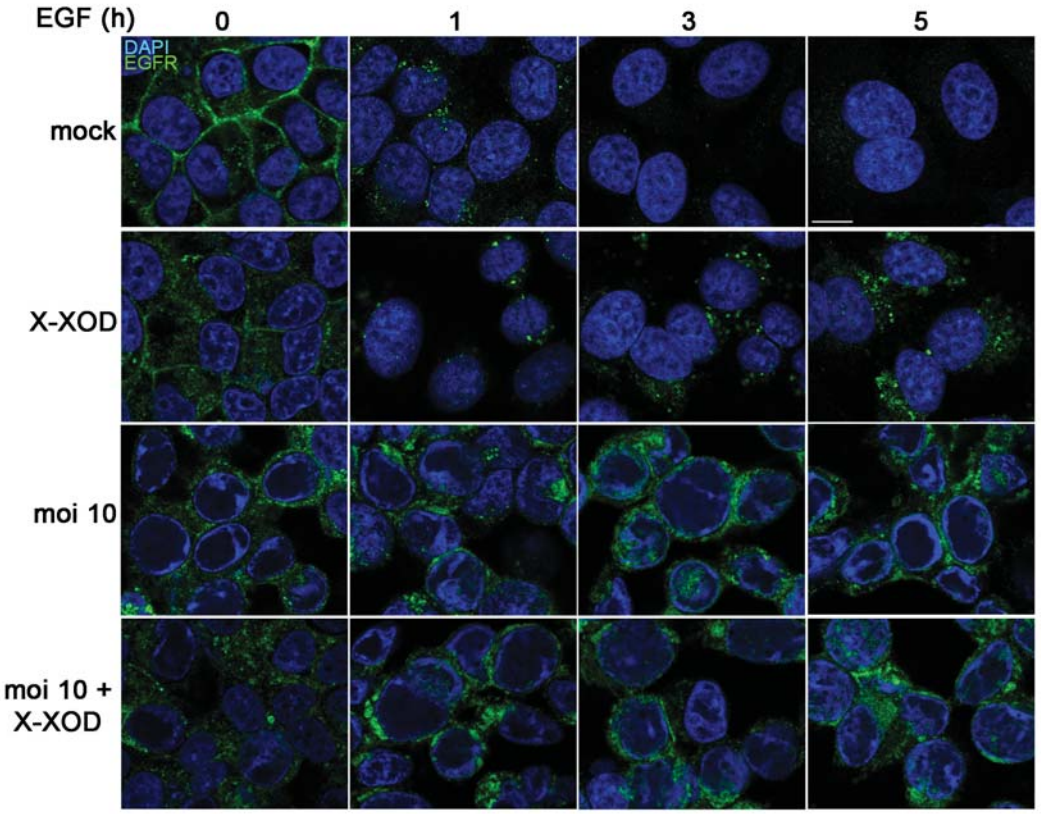

Figure 17. HSV-1 and OS impair EGFR lysosomal degradation.
HeLa cells were treated with HSV-1 (moi 10) and X-XOD for 13 hours and then EGFR degradation was determined by stimulating the cells with 40 ng/mL EGF for the indicated times to induce EGFR internalization. Immunofluorescence images of HeLa cells using an anti-EGFR antibody are shown. Dapi was used to counterstain the nuclei. Note the intracellular accumulation of EGFR in cells exposed to OS and HSV-1. Scale bar: 10 µm.

Given that EGFR is internalized by the endocytic machinery and then degraded by the lysosomes, tests were made to determine whether EGFR accumulation induced by HSV-1 and OS takes place in some compartment of this pathway. To do this, confocal microscopy analyses using antibodies specific to marker proteins of early endosomes (EEA1), late endosomes (insulin-like growth factor 2 receptor, CD222) and lysosomes (CD63) were performed. The distribution of EGFR was examined by 5 hours after EGF addition when the EGFR accumulation has already occurred (Figure 18). In non-treated cells, EGFR staining is not detected confirming the EGFR degradation. At 18 hpi no significant colocalization of EGFR with early endosomal or lysosomal markers was detected in all conditions tested showing that EGFR does not reach the lysosome. In contrast, confocal images revealed EGFR to colocalize significantly with CD222 in HSV-1 infected cells indicating that HSV-1 caused the accumulation of EGFR in late endosomes. This colocalization was already observed at 16 hpi—3 hours after EGF addition. Interestingly, a change in the pattern of EGFR staining was observed in cells exposed to X-XOD indicating that OS

induced the EGFR accumulation in different cell compartments. To proof the specificity of the experiments, all time-points were also analysed in absence of EGF showing that without ligand the EGFR was not changing its location (data not shown). These findings indicate that the EGFR transport to the lysosomes was impaired in cells exposed to HSV-1 and OS confirming that both factors strongly impair the functionality of the lysosomal pathway.

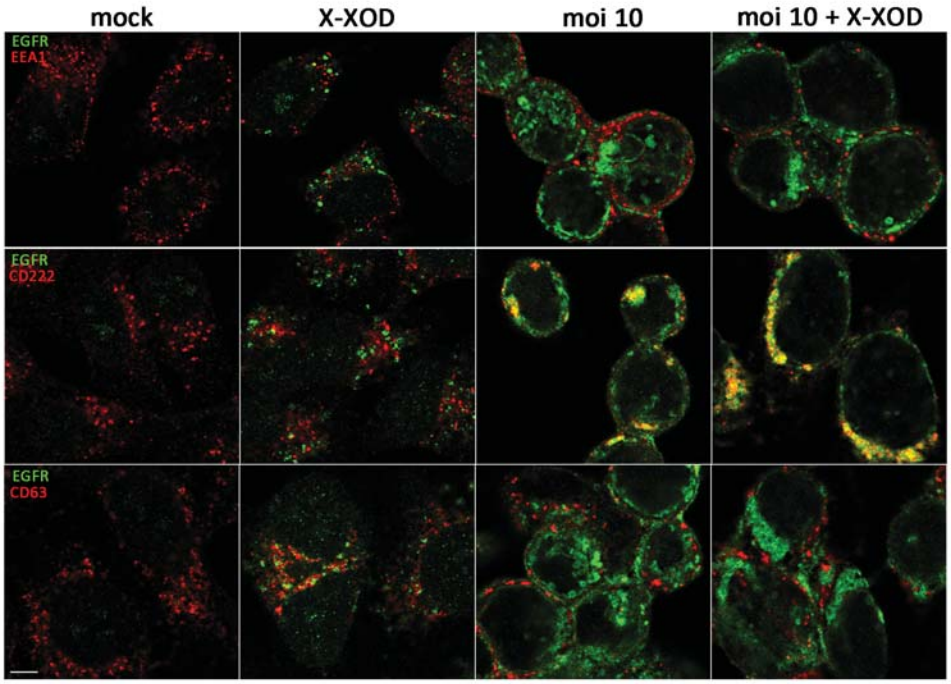

Figure 18. Internalized EGFR colocalizes with late endosomal markers in HSV-1 infected cells.
HeLa cells were exposed to HSV-1 (moi 10) and X-XOD for 18 hours. 5 hours before the end of treatments, HeLa cells were stimulated with 40 ng/mL EGF and the colocalization of EGFR with early endosomal (EEA1), late endosomal (CD222), and lysosomal (CD63) markers was analysed by confocal microscopy. The presence of yellow color in the merged panels indicates colocalization of signals. Scale bar: 5 µm.

2.4. HSV-1 infection and OS increase intracellular cholesterol levels

A growing body of evidence suggest that alterations of cholesterol homeostasis could be implicated in the lysosomal dysfunction observed in the pathogenesis of AD (Chen et al., 2014). Our results also support this relationship because the candidate showing a positive association with the AD-group in the genetic association study (described in section 3.1)—*LAMP2*—has been directly associated with cholesterol. LAMP2 is localized to late endosomes/lysosomes and is thought to be implicated in cholesterol transport out of late endosomes/lysosomes to other cellular compartments (Schneede et al., 2011).

Unesterified cholesterol (also referred to as free cholesterol) is mainly localized to the plasma membrane (60-80% of the cholesterol in the cell), whereas cholesterol esters are packed into intracellular lipid particles and are mainly found in plasma. To address if HSV-1 infection and OS affect cholesterol levels in SK-N-MC cells, total unesterified cholesterol amount was quantified using the Amplex Red Kit. OS did not affect cellular cholesterol, however, HSV-1 infection provoked a significant increase of cholesterol levels (Figure 19A). The combination of both treatments led to an increase of cholesterol levels, though not significant. These results rule out that there is a synergic effect of HSV-1 infection and OS on cholesterol accumulation.

Another popular method to visualize cellular cholesterol by fluorescence microscopy can be achieved with filipin staining. Filipin is a naturally fluorescent polyene antibiotic that binds to cholesterol but not to esterified sterols. Thus, we used this method to detect free (i.e., unesterified) cholesterol in our cell model (Figure 19B). In mock cells, almost all cholesterol is localized to the plasma membrane. Both conditions, HSV-1 infection and OS, provoked a strong accumulation of intracellular cholesterol. As a positive control, cells were treated with bafilomycin A1. This drug specifically inhibits the V-type H^+-ATPase thereby blocking lysosomal acidification causing cholesterol accumulation in endo-lysosomal compartments (Furuchi et al., 1993). Interestingly, the staining pattern of the cells infected with HSV-1—in the presence or absence of X-XOD—was quite similar to that observed with Bafilomycin A1. Also the round shape of filipin positive structures remind of vesicles, suggesting that HSV-1 infection might induce the accumulation of cholesterol in endo-lysosomal compartments.

As seen in Figure 19B, most cellular cholesterol locates to the plasma membrane. To focus on lysosomal cholesterol content, we first partially purified lysosomes from total cell lysates previous to measuring their cholesterol levels (Avrahami et al., 2013). As quality control of the purification, analysis of LAMP1 protein levels was monitored in the different fractions obtained during the process (Figure 19C). These results show that LAMP1 was mainly present in the fraction enriched in lysosomes (F4) and absent in the cytosolic fraction (F3) proofing the efficiency of this method. After purification of the lysosomes, these enriched lysates were analysed with the Amplex Red kit to measure the cholesterol levels. In consistence with the results obtained in total cholesterol levels, HSV-1 infection—in the presence or absence of X-XOD—caused an increment of the cholesterol amount in the fractions enriched with lysosomes (Figure 19D). These findings indicate that HSV-1 and to a lesser extent OS provoke an alteration of cholesterol homeostasis. Further experiments are required to test whether this alteration is responsible for lysosomal dysfunction induced by HSV-1 and OS.

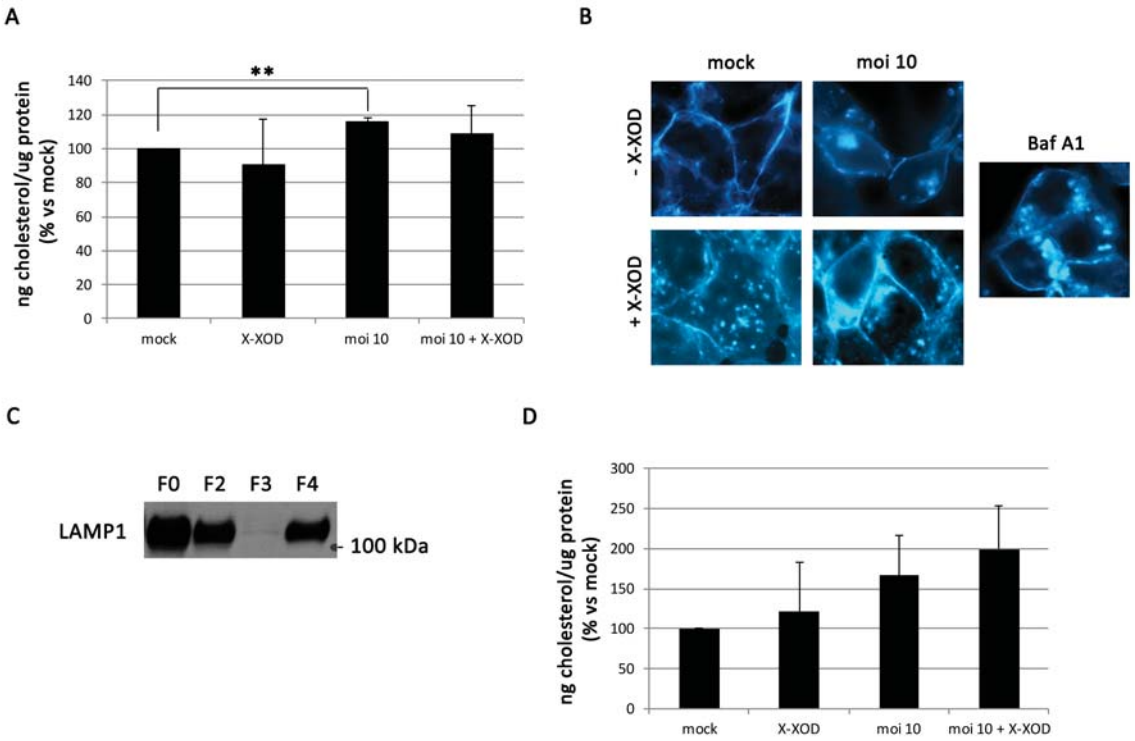

Figure 19. Effect of HSV-1 infection and OS on cholesterol levels and its cellular localization.
Cholesterol quantification was measured with the Amplex Red cholesterol kit in (A) total cell lysates or (D) lysosome-enriched lysates of SK-N-MC cells infected with HSV-1 at a moi of 10 pfu/cell for 18 h and in the presence or absence of X-XOD. Results are expressed in ng of cholesterol per µg of protein (% vs mock) and represent the mean ± SEM of 5 or 3 independent experiments, respectively (**p<0.01). (B) Fluorescence microscopy images of free cholesterol by filipin staining of the cells. As control, cells were treated during 18 h with bafilomycin A1 (Baf A1). (C) Western blot analysis of LAMP1 protein levels in the fractions obtained during partial purification of lysosomes. F0: initial lysate; F2: nuclei-free fraction; F3: cytosolic fraction; F4: fraction enriched in lysosomes.

In summary, using the human neuroblastoma cell line SK-N-MC, we observed that HSV-1 infection and OS deeply alter the lysosomal pathway. Infection and OS lead to an increase of lysosomal burden, decreased activity of lysosomal enzymes, altered lysosomal degradation of the EGFR, and intracellular accumulation of cholesterol. All these findings suggest that our cell model of sporadic AD present severe perturbations of the lysosomal pathway and confirm the hypothesis that it might be a good therapeutic target for AD.

3. Role of LAMP2 in the AD-like neurodegeneration events induced by HSV-1 and OS

3.1. *LAMP2* polymorphisms are associated with sporadic AD

Microarray analysis of our cell models identified the lysosomal pathway as important player in the pathology of AD. To determine whether the candidates identified in our experimental models could be related to the real disease, potentially functional SNPs in six genes were selected (Table 8) and their association with sporadic AD investigated in case/control samples. The sample

was composed of 612 AD cases and 654 age-matched controls from northern and central areas of Spain as described in section 19 of Materials and Methods. The *APOE* genotype was analysed previously (Recuero et al., 2009; Rodriguez-Rodriguez et al., 2010). After the analysis of the individual SNPs in the whole sample, we looked for possible interactions with age, gender and *APOE-ε4* genotype by sample stratification and in logistic regression models. We found no significant associations in the samples stratified (data not shown), except for LAMP2. Interestingly, we found that for this gene encoded on the X chromosome—especially in haplotype blocks 1 and 2—there was a significant association with AD in males, with increased risk for *APOE-ε4* carriers (Table 9).

Table 8. Allele frequencies of the studied SNPs in the AD-case/control sample.

Gene Symbol	dbSNP ID	Haplotype block	MAF (cases/controls)
LAMP2	rs7889047	1	0.37 / 0.42
LAMP2	rs2283738	1	0.38 / 0.38
LAMP2	rs42892	2	0.43 / 0.41
LAMP2	rs42894	3	0.17 / 0.15
LAMP2	rs42901	4	0.17 / 0.15
CTSF	rs4576	1	0.22 / 0.18
CTSF	rs572846	2	0.47 / 0.47
CTSF	rs77760653	4	0.035 / 0.035
CTSF	rs2242663	3	0.27 /0.27
NPC1	rs1805082	1	0.43 / 0.43
NPC1	rs1788799	2	0.34 / 0.36
NPC1	rs1620047	3	0.28 / 0.27
MAP1LC3B	rs11117269	NA	0.44 / 0.48
SORL1	rs668387	NA	0.43 / 0.42
SORL1	rs12364988	NA	0.47 / 0.47
UBC	rs13624	NA	0.17 / 0.17

Table 9. AD risk associated with LAMP2 SNPs in the sample stratified by gender and *APOE* genotype.
Odds ratios (OR) for the association of Alzheimer's disease with the minor allele of the indicated LAMP2 SNPs (vs. the major allele) in different sample strata defined by gender and *APOE* genotypes. †The number of individuals (cases/controls) in each stratum is shown. ‡The p-value for the X^2 test is shown in parenthesis. *ns*, non significant.

		OR (*p-value*)			
dbSNP ID	Haplotype block	Whole sample (523/587)†	Women (333/372)	Men (190/188)	**APOE4 Men (108/30)**
rs7889047	**1**	1.19 (*0.05*)‡	1.03 (*ns*)	**1.59 (*0.03*)**	**3.94 (*0.02*)**
rs2283738	**1**	1.27 (*ns*)	1.01 (*ns*)	**1.59 (*0.03*)**	**3.47 (*0.008*)**
rs42892	**2**	1.08 (*ns*)	0.92 (*ns*)	1.50 (*ns*)	**4.40 (*0.008*)**
rs42894	3	1.18 (*ns*)	1.18 (*ns*)	1.24 (*ns*)	1.85 (*ns*)
rs42901	4	1.18 (*ns*)	1.16 (*ns*)	1.24 (*ns*)	3.59 (*ns*)

Further studies will be performed to assess the genetic association of the genes of interest with SAD, including the analysis of epistatic effects (functional gene-gene interactions), like the one we found in the same sample between NPC1 and ATP-binding cassette transporter A1 (ABCA1) (Rodriguez-Rodriguez et al., 2010). Therefore, we will further extend the sample size with additional samples in the context of the Spanish Consortium of Dementia Genetics (DEGESCO). In any case, our current data suggest that *LAMP2*, most probably integrated into "epistatic machineries", could be a genetic risk factor for SAD.

3.2. Generation of SK-N-MC cell lines with a stable knockdown for LAMP2

After identifying *LAMP2* in the genetic association study and the observation that LAMP2 was strongly upregulated in the neuronal cell model of infection and OS, our next step was to generate a suitable cell model to study the role of LAMP2 in the lysosomal dysfunction and AD-like neurodegeneration events induced by HSV-1 infection and OS. To achieve this, SK-N-MC cells were stably transfected with shRNAs specific for LAMP2. Five different shRNA clones (nos. 1-5) and one scrambled control plasmid (no. 6) were transfected individually and several LAMP2 knockdown cell lines were selected and expanded. Figure 20A shows Western blot analyses of LAMP1 and LAMP2 in these cell lines. In comparison with SK-N-MC cells, the LAMP2-deficient cell lines showed a clear reduction in LAMP2 protein levels (1-B1: 52%; 2-A4: 76%, 5-A6: 60% reduction) without affecting the amount of the lysosomal protein LAMP1. The scrambled control-transfected cell line showed no decrease in LAMP2 (6-A2: 106%). Interestingly, the 5-A6 cell line also showed reduced LAMP1 protein levels (45% less) although the expression of this gene should not be affected by the knockdown of LAMP2.

Determination of the relative LAMP2 mRNA levels of all LAMP2 isoforms by RT-qPCR confirmed the results obtained by Western blot (Figure 20B). Given that alternative splicing of *LAMP2* generates 3 different isoforms and that their expression is tissue dependent, we additionally measured the expression of LAMP2B by using specific primers for this isoform. Both results were almost identical indicating the strong reduction of LAMP2 mRNA levels observed in these cell lines. In conclusion, the in-house generated LAMP2 knockdown cells are suitable for further studies about the involvement of LAMP2 in the events induced by HSV-1 and OS.

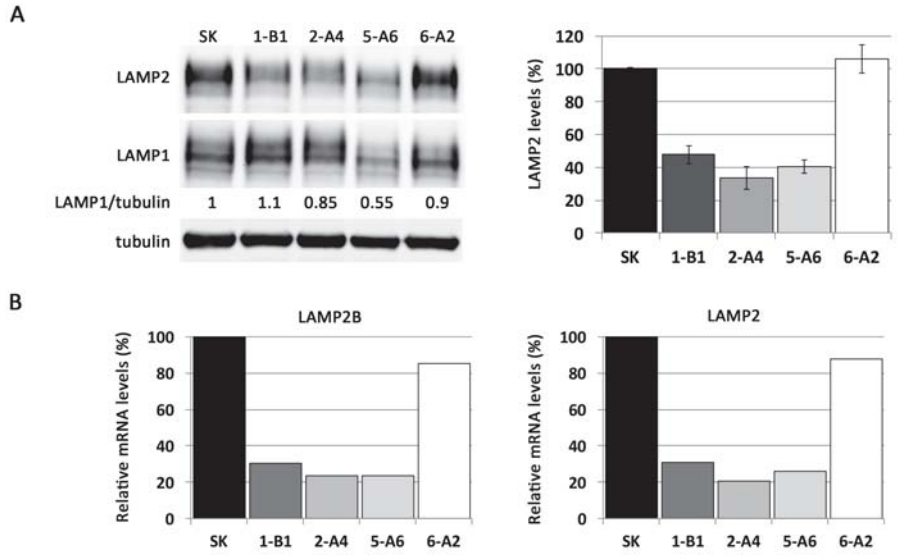

Figure 20. Analysis of LAMP2 expression in SK-N-MC cells transfected with shRNA clones against LAMP2. (A) Western blot analyses of LAMP1 and LAMP2 of SK-N-MC (SK) cell line or shRNA transfected cells (called 1-B1, 2-A4, 5-A6 and 6-A2). The ratio of LAMP1 to tubulin with respect to the parental SK cell line is indicated below the blots. The blots are representative of 5 independent experiments. A tubulin blot is shown as control for equal loading. The remaining amount of LAMP2 normalized by tubulin is represented as mean ± SEM in percentages with respect to SK-N-MC. (B) Quantification of LAMP2B and LAMP2 mRNA levels by RT-qPCR in LAMP2-deficient cell lines. Data are represented in percentages with respect to non-transfected SK-N-MC cells. A representative experiment is shown.

The group of P. Saftig in Germany generated LAMP2-deficient MEF and murine neuroblastoma N2a cells to study molecular mechanisms implicated in Danon disease, a X-linked disorder included in the LSDs caused by mutations in the *LAMP2* gene and characterized by hypertrophic cardiomyopathy and mental retardation. MEF cells have a genetic knockout of the *LAMP2* gene and the N2a cell line presents a stable knockdown of LAMP2 via shRNAs. For simplification, no differentiation between knockout and knockdown will be made in the text and it will be referred to both as "LAMP2-deficient cells". These cell lines were kindly provided by Saftig's laboratory to be included in this study.

Before all else, LAMP2 mRNA and protein levels were analysed to verify the deficiency of LAMP2. Western blot experiments using a specific antibody for the murine LAMP2 confirmed the absence/reduction of LAMP2 in MEFs/N2a, respectively (Figure 21A). LAMP2-deficient N2a cells showed also a slight reduction of LAMP1 protein amount. Quantification of LAMP2 mRNA by RT-qPCR confirmed the results obtained by Western blot (Figure 21B).

Considering that the remaining levels of LAMP2 protein in our deficient SK-N-MC cell lines were notably higher than those measured in deficient MEF and N2a cells and, consequently, differences between wt and LAMP2-deficient cells will be much more appreciable in these cell lines, we decided to perform the functional studies of the role of LAMP2 in MEF and N2a cells.

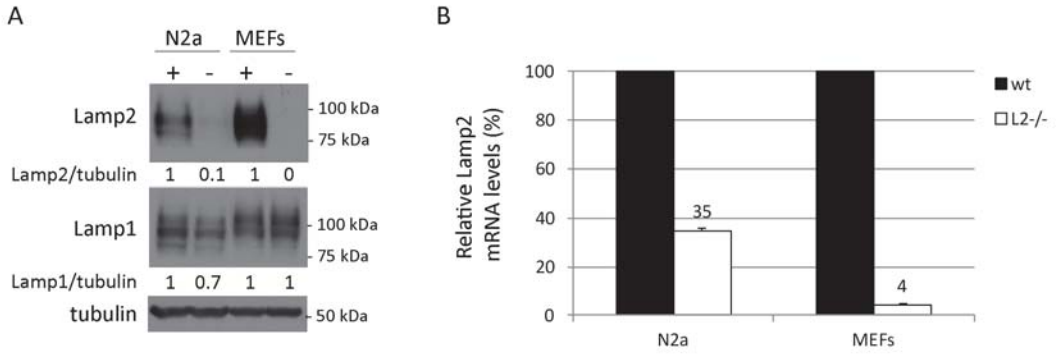

Figure 21. Analysis of LAMP2 protein and mRNA levels of murine cell lines.
(A) Western blot analyses of LAMP1 and LAMP2 in wt (+) and LAMP2-deficient N2a and MEF (-) cell lines. The ratio of LAMP1 or LAMP2 to tubulin with respect to the corresponding wt cell line is indicated below the blots. A tubulin blot is shown as control for equal loading. (B) RT-qPCR of LAMP2 mRNA levels in LAMP2-deficient cell lines (L2-/-) with respect to wt cell lines.

As a next step, the effects of LAMP2 expression on HSV-1 infection, lysosomal alterations and AD-like neurodegenerative markers induced by HSV-1 and OS were evaluated in these models.

3.3. LAMP2 deficiency does not affect cell viability after X-XOD treatment

The response to X-XOD treatment in SK-N-MC cells was extensively studied by our group (Recuero et al., 2009), e.g. it is known that 24 hours of treatment does not affect significantly cell viability. OS-induced apoptosis is known to appear upon 36-48 hours of X-XOD exposure. To determine whether the two murine cell lines—N2a and MEFs—behave the same way and secondly, if there is a differential response to X-XOD-induced mild OS in the presence/absence of LAMP2, the cell viability was determined using the MTT assay. No variations were observed in cell viability at 18 or 24 hours in none of the tested cell lines (Figure 22) indicating that LAMP2 has no effect on cell viability in the presence of OS.

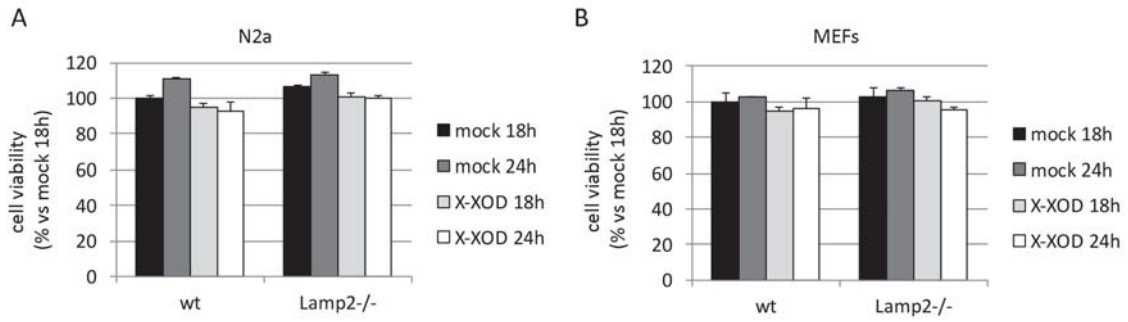

Figure 22. LAMP2 deficiency does not affect cell viability of cells exposed to oxidative stress.
Cells were treated with X-XOD for 18 and 24 hours and the cell viability of (A) N2a and (B) MEF cells was monitored using the MTT reduction assay. Graphs represent the mean ± SD of a representative experiment performed in triplicate and data are expressed as the percentage with respect to untreated cells (wt mock 18 hours).

3.4. LAMP2 deficiency decreases efficiency of HSV-1 infection

As done for the X-XOD treatment, in the next experiments we first wanted to evaluate if the absence of LAMP2 affects HSV-1 infection. To do this, cells were infected with increasing viral dose (ranging from 0.1 to 10 pfu/cell) for 18 hours and viral protein levels were investigated. Western blot analyses showed an increase of the viral glycoprotein gC in a dose-dependent manner in wt and LAMP2-deficient cells. However, LAMP2 deficiency led to lower levels of gC compared to wt cells (Figure 23A and Figure 24A). The glycoprotein gC is a true late gene and the expression of this gene depends on viral DNA synthesis. The decrease in gC levels in LAMP2-deficient cells could therefore indicate altered viral replication and motivated us to further analyse viral DNA levels and the production of infectious particles. The quantification of viral DNA and extracellular infectious titer showed similar results for both cell lines (Figure 23B, C and Figure 24B), with less viral DNA and infectious particles in LAMP2-deficient cells. These results indicate that the absence of LAMP2 decreases the efficiency of HSV-1 infection.

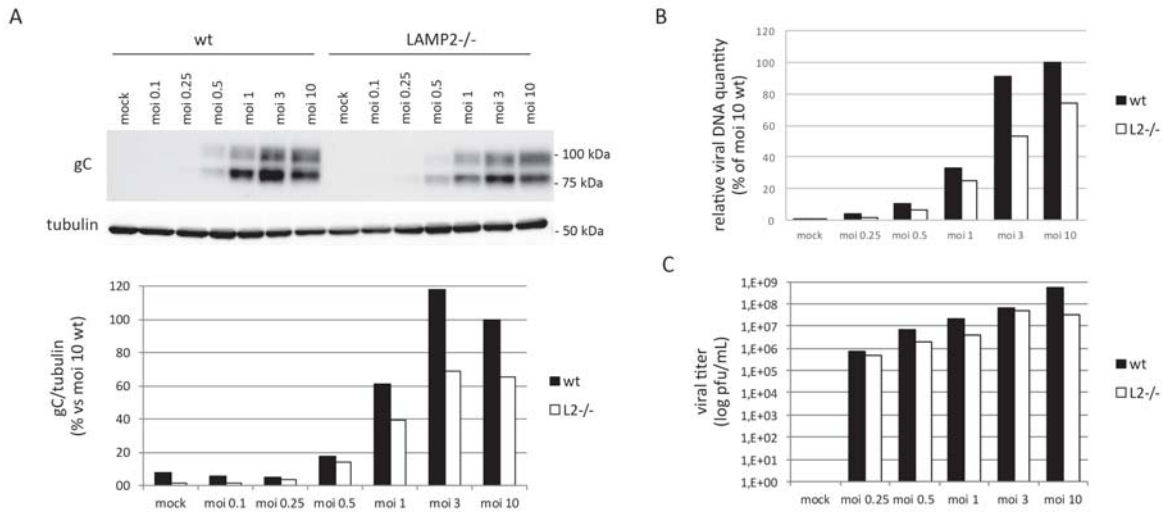

Figure 23. Effect of LAMP2 deficiency on HSV-1 infection in N2a cells.
Wt and LAMP2-deficient (L2-/-) N2a cells were infected with HSV-1 at a moi of 0.1, 0.25, 0,5, 1, 3, and 10 pfu/cell for 18 hours. (A) Western blot analysis with a specific antibody for the viral glycoprotein gC was performed and quantified by densitometric analysis (lower panel). A tubulin blot is shown as control for equal loading. A representative experiment of two performed is presented. (B) Quantification of viral DNA by qPCR. Data represent the mean from triplicate samples of a representative experiment. (C) Viral extracellular titers were analysed by plaque assays.

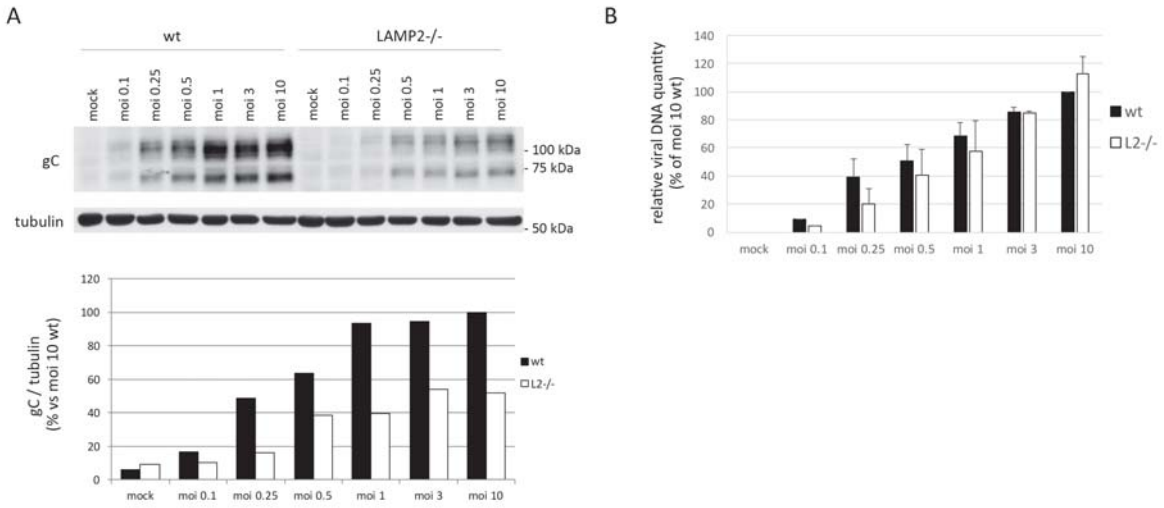

Figure 24. Effect of LAMP2 deficiency on HSV-1 infection in MEF cells.
Wt and LAMP2-deficient (L2-/-) cells were infected with HSV-1 at a moi of 0.1, 0.25, 0,5, 1, 3, and 10 pfu/cell for 18 hours. (A) Western blot analysis with a specific antibody for the viral glycoprotein gC were performed and quantified by densimetric analysis (lower panel). A tubulin blot is shown as control for equal loading. A representative experiment of two performed is presented. (B) Quantification of viral DNA by qPCR. Data represent the mean ± SD of two experiments.

Given that at a viral dose of moi 10 for 18 hours both cell lines, but especially MEF cells, seem to be severely affected (visual observations) and no large differences in the amount of viral protein and DNA were observed comparing moi 3 and moi 10 viral dose, the posterior experiments were performed at a moi of 3 pfu/cell. Immunofluorescence analysis confirmed that almost all cells were infected at this viral dose and time of infection (Figure 25).

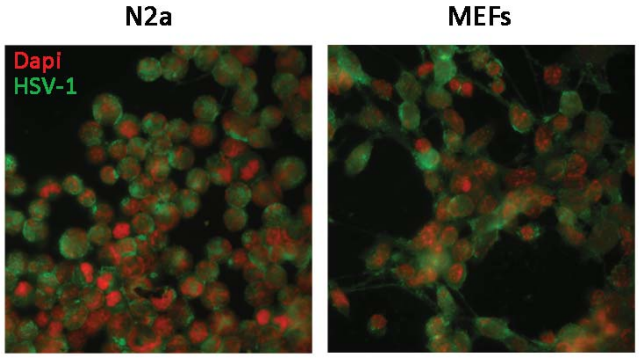

Figure 25. Analysis of infected cells by immunofluorescence experiments
Wt N2a and MEF cells were HSV-1 infected at 3 pfu/cell for 18 hours and immunofluorescence analysis were done with double labelling of dapi (shown in red) and the anti-gC antibody (in green). Magnification 63x.

Our group has previously reported that HSV-1 replication is severely compromised in SK-N-MC cells subjected to OS (Santana et al., 2013). In order to determine the effects of OS in LAMP2-deficient cell models, N2a cells were HSV-1 infected with different viral dose in the presence or absence of X-XOD and the amount of viral protein and DNA was quantified by Western blot and qPCR, respectively. Extracellular infectious particles were also determined by plaque assays. The combination of X-XOD and HSV-1 reproduced the results published from our group in SK-N-MC cells, showing that X-XOD decreases viral protein and DNA levels, as well as infectious titers in N2a cells. This inhibitory effect was also observed in the absence of LAMP2. In addition, lower viral protein and DNA levels were observed in LAMP2-deficient cells compared to wt (Figure 26). The reduction of viral gC levels induced by OS was also observed in MEF cells (Figure 27). These results indicate that, as occurs in SK-N-MC, OS is able to reduce HSV-1 infection in N2a and MEF cells, independently of LAMP2 expression, and confirm the lower efficiency of infection in LAMP2-deficient cell lines.

To evaluate if HSV-1 infection and OS affect LAMP2 expression, Western blot experiments of LAMP2 were also performed. These experiments confirmed again the absence/reduction of LAMP2 in the deficient cell lines. In N2a cells, HSV-1 decreased LAMP2 in a dose-dependent manner, whereas OS strongly increased LAMP2 protein levels (Figure 26). This effect was also observed in LAMP2-deficient cells. In contrast, in wt MEF cells, HSV-1 infection increased LAMP2 levels (Figure 27). OS also increased LAMP2—as observed in N2a cells—independent of their infection status. These data are in agreement with the increase of expression of lysosomal genes induced by OS observed in the functional genomic analysis.

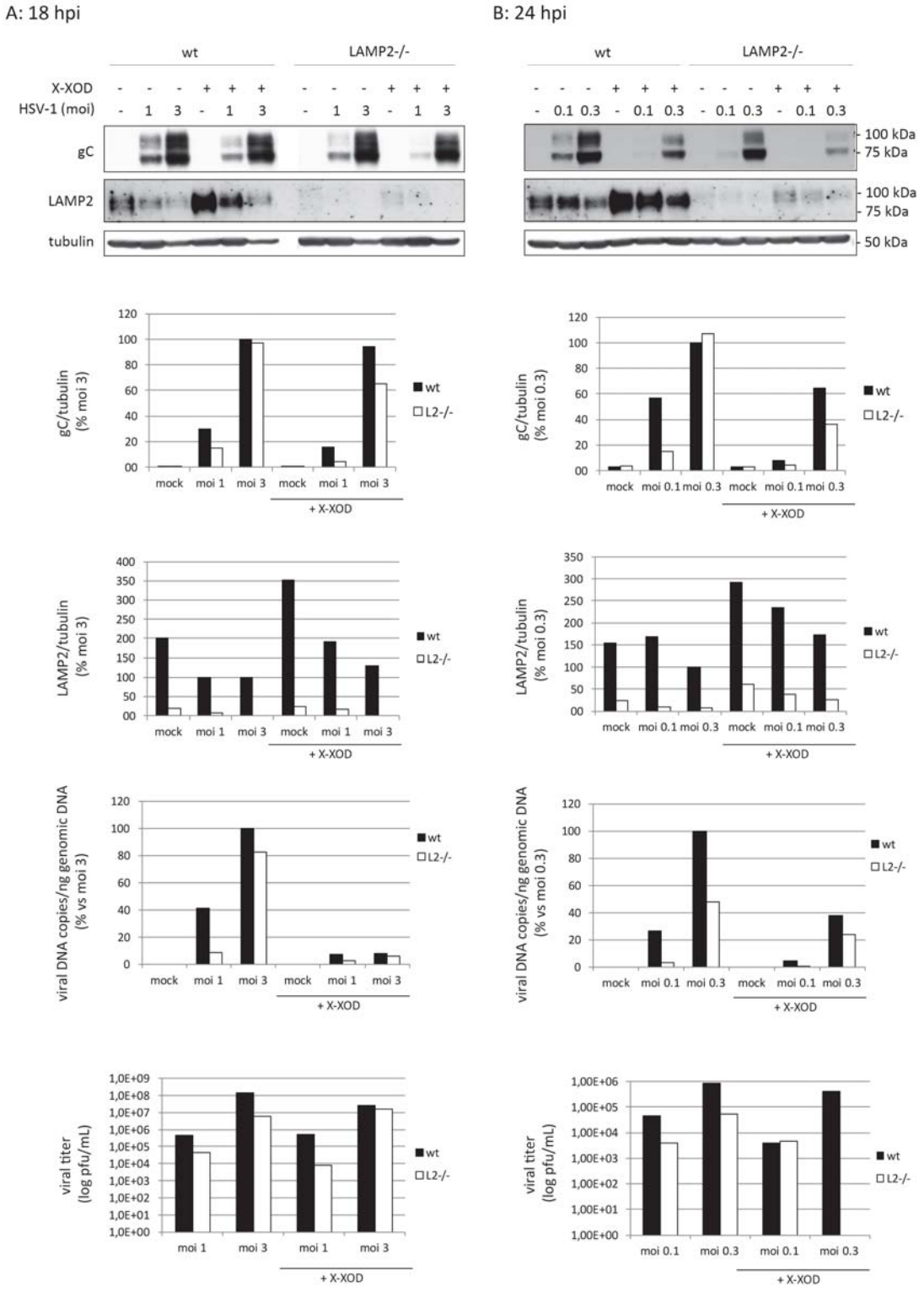

Figure 26. LAMP2 deficiency and OS reduce HSV-1 infection in N2a cells.
Wt and LAMP2-deficient N2a cells were infected with HSV-1 at a moi of 1 and 3 pfu/cell for 18 hours (A: left panel) and at a moi of 0.1 and 0.3 pfu/cell for 24 hours (B: right panel) in the presence/absence of X-XOD. Protein levels of the viral glycoprotein gC and LAMP2 were analysed by immunoblotting and quantified by densitometric analysis. Quantification of viral DNA by qPCR and extracellular viral titers determined by plaque assays are shown. All data are from a representative experiment.

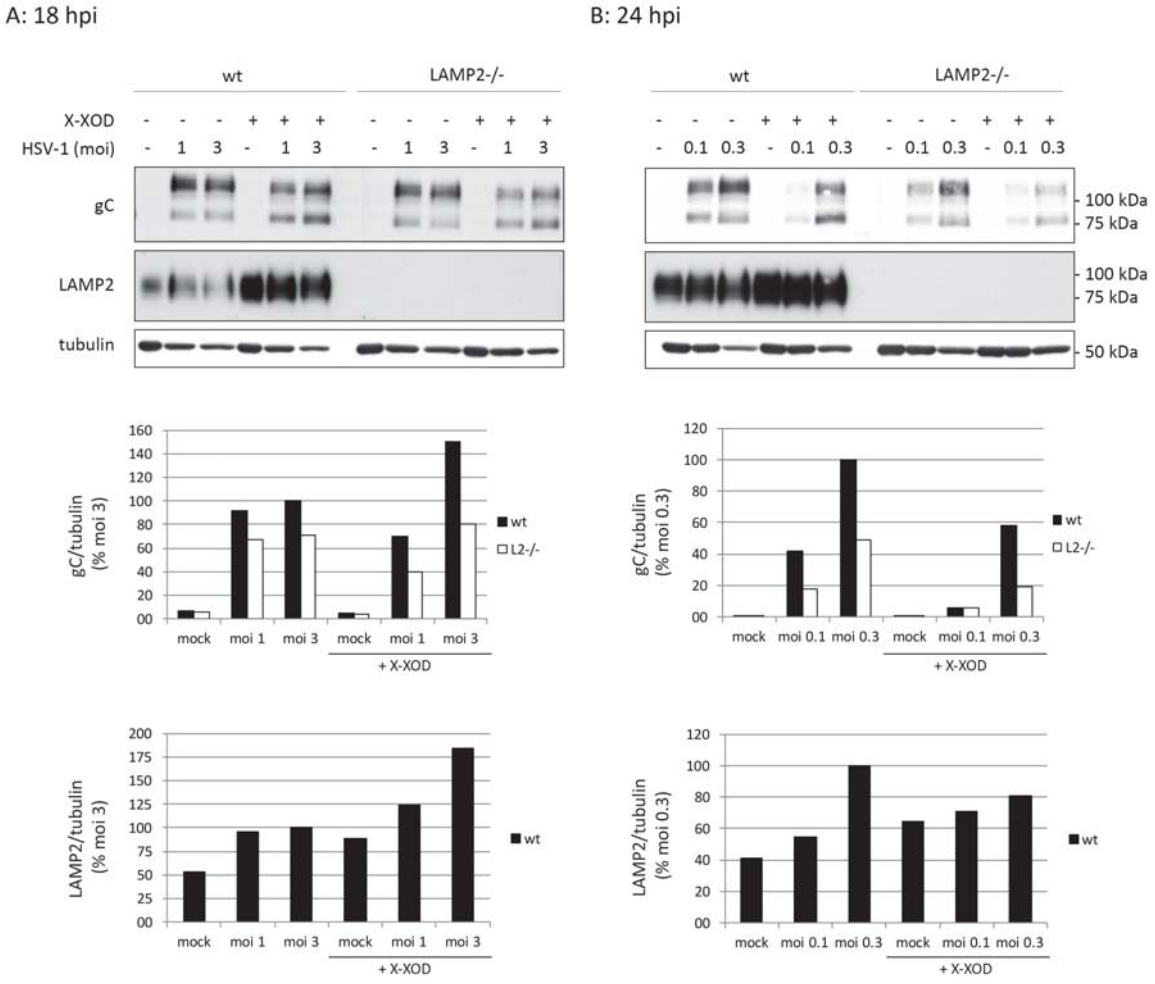

Figure 27. LAMP2 deficiency and OS reduce HSV-1 infection in MEF cells.
Wt and LAMP2-deficient MEF cells were infected with HSV-1 at a moi of 1 and 3 pfu/cell for 18 hours (A: left panel) and at a moi of 0.1 and 0.3 pfu/cell for 24 hours (B: right panel) in the presence/absence of X-XOD. Protein levels of the viral glycoprotein gC and LAMP2 were analysed by immunoblotting and quantified by densitometric analysis. A tubulin blot was performed as control for equal loading. Data are from a representative experiment.

3.5. Effect of LAMP2 deficiency on lysosomal activity

In the following block of results, MEF and N2a cells were analysed to assess whether the HSV-1-induced lysosomal dysfunction observed in SK-N-MC cells were reproduced in these murine cell lines, and secondly, the differential response of wt and LAMP2-deficient cells.

In a first set of experiments, we evaluated the effect of HSV-1 and OS on lysosomal activity analysing the proteolytic activity of CTS D/E and β-hexosaminidase. As observed in SK-N-MC cells, HSV-1 significantly decreased the proteolytic activity of β-hexosaminidase in N2a and MEF cells (Figure 28B). This trend was also observed when the activity of CTS D/E was measured (Figure 28A), but reached significance only in combination with X-XOD.

OS strongly reduced the activity of CTS D/E in N2a and MEF cells (Figure 28A). However, unlike SK-N-MC, X-XOD treated MEF and N2a cells did not show reduced activity of β-hexosaminidase (Figure 28B). These OS and HSV-1-induced effects were observed likewise in wt and LAMP2-deficient cells.

When comparing the proteolytic activities of CTS D/E and β-hexosaminidase in HSV-1 infected cells between wt and LAMP2-deficient cells, a general reduction of enzymatic activity in LAMP2-deficient N2a and MEF cells was observed, although no significance was reached or statistical analyses could not be performed yet (n=2). These data suggest that the HSV-1-induced decrease of lysosomal hydrolase activity is even more pronounced in LAMP2-deficient cells, even though more experiments are required to demonstrate this effect.

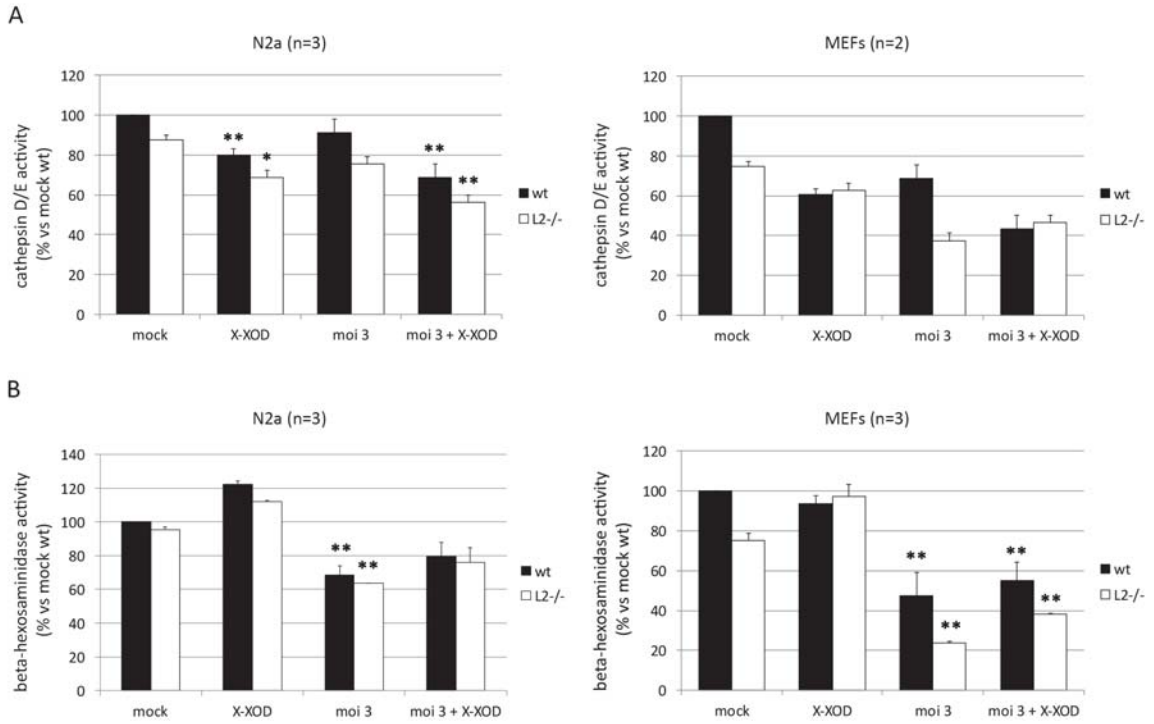

Figure 28. Effect of LAMP2 deficiency on activity of lysosomal hydrolases.
Cells were infected with HSV-1 at a moi of 3 pfu/cell for 18 hours in the presence/absence of X-XOD. (A) The relative enzymatic activity of CTS D/E with respect to wt mock cells is presented as the mean ± SEM (2 or 3 independent experiments) (B) The relative enzymatic activity of β-hexosaminidase with respect to wt mock cells is shown. Data are the mean ± SEM of 3 experiments (*p<0.05, **p<0.01).

3.6. Effect of LAMP2 deficiency on AD-like neurodegeneration markers

With the aim of assessing the role of LAMP2 in the appearance of neurodegeneration markers induced by HSV-1 and OS, the levels of tau phosphorylation, Aβ and LC3 were monitored in LAMP2-deficient MEF and N2a cells.

3.6.1. Analysis of tau phosphorylation

Western blot analyses were used to evaluate tau phosphorylation in the epitope thr205, which is known to be phosphorylated in AD brains (Goedert, 1993) and in HSV-1 (Zambrano et al., 2008) and HSV-2 infected cells (Kristen et al., 2015). The effects of LAMP2 deficiency on tau phosphorylation were also studied. A strong increase of tau phosphorylation was observed in HSV-1 infected N2a and MEF cells (Figure 29A and B), reproducing the results published by our laboratory in SK-N-MC cells (Alvarez et al., 2012). These results were confirmed by immunofluorescence analysis (Figure 30). In non-infected cells, almost no signal was seen. A week signal was only detected in mitotic cells, which is consistent with the fact that AD-like tau phosphorylation occurs during mitosis (Delobel et al., 2002). In contrast, HSV-1 infection strongly increased the levels of phosphorylated tau in the cells. No apparent differences were noted between wt and LAMP2-deficient cells.

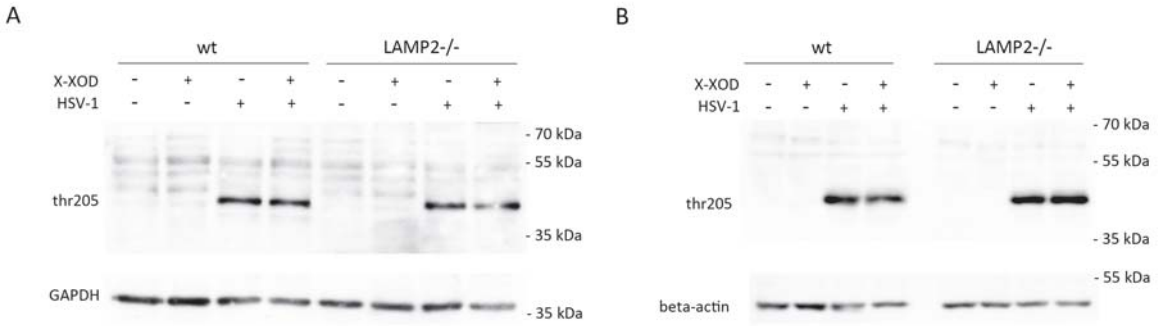

Figure 29. Effect of LAMP2 deficiency on tau phosphorylation site thr205.
Wt and LAMP2-deficient cells were exposed to HSV-1 at a moi of 3 pfu/cell for 18 hours in the presence/absence of X-XOD, and tau phosphorylation was assessed using the phosphorylation-sensitive antibody thr205. A representative experiment of the analysis of endogenous tau levels by Western blot in (A) N2a (n=1) and (B) MEF (n=3) cells is shown. GAPDH or β-actin blots are shown as a control to ensure equal loading.

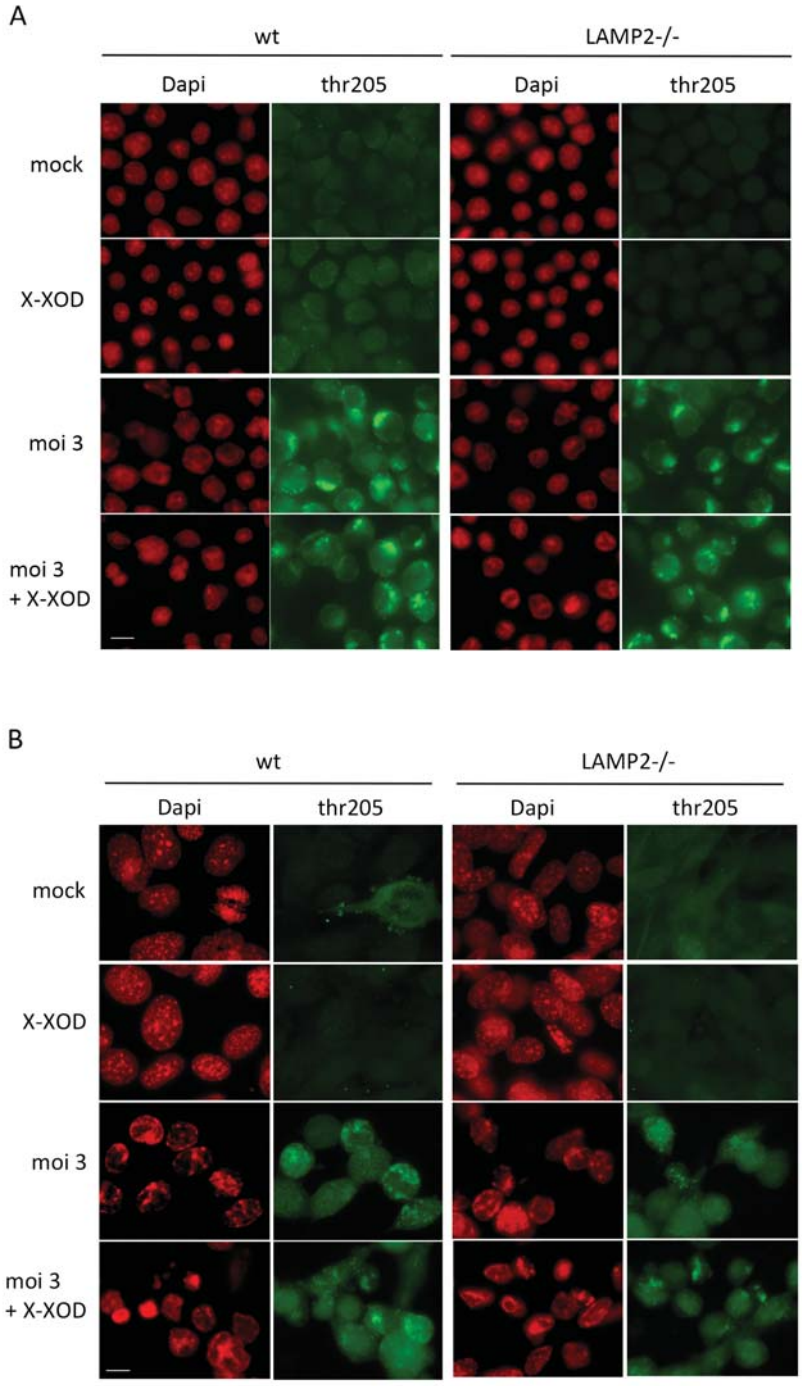

Figure 30. Effect of LAMP2-deficiency on tau phosphorylation site thr205.
Wt and LAMP2-deficient N2a (A) and MEF (B) cells were infected with HSV-1 at a moi of 3 pfu/cell and exposed to X-XOD for 18 hours. Immunofluorescence images using the phosphorylation-sensitive antibody thr205 and dapi-stained nuclei are shown. Original magnification: 63x. Scale bar: 10 µm.

3.6.2. Analysis of Aβ levels

Firstly, immunofluorescence analysis was used to determine if HSV-1 infection and OS modify Aβ levels in wt and LAMP2-deficient N2a and MEF cells. As it has been described that most intraneuronal Aβ ends at residue 42 (Gouras et al., 2000; Takahashi et al., 2002),

immunofluorescence experiments using an antibody specific for Aβ42 were performed. No staining for Aβ42 was observed in mock or X-XOD treated cells. In contrast, accumulation of Aβ42 was observed in HSV-1 infected cells, a trend that seemed to be potentiated in combination with X-XOD (Figure 31). No differences were apparent between wt and LAMP2-deficient cells.

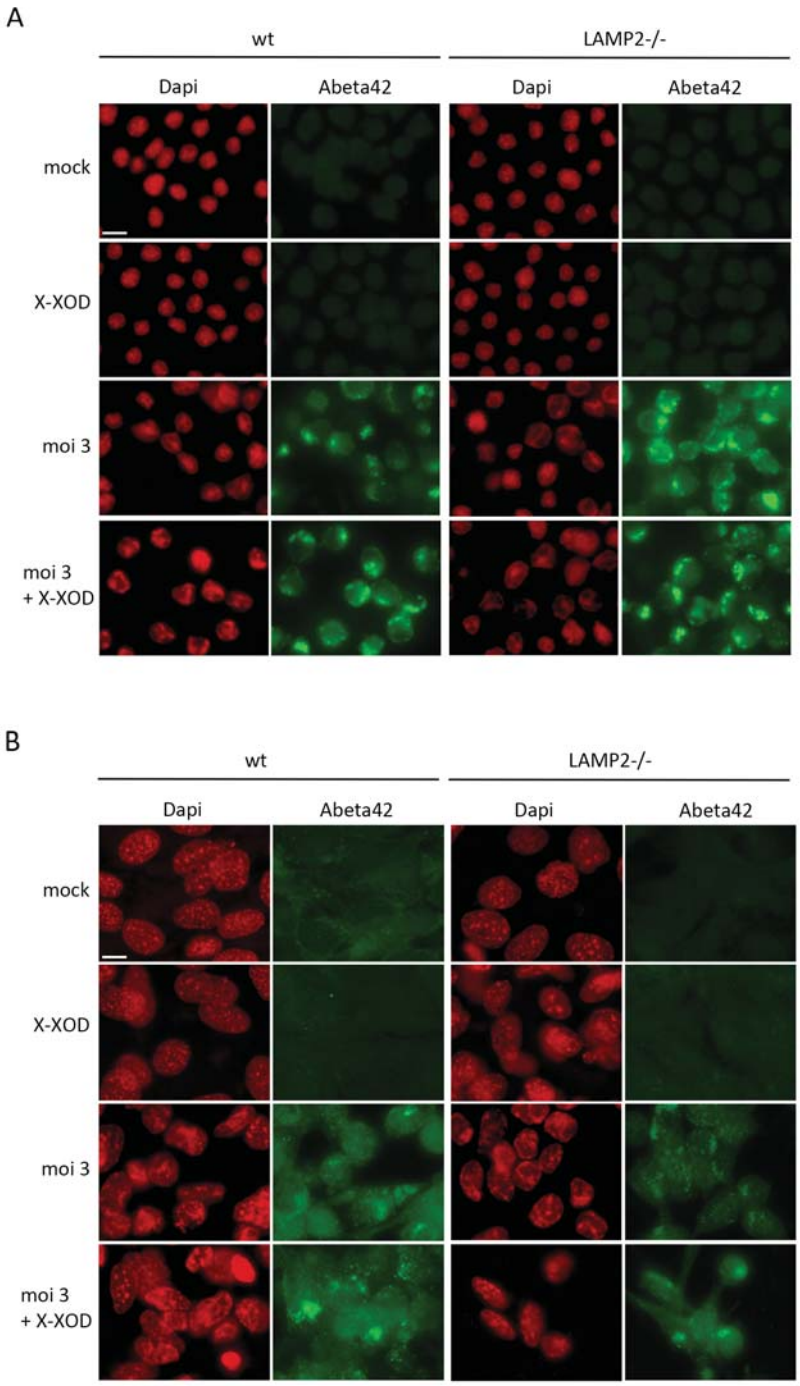

Figure 31. Effect of LAMP2 deficiency on Aβ42 accumulation.
Wt and LAMP2-deficient N2a (A) and MEF (B) cells were infected with HSV-1 at a moi of 3 pfu/cell and exposed to X-XOD for 18 hours. Immunofluorescence images using an antibody specific for Aβ42 and dapi-stained nuclei are shown. Original magnification: 63x. Scale bar: 10 µm.

We have reported that intracellular Aβ accumulation induced by HSV-1 in neuronal cells is partly mediated by decreased efficiency of the cells to secrete this peptide (Santana et al., 2012). Therefore, the levels of secreted Aβ40 and Aβ42 in conditioned media were measured by ELISA. As expected, HSV-1 caused a marked reduction in secreted Aβ40 and Aβ42 levels in N2a and reached undetectable levels in MEF cells (Figure 32). These results indicate that HSV-1 infection strongly reduces secretion of both Aβ peptides leading to intracellular accumulation of Aβ. Again, LAMP2 deficiency had no effect on the levels of secreted Aβ.

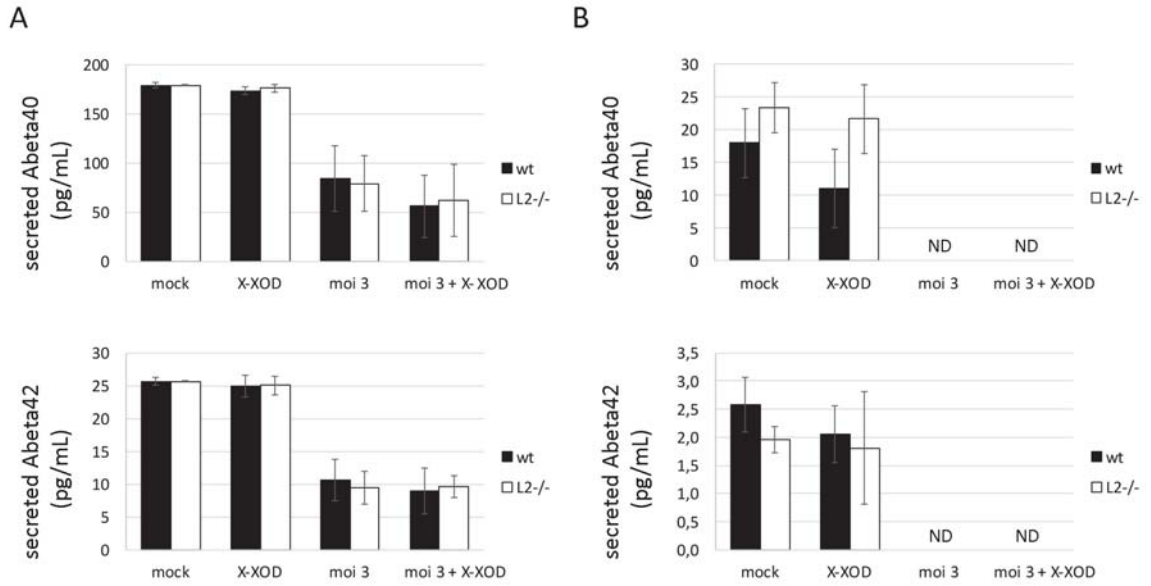

Figure 32. Effect of LAMP2 deficiency on Aβ secretion.
ELISA analysis of Aβ40 and Aβ42 levels in the medium of wt and LAMP2-deficient N2a (A) and MEF (B) cells treated with X-XOD and infected with HSV-1 at a moi of 3 pfu/cell for 18 hours. Values are the mean ± SD of two independent experiments represented in pg/mL (ND: not detected).

3.6.3. Analysis of LC3 levels

Severe alterations of the autophagic pathway were observed in HSV-1 infected SK-N-MC cells (Santana et al., 2012). To test if HSV-1 interferes with autophagy in N2a and MEF cells, we analysed the autophagic marker LC3 by Western blotting. Upon the activation of autophagy, LC3 is converted from its cytosolic form LC3-I to the autophagic membrane-bound form LC3-II. As shown in Figure 33, OS and HSV-1 infection strongly increased LC3-II levels in N2a and MEF cells suggesting an accumulation of autophagic vesicles in HSV-1 and OS treated cells, as occurred in SK-N-MC cells exposed to HSV-1 and OS (Santana et al., 2013). Similar results were observed in wt and LAMP2-deficient cells.

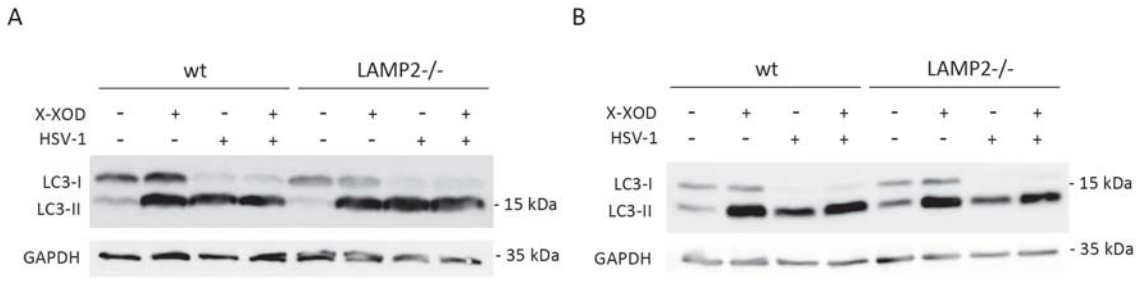

Figure 33. Effect of LAMP2 deficiency on LC3-II levels.
Cells were infected with HSV-1 at a moi of 3 pfu/cell for 18 hours in the presence/absence of X-XOD. Analysis by Western blotting using an anti-LC3 antibody in (A) N2a cells (n=2) and (B) MEFs (n=3). GAPDH blots are shown as control for equal loading.

In summary, preliminary results in N2a and MEF cells showed that HSV-1 and OS induce the appearance of the main AD-like neurodegenerative markers including the increase of phosphorylated tau and LC3-II levels, accumulation of intracellular Aβ42, as well as reduced secretion of the Aβ peptides, therefore recapitulating the effects found in SK-N-MC cells. HSV-1 and OS also caused a reduction of the activity of lysosomal hydrolases. So far, no differential response between wt and LAMP2-deficient cells was observed, except for the proteolytic activity of hydrolases. LAMP2-deficiency weakly accentuated the HSV-1-induced decrease in activity indicating a more severe lysosomal dysfunction in the absence of LAMP2.

4. Generation of induced pluripotent stem cells

The findings obtained so far result from work with cell models mimicking AD. The question is whether the molecular alterations observed are also present in the "real" disease. To overcome this gap, we proposed to study the lysosomal pathway in a more physiological model.

Since the discovery of the Yamanaka factors and the fact that human/mouse somatic cells can be reprogrammed into pluripotent stem cells (iPSCs), this field has made great advances. Especially for multifactorial and sporadic diseases where a clear pattern of inheritance and good animal models are missing, this new technology is of great importance. Researchers worldwide have generated patient-specific iPSC lines to gain insight into disease mechanisms and have used them for drug screening, identification of biomarkers and clinical trials of personalized therapies.

The experimental set-up is quite complicated and lengthy and there are still many unanswered questions to fully understand reprogramming and pluripotency, but mainly the protocol efficiency has to be improved (reviewed in depth in Li et al., 2016). The "iPS" segment of the present thesis is subdivided into four parts:

I. Generation of primary culture of fibroblasts derived from one AD patient and control.
II. Reprogramming of fibroblasts into iPSCs.
III. Characterization.
IV. Differentiation of iPSCs into neurons.

Finally, the generated iPSCs/differentiated neurons will then be analysed to confirm the alterations of the lysosomal pathway observed in SK-N-MC, N2a and MEF cells. They will also be used to study if there is a differential behaviour in response to HSV-1 infection and/or OS in neurons derived from AD patients and control individuals.

In this study we used samples from two individuals that were selected from a group of volunteers participating in a longitudinal study (ELMO: Longitudinal Multicentric Observational Study) about AD in collaboration with Dra. Ana Frank of the Hospital Universitario La Paz. One was classified as sporadic AD patient that, at the moment of sample removal, presented clinical features of a person with mild cognitive impairment (herein referred to as patient [P]) and the second individual was an age-matched control (C).

In the following sections the results obtained so far concerning part I. to III. will be described:

4.1. Establishing primary cell cultures from patient biopsies

iPSCs can be generated from diverse adult somatic cells. The less invasive option for the donors is the use of dermal fibroblasts as starting material. In our case, these fibroblasts were obtained by the processing of a skin punch biopsy of the individuals. Therefore, a 6 mm skin specimen was extracted from their forearms. These skin samples were then cut into smaller pieces and attached to the bottom of a cell culture flask (Figure 34; Day 0). After a few days, outgrowth of keratinocytes surrounding the attached biopsy was noticed. 10 days post-biopsy the outgrowth of early fibroblasts was observed in both samples. By 18 days a dense monolayer of fibroblasts (HDF) was observed and cells were passaged into bigger flasks for expansion. Only a small amount of cells was required for the following reprogramming experiment, so the rest was frozen down. No apparent differences of cell morphology (shape and size) and cell proliferation between patient and control fibroblasts were observed (Figure 34).

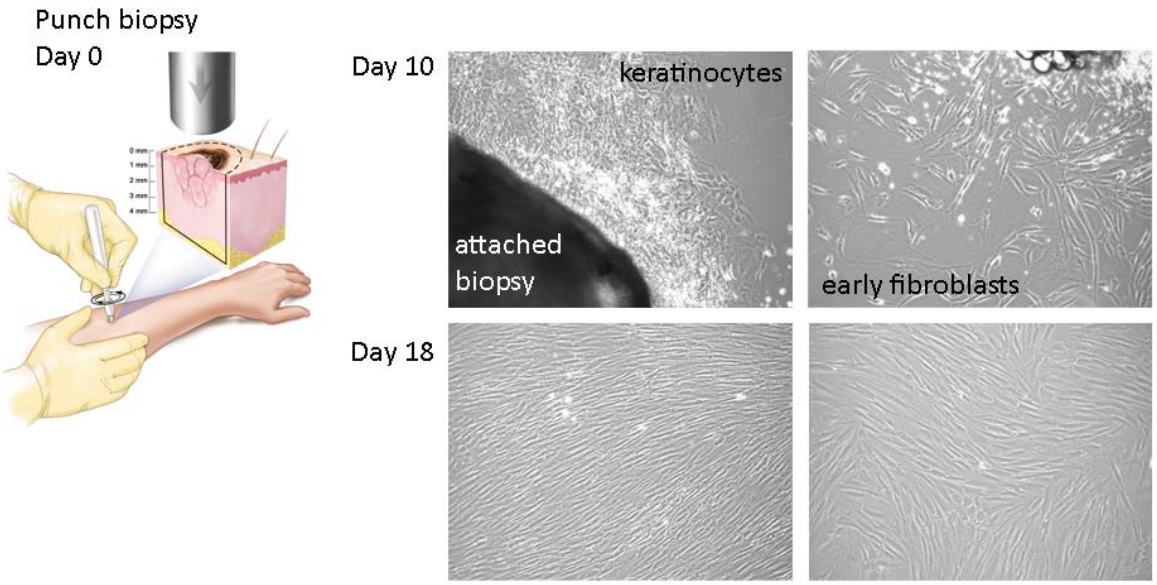

Figure 34. Overview of processing and growth of human dermal fibroblasts.
Specimens from 6 mm skin punch biopsies are dissociated, and plated to expand dermal fibroblasts. Phase contrast images were taken with a standard microscope. Magnification: 10x.

4.2. Generation of iPSCs

The generated fibroblasts were then used to be reprogrammed into iPSCs using integration-free CytoTune®-iPS 2.0 Sendai Reprogramming Kit that includes Sendai virus particles of the four Yamanaka factors (OCT3/4, SOX2, KLF4, and c-MYC). Figure 35A shows the timeline respected during this reprogramming experiment. On day 0, HDFs were transduced with the four Yamanaka factors. After 7 days, cells were replated onto a monolayer of irradiated MEFs. By 12 days, the first clumps were spotted and by 18 days, colonies with iPSC morphology were observed in both preparations (Figure 35B). Several iPSC lines were generated from individual colonies. Some colonies did not grow after the first round of mechanical passaging. From those who did expand, two patient-derived (called P-I and P-II) and two control-derived cell lines (C-I and C-II) were selected for further maintenance and analysis.

iPSC colonies have a very characteristic phenotype. Recent studies reported the quality evaluation of iPSCs by their colony morphologies (Scherf et al., 2012; Suga et al., 2015; Tokunaga et al., 2014). Figure 36 shows representative images of the grown colonies. They showed the expected sharp edges and the dense packaging of cells inside the colonies (Robinton et al., 2012; Wakao et al., 2012). The four cell lines were mechanically passaged every other week for expansion and characterization.

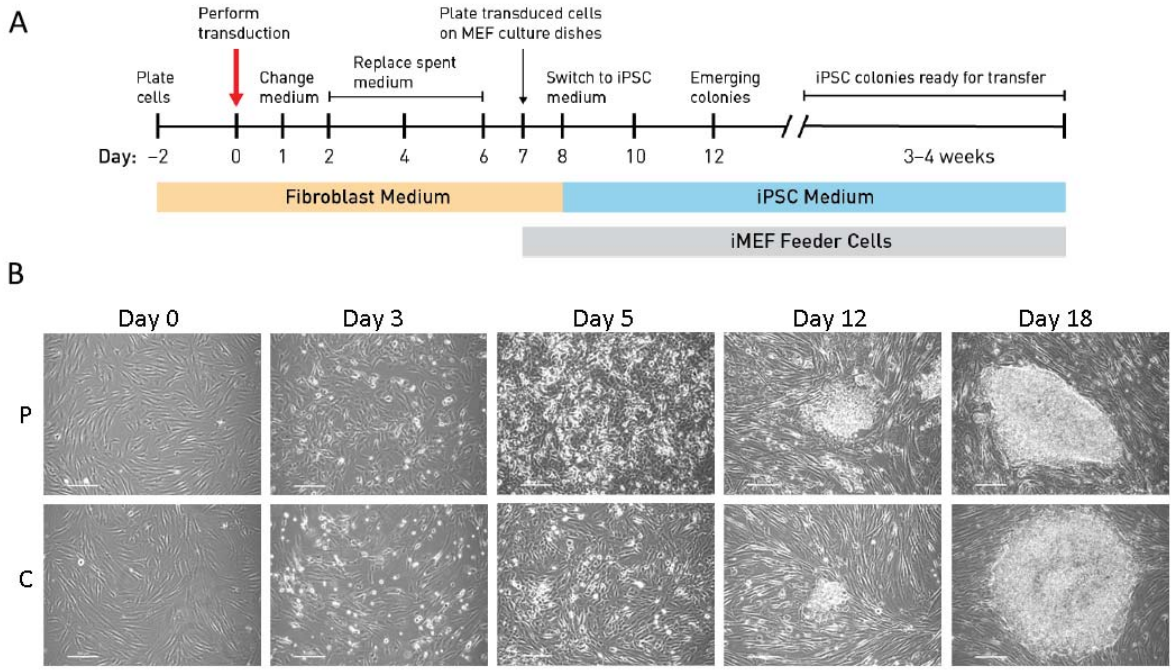

Figure 35. Sendaiviral transduction of fibroblasts and generation of iPSCs.
(A) Time schedule of HDF reprogramming and iPSC generation. (B) Phase contrast images (magnification: 10x) of different phases of reprogramming until the appearance of colonies with typical iPSC morphology. P: patient-derived. C: age-matched control. Scale bar: 200 µm.

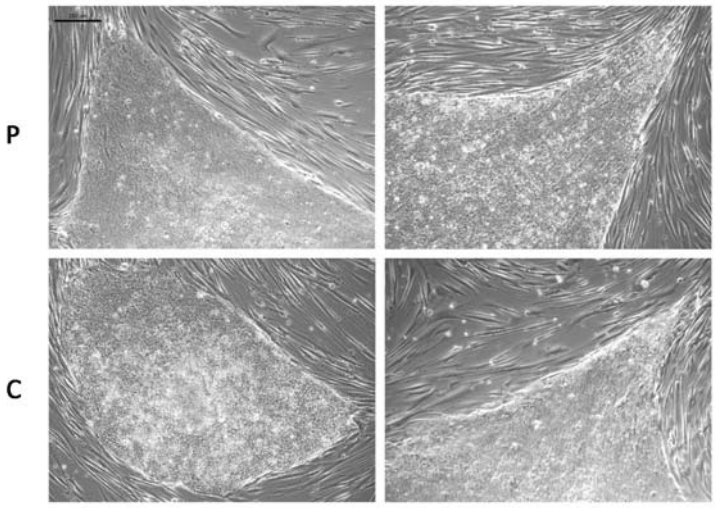

Figure 36. iPSC morphology of mature colonies.
Representative phase contrast images of iPSC colonies of patient (P) and control (C) cell lines on a monolayer of feeder cells. Magnification: 10x. Scale bar: 200 µm.

5. Characterization of iPSC lines

It is of great importance to characterize exhaustively the developed iPSC lines in order to demonstrate their pluripotency. The International Stem Cell Banking Initiative (ISCBI) (Crook et al., 2010) recommends several tests, which has served us as guideline.

5.1. Alkaline phosphatase and TRA1-60 staining

Alkaline phosphatase (AP) staining is normally the first assay to perform. The AP enzyme is able to change the conformation of a colorimetric reagent from a soluble to a precipitated state. A clear blue signal in the colonies and no staining of the feeder cells should be observed. In Figure 37A microscope images of an individual iPSC colony are shown before and after staining with AP. The colony revealed a partial positive staining, but the border of the colony seemed to be less intense. To clarify whether our iPSC cell lines were pluripotent, they were live stained with an antibody specific for TRA1-60—one of the fastest and most reliable methods for identifying a reprogrammed colony. Figure 37B shows that all cells of the colonies are TRA1-60 positive, whereas the cells from the surrounding feeder layer were clearly negative. In conclusion, all four established iPSC lines are positive for TRA1-60 indicating their pluripotent state.

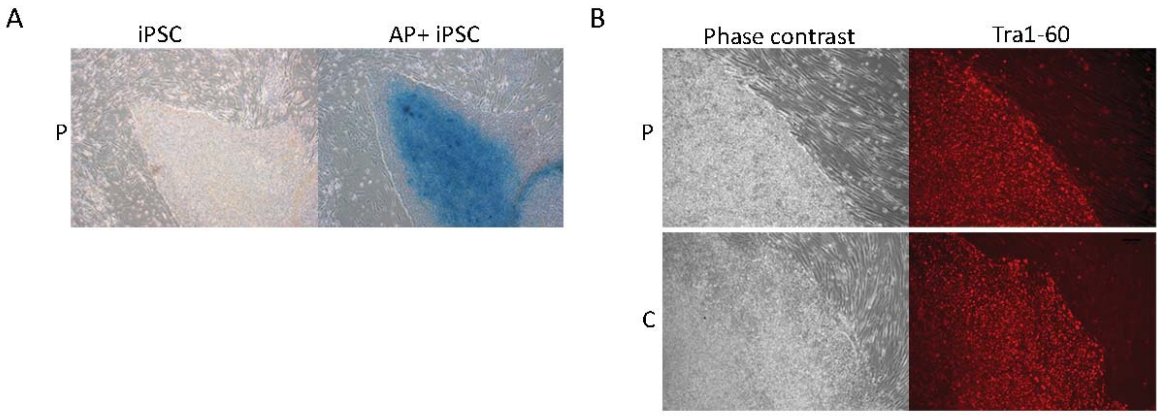

Figure 37. Alkaline phosphatase (AP) and TRA1-60 live staining of iPSC lines.
(A) Microscope images of the same patient-derived (P) iPSC colony before and after the staining with alkaline phosphatase (AP; in blue). (B) Representative immunofluorescence images of patient (P) and control (C) derived iPSC colonies before and after the staining with an antibody specific for the pluripontency marker TRA1-60 (in red). Magnification: 10x.

After several weeks of passaging, the two control cell lines started to differentiate. Inside the colonies the appearance of other cell types were noticed (Figure 38; marked with asterisk). To confirm that the colonies did lose their undifferentiated/pluripotent state, TRA1-60 live staining was performed again. Unlike the staining pattern seen in recent reprogrammed colonies (Figure

37B), those colonies now represented a heterogeneous staining with mainly negative cells confirming the differentiation of these colonies. Both control cell lines were affected by these differentiation events and were therefore discarded. The following characterization experiments were performed consequently only with the two iPSC lines generated from the AD patient.

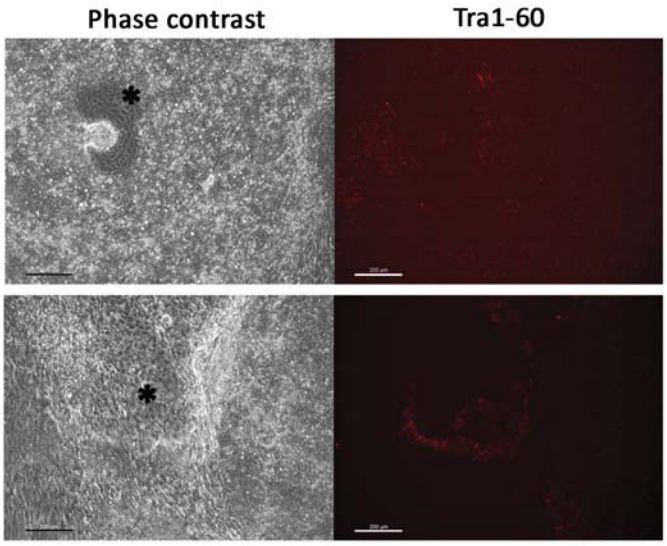

Figure 38. Morphology of partially differentiated iPSC colonies.
Phase contrast images of control iPSC colonies with differentiated cells in the center (marked with asterisk). TRA1-60 live staining (in red) of the same colonies showed negative signal of these colonies. Scale bar: 200 µm.

5.2. Analysis of the expression of pluripotency markers in iPSC lines

Once TRA1-60 positive colonies are determined, the next step is to confirm their pluripotency by immunostaining. A set of biochemical and molecular markers has been identified that are specific for iPSCs and fundamental to maintaining the undifferentiated state (Ohnuki et al., 2009). Immunofluorescence analysis of the two remaining cell lines (P-I and P-II) revealed expression of nuclear transcription factors OCT4, NANOG, SOX2; keratin sulphate surface antigens TRA1-60 and TRA1-81; and glycolipid antigens SSEA3 and SSEA4 (Figure 39A and B).

In addition, quantitative RT-PCR analysis also demonstrated high levels of expression of the pluripotency markers including OCT4, SOX2, REX1, NANOG and CRIPTO (Figure 39C). Additionally, expression levels of differentiation markers for the three germ layers were analysed. Only PAX6—an early differentiation marker for ectoderm—showed a slight increase in both iPSC lines compared to fibroblasts. The other ectodermal marker (TUBB3), and the early differentiation markers for mesoderm (HNF4), endoderm (SOX17, FOXA2) or cardiomyocytes (MEF2C, TBX5) showed no expression in the iPSC lines.

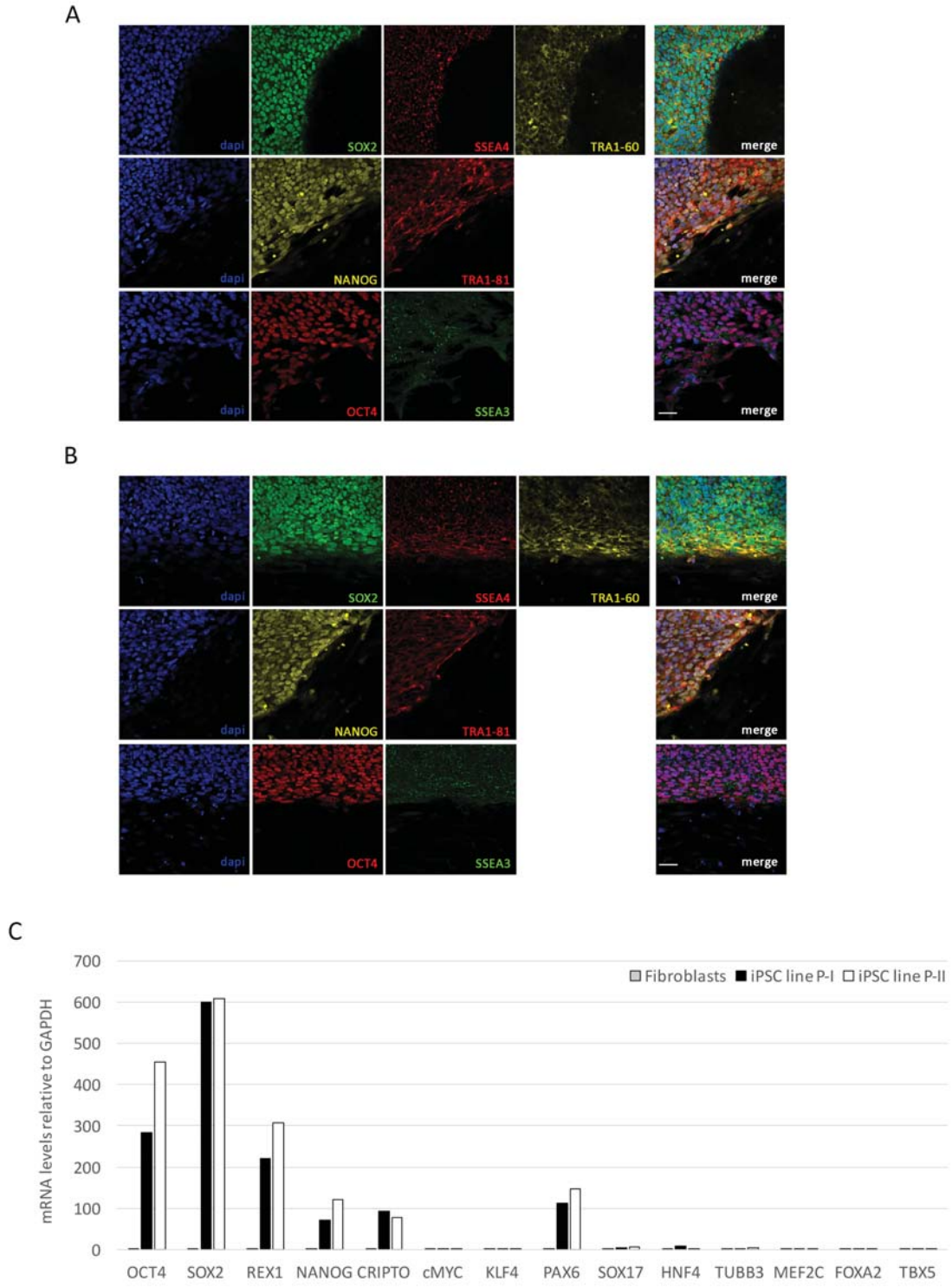

Figure 39. Analysis of the expression of pluripotency markers in iPSC lines.
Immunofluorescence analysis of iPSC lines P-I (A) and P-II (B) showing expression of typical pluripotent iPS cell markers such as the transcription factors OCT4, SOX2, NANOG and the cell surface markers SSEA3, SSEA4, TRA1-60 and TRA1-81. Objective: 25x oil-immersion. (C) RT-qPCR showing the expression relative to GAPDH of the pluripotency associated markers (OCT4, SOX2, REX1, NANOG, CRIPTO, cMYC, and KLF4) and markers for early differentiation into specific cell types (endoderm: SOX17, FOXA2; mesoderm: HNF4; ectoderm: PAX6, TUBB3; or cardiomyocytes: MEF2C, TBX5).

To finish their characterization, the following experiments need to be performed:

(i) Bisulfite pyrosequencing of the OCT4 and NANOG promoters for the determination of their methylation states. Promoters of pluripotency-associated genes are methylated in the original fibroblasts but almost completely demethylated in iPSC lines.

(ii) Karyotype analysis for the evaluation of genomic integrity.

(iii) Differentiation tests to demonstrate that the generated iPSCs can differentiate into the three germ layers of the embryo (endoderm, mesoderm and ectoderm). This can be shown via *in vitro* (via the formation of embryoid bodies) or *in vivo* (teratoma formation) tests.

(iv) DNA fingerprinting analysis for the verification that the iPSC lines are genetically matched to the donor cells.

DISCUSSION

1. Identification of the lysosomal pathway as involved in SAD

Oxidative stress and HSV-1 infection play critical roles in the pathogenesis of AD (Harris et al., 2015; Persson et al., 2014; Tonnies et al., 2017). In addition, other members of the herpesvirus family have been associated to AD—HSV-2, HHV6 and CMV (Harris et al., 2015; Kristen et al., 2015; Lin et al., 2002). Over the last years, our group has contributed to the growing number of experimental evidence supporting the damaging relationship of both factors. To study the molecular mechanisms involved in AD, we developed a neuronal cell model of mild OS and HSV-1 infection. We showed that HSV-1 induces the main AD-like neurodegenerative events, such as aberrant tau phosphorylation (Alvarez et al., 2012), autophagy impairment (Santana et al., 2012), altered trafficking and metabolism of APP protein and the accumulation of the β-amyloid peptide (Santana et al., 2012). We also showed that mild OS—induced by the X-XOD system—activates cholesterol synthesis (Recuero et al., 2009) and alters autophagy/lysosome system (Recuero et al., 2013). Finally, OS is able to enhance the neurodegenerative events associated with HSV-1 infection (Santana et al., 2013).

To identify genes and pathways altered by HSV-1 infection and OS that might be implicated in AD, microarray analyses were performed to profile global changes in gene expression modulated by HSV-1 and OS. The main objective of the present thesis was to identify genetic risk factors common for the sporadic and familial forms of the disease. Although the underlying causes for both forms are different, the clinical and pathological manifestations are very similar. They share the two pathological hallmarks of the disease—NFTs and SPs—and it is widely thought that both forms have similar molecular mechanisms. To generate a cell model of FAD (herein referred to as monogenic model), our laboratory developed a cell line, based on SK-N-MC cells, expressing human APP695 harbouring the Swedish mutation (APP_{swe}). We then compared the list of OS-modulated genes in our infection model with those obtained in our monogenic model and focused on the overlap between the two datasets. By doing so, a list of 68 genes was obtained. Although two time points (24 and 36 hpi) were prepared for analysis by microarrays, we focused on 24 hpi because this is the first time point at which expression is modulated in a significant number of genes and functional changes are just initiated (previous laboratory data). Since large amount of data were generated by such microarrays, bioinformatics tools were used to further analyse the lists of differentially expressed genes. These tools use statistical analyses to identify categories (like biological processes or functions) that are over- or underrepresented in a given condition. These data mining techniques revealed significant annotations to the lysosomal pathway (identified by two independent analyses, GeneCodis and IPA) and to a lesser extent to the metabolism of sterols (only with IPA). The five genes from our dataset that form part of the lysosomal pathway are involved in different aspects of this pathway: (i) *ATP6AP1* encodes for a component of the V-ATPase, though plays a role in V-ATPase-mediated acidification of acidic organelles. (ii) *CTSF* is

a member of the papain family of cysteine proteinases and is a component of the lysosomal proteolytic system. (iii) LAMP2 is one of the major lysosome-associated membrane proteins important for the protection, maintenance and adhesion of the lysosome. (iv) *LIPA* encodes a lysosomal acid lipase that catalyses the hydrolysis of cholesteryl esters and triglycerides. (v) NPC1 is primarily located to lysosomes and endosomes, and mediates intracellular cholesterol trafficking. Our findings are supported by several GWAS studies identifying polymorphisms associated with AD involved in endocytosis and lipid metabolism (Harold et al., 2009; Jones et al., 2010; Lambert et al., 2009) (Figure 2). Among them, *PICALM*, *SORL1*, CD2-associated protein (*CD2AP*), and bridging integrator 1 (*BIN1*) are those involved in endocytosis and *APOE*, *SORL1*, *CLU,* and *ABCA7,* are involved in lipid metabolism. How exactly they contribute to neurodegeneration is under intense investigation, but it has been already shown that some of these variations result in abnormal trafficking in the endo-lysosomal and autophagic networks (Cormont et al., 2003; Moreau et al., 2014). Interestingly, several of them—namely *APOE*, *ABCA7*, *CD2AP*, and *PICALM*—have been associated directly or indirectly with the herpes simplex life cycle supporting the implication of HSV-1 in AD pathogenesis (Licastro et al., 2011; Porcellini et al., 2010). The authors suggest that these genes (among others) cause a genetic signature that might affect the individual CNS ability to cope with and fight against invasion of herpesviruses. All these evidence from GWAS are in concordance with and confirm our results obtained from cellular models of AD, not only pointing to the lysosomal system as relevant pathway but also strengthen the hypothesis of a causal role for HSV-1 in AD. This concordance shows nicely that basic research based on cell models is adequate to study molecular mechanisms involved in complex diseases.

The link between lysosome dysfunction and neurodegeneration has been evidenced by numerous research groups and is still under intense investigation because of its great potential as pharmacological target (Appelqvist et al., 2013; Whyte et al., 2017). Neurons are especially vulnerable to lysosome dysfunction and rely deeply on functional autophagic and endocytic pathways because these postmitotic cells are otherwise unable to dilute debris and undigested material through cellular divisions. Their size and polarity add further difficulties since very long neurites force the cellular machinery to manage the transport of material to mature lysosomes over long distances (Neefjes et al., 2014). Abnormalities of the lysosomal system in AD include very early-appearing endosome enlargement, accumulation of autophagic vesicles, increased lysosome biogenesis and lysosomal proteolysis deficits (Nixon et al., 2011). Insights in disease-causing mechanisms associated to lysosomal failure came from observations in cell models for FAD. PSENs have been intensively studied because of their proteolytic action on APP within the γ-secretase complex. Additional γ-secretase-independent functions have been reported, including cellular signalling, intracellular calcium homeostasis, endo-lysosomal trafficking and autophagy (reviewed in Peric et al., 2015). PSEN-deficient cells show accumulation of autophagic vesicles

and multivesicular bodies (MVBs) (Dobrowolski et al., 2012), as well as defects in lysosomal acidification and degradation. These defects cumber the degradation of Aβ thereby favouring AD pathogenesis (Lee et al., 2010). Other authors reported compromised lysosomal calcium storage and release in PSEN-deficient cells and neurons causing lysosomal dysfunction (Coen et al., 2012). Taken together, these data support the role of the lysosomal pathway in FAD.

Lysosomal storage diseases (LSDs) are a group of disorders that are caused by dysfunction of lysosomal hydrolases or in a lesser extent by defective lysosomal membrane proteins (Filocamo et al., 2011). This leads to the accumulation of undigested material in compartments of the autophagic and endocytic machinery, along with the accumulation of autophagic and endocytic compartments themselves, resulting in the appearance of neurodegenerative phenotypes (Nixon et al., 2008). These abnormalities have also been reported in AD models and in our cell model of HSV-1 infection and OS, highlighting the implication of the lysosomal system in CNS pathologies and supporting the hypothesis that lysosomal dysfunction can cause the neurodegeneration induced by HSV-1 and OS.

2. Alterations of lysosomal function induced by HSV-1 and OS

To confirm the data of the functional genomic analysis indicating that the lysosomal pathway could be affected in our neuronal cell model, we studied different aspects of this pathway in depth. We first analysed the effect of HSV-1 and OS on the amount of lysosomal proteins. Our experiments showed that HSV-1 infection and OS increased the amount of the endo-lysosomal proteins Rab7, LAMP1 and LAMP2, suggesting increased lysosomal burden in these cells. In this respect, increased levels of these proteins were found in the cerebrospinal fluid (CSF) of AD patients (Armstrong et al., 2014), and Rab7 and LAMP1 have been previously reported to be upregulated in the AD brain (Barrachina et al., 2006; Ginsberg et al., 2010).

Another more quantitative method to measure lysosomal content is the use of lysosomotropic dyes. Two different ones were used—LysoSensor Green (LSG) and LysoTracker Red (LTR). The LSG fluorescence is pH-sensitive and can indicate not only changes in number but also in lysosomal pH. The maximum of LSG fluorescence is obtained close to the lysosomal pH. In contrast, LTR accumulates in cellular compartments with low internal pH but exhibits fluorescence largely independent of pH. HSV-1 infection increased the fluorescence intensity of both dyes confirming the increase of lysosomal burden induced by the infection. Accumulation of lysosomes is a well known hallmark of AD brains (Gowrishankar et al., 2015). OS only showed enhanced fluorescence of LTR, but had no effect on LSG fluorescence. These differences might be explained by the fact that OS is known to cause lysosomal membrane permeabilization, thereby releasing hydrolases from the lysosomal lumen into the cytosol and causing the alkalization of lysosomes (Johansson et al., 2010). In this context, a recent report showed that sub-lethal oxidative stress is

able to induce lysosome biogenesis and lysosomal membrane permeabilization in rat myoblasts (Leow et al., 2017). A possible scenario might be that X-XOD, which also induces a sub-lethal oxidative stress in our cell models, provokes an increase of lysosomal burden but at the same time increases lysosomal pH through the induction of lysosomal membrane permeabilization. Taken together, these results indicate that HSV-1 infection and OS increase lysosomal content. This could be either due to increased induction of lysosome biosynthesis or due to defective lysosomal clearance or a combination of both.

Given the increased number of lysosomes caused by HSV-1 and OS, we then focused on the effect of both stimuli on lysosomal proteolytic activity. The lysosome contains over 50 different hydrolases with particular importance of proteases. We found that HSV-1 infection significantly decreased activity of all analysed cathepsins (CTS B, K, S, and D/E). OS itself strongly reduced their activity as described previously by Porter et al. (2013). They observed decreased activities of serine, cysteine, and aspartyl protease activities, and defective cathepsin B maturation in trabecular meshwork cells (Porter et al., 2013). Numerous examples showing inhibition of lysosomal enzymatic activity by OS have been reported. Importantly, mutations in *CTS D* cause neuronal ceroid lipofuscinosis (NCL)—a human LSD with severe mental retardation and dementia, and *CTS F* and *D* deficiency in mice lead to a phenotype that resembles NCL (Koike et al., 2000; Tang et al., 2006). In addition, inhibition and/or loss of the cathepsins B and L lead to lysosomal dysfunction and accumulation of intracellular cholesterol and Aβ (Cermak et al., 2016). These findings indicate the importance of cathepsin activity for maintaining lysosomal function and preventing neurodegenerative processes.

The activity of the lysosomal hydrolase β-hexosaminidase is also reduced by HSV-1 infection and strongly inhibited by OS. In contrast, increased β-hexosaminidase activity was measured in skin fibroblasts from AD patients, presymptomatic individuals with FAD mutations (Emiliani et al., 2003; Pitto et al., 2005) and in the cortex of a murine model of FAD (Magini et al., 2015). However, there are several reports in line with our findings describing decreased activity of lysosomal enzymes in association with AD (recently reviewed in Whyte et al., 2017). Lysosomal hydrolases are synthesized as inactive precursors and activated during transport through endosomes to lysosomes by acidification and proteolysis (Repnik et al., 2012). HSV-1 and OS might affect their maturation, maybe due to interference with other proteases required for proteolytic cleavage. In agreement with this hypothesis, an alteration of endosomal trafficking mediated by the glycoprotein B of HSV-1 has recently been reported (Niazy et al., 2017). The analysis of cathepsins by Western blot using antibodies that recognize immature precursors and mature forms of the protein could help to elucidate if alterations in cathepsins maturation could be the case in our infection cell model. The activation of endogenous inhibitors of cathepsins could be another mechanism causing the reduction in their activity. To evaluate this option, we could measure if the

levels of natural cathepsin inhibitors—like cystatins—are modulated by HSV-1 and OS in our cell model. In conclusion, HSV-1 and OS were found to induce an increase of lysosomal burden that did not correlate with an increase of lysosome enzyme activity. By contrast, HSV-1 and OS severely impair the proteolytic activity of lysosomes.

Considering the significant decrease in lysosomal enzyme activities, enhancing lysosome efficiency might be a possible therapeutic strategy in AD. Genetic depletion of cystatin B—the natural inhibitor of cysteine proteases—rescues autophagic/lysosomal dysfunction and attenuates amyloidogenesis and related memory and cognitive deficits in an AD mouse model (Yang et al., 2011; Yang et al., 2014). Improvement of synaptic function has been described in APP transgenic mice by deletion of cystatin C—the endogenous inhibitor of cysteine proteases like CTS B—(Sun et al., 2008), overexpression of CTS B (Mueller-Steiner et al., 2006) or pharmacological stimulation of cysteine protease activities (Butler et al., 2011). These strategies are already under investigation in research and clinical trials for the treatment of several LSDs showing promising results (Schultz et al., 2011) and could be of great interest for the treatment of AD. In concordance, modulation of the transcription factor EB (TFEB) function—the master regulator of lysosomal biogenesis—has recently been suggested to be neuroprotective in different studies. Overexpression of TFEB reduced NFT pathology and rescued behavioural and synaptic deficits and neurodegeneration in mice (Polito et al., 2014) and promoted the clearance of intracellular Aβ42 in SH-SY5Y cells (Xiao et al., 2015). These studies support the implication of lysosomal dysfunction in neurodegeneration. We have already started to test the effects of TFEB overexpression in our SAD cell model. Preliminary results showed that HSV-1 infection enhanced the TFEB gene expression and affected the cellular distribution of TFEB provoking its translocation to the nucleus—a sign of TFEB activation (unpublished data from our laboratory). These data suggest that HSV-1 could increase lysosome biogenesis through the activation of TFEB pathway.

Defects in the endocytic pathway have also been associated with lysosomal dysfunction and were evaluated in our cell model. Moreover, impairment of this pathway is one of the earliest observations in AD (Peric et al., 2015). A popular method to analyse the endocytic pathway is to monitor the degradation of the EGF receptor (EGFR) upon stimulation by its ligand. After activation by EGF, the receptor-ligand complex is internalized and sent to endosomes. From there the complex reaches the lysosome for degradation, and the receptor is recycled back to the plasma membrane (Madshus et al., 2009). With the aim of studying the EGF-induced EGFR degradation in our cell model of infection, SK-N-MC cells were transfected with a pEGFR-c-myc expression plasmid due to the lack of expression of endogenous EGFR in SK-N-MC cells. In untreated cells, upon EGF stimulation, no differences in the EGFR levels were found. However, in HSV-1 infected cells, there was a strong accumulation of EGFR indicating a defect in EGFR degradation. The fact that no differences in the EGFR levels were observed in untreated cells could be related to EGFR

overexpression. In fact, ligand-induced EGFR degradation has a low capacity and the pathway is easily saturated (Lund et al., 1990; Wiley, 1988). The experiments regarding EGFR were therefore performed in another well known model by our group—HeLa cells. This cell line expresses EGFR and numerous reports of EGFR internalization and degradation have been published. Our results with HeLa cells showed that OS and HSV-1 strongly inhibit EGFR degradation stimulated by EGF, indicating that under those conditions lysosomal degradation was impaired. This might be explained by HSV-1 and OS-induced defects in endocytic trafficking. In this sense, overexpression of HSV-1 glycoprotein B cause an impairment of the endosomal trafficking (Niazy et al., 2017). To measure if the EGFR reaches the lysosome, confocal microscopy experiments were performed. The results revealed colocalization of EGFR with late endosomes in HSV-1 infected cells suggesting that the final step of this pathway—probably the fusion of late endosomes with lysosomes—is altered. The fusion of lysosomes with autophagosomes is also deeply altered in HSV-1 infected cells (Santana et al., 2012) indicating that both pathways converging in the lysosome are not able to deliver cargo to the lysosome causing accumulation of autophagosomes and endosomes in our infection model. This hypothesis is supported by a study from Coen et al. (2012). They observed defective endosome-lysosome fusion in PSEN-deficient cells. In their view, altered lysosomal calcium storage and release is the primary cause of these fusion defects that subsequently cause endosome accumulation. It would be interesting to explore alterations in lysosomal calcium in our cell model to evaluate if HSV-1 and OS affect calcium homeostasis. Considering that APP and APOE—two important players in AD etiology—are localized in endocytic compartments, it is not surprising that the observed fusion defects might contribute to neurodegeneration. Accordingly, endosomal alterations have been observed in pyramidal neurons of AD patients (Cataldo et al., 1997). They observed accumulation of enlarged endosomes and altered trafficking of hydrolase-containing endosomes leading to accelerated β-amyloidogenesis. In conclusion, the lysosomal alterations found in our cell model, like increased lysosomal burden, decreased activity of several lysosomal hydrolases and defective endocytosis-mediated EGFR degradation provoked by HSV-1 and OS, validate our results obtained from the functional genomic analysis pointing to the lysosome as the main altered pathway. In addition, these alterations induced by HSV-1 and OS might contribute to neurodegeneration by increasing Aβ production and tau phosphorylation and decreasing degradation of toxic aggregates.

The second pathway enriched in our data set from microarray analysis was the metabolism of sterols. Previous data from our group showed that OS induces cholesterol biosynthesis and that polymorphisms in *HMGCR*—the rate-limiting enzyme for cholesterol synthesis—are associated with AD risk (Recuero et al., 2009). Cholesterol is the major source of sterols in mammals and numerous studies suggest that cholesterol homeostasis alterations could be causing the lysosomal dysfunction observed early in neurodegeneration, in particular in AD (Chen et al., 2014). In diverse

LSDs, cholesterol accumulates in endo-lysosomal membranes affecting either the lysosome ability to fuse with endocytic or autophagic vesicles, maturation of autophagosomes or lysosomal proteolysis (Fraldi et al., 2010; Maetzel et al., 2014). All these evidence links cholesterol homeostasis and lysosomal dysfunction motivating us to investigate whether changes in lysosomal cholesterol levels could be causing the lysosomal defects in our cell models.

To evaluate cholesterol levels in our cell models two different methods were applied. First, a quantitative enzymatic assay measuring cellular unesterified cholesterol and second, filipin staining to visualise free cholesterol by fluorescence microscopy. Our results show that HSV-1 infection caused a significant increase of cholesterol levels, a trend that was not potentiated by the addition of OS. On the other hand, OS alone did not modify significantly the amount of cellular cholesterol. In addition, filipin experiments revealed the accumulation of cholesterol in intracellular compartments in cells exposed to HSV-1 and OS. These data suggest that HSV-1 infection affects cholesterol homeostasis more than OS does. To date, there are few reports linking herpes virus infections with alterations of cholesterol homeostasis. HSV-1 infection impaired the cholesterol metabolism of human arterial smooth muscle cells producing accumulation of cholesteryl esters (Hajjar et al., 1987). Accordingly, another study reported altered cholesterol trafficking in HSV-1 infected arterial smooth muscle cells (Hsu et al., 1995).

Filipin staining indicated that in untreated control cells most of the cell free cholesterol is located to the plasma membrane. In contrast, HSV-1 and OS treated cells showed a filipin staining pattern similar to that seen in Bafilomycin A1 treated cells. Bafilomycin A1 specifically inhibits the V-ATPase thereby blocking lysosomal acidification causing cholesterol accumulation in endo-lysosomal compartments (Furuchi et al., 1993). These results suggest that HSV-1 and OS cause cholesterol accumulation in compartments of the endo-lysosomal pathway. To further verify this hypothesis, double labelling of cells with filipin and diverse markers specific for compartments of this pathway will be done. All these evidence drove us to focus on lysosomal cholesterol levels in our cell model. Furthermore, the fact that cellular cholesterol is mainly located to the plasma membrane could disguise small changes in lysosomal cholesterol levels. Therefore we adapted a protocol for the partial purification of lysosomes. Analysis of the fraction enriched in lysosomal membranes showed increased cholesterol after HSV-1 infection. These results are in concordance with those obtained for total cholesterol levels, although the HSV-1-induced increase of lysosomal cholesterol is higher than of total cholesterol amount (166% and 116%, respectively). In this sense, cholesterol and other lipids accumulate in several LSDs and have been proposed to be causative for lysosomal dysfunction (Sobo et al., 2007; Walkley et al., 2009) and impairment of endocytic pathways (Rappaport et al., 2016). In two severe neurodegenerative LSDs—multiple sulphatase deficiency and mucopolysaccharidosis type IIIA—the accumulation of cholesterol alters the organisation of endo-lysosomal membranes affecting the fusion of lysosomes with endosomes and

with autophagic vesicles (Fraldi et al., 2010). These autophagic defects have also been reported in our infection cell model (Santana et al., 2012) supporting an active role of cholesterol accumulation in the vesicular fusion defects induced by HSV-1 and OS. Also, in Niemann-Pick disease C1 (NPC1) the primary accumulation of sphingosine causes altered calcium homeostasis, what in turn causes the secondary accumulation of sphingolipids and cholesterol inhibiting the endocytic pathway (Lloyd-Evans et al., 2008). In conclusion, our data support the hypothesis that altered cholesterol homeostasis could be one of the mechanisms causing the lysosomal dysfunction induced by HSV-1 infection and OS.

High levels of neuronal cholesterol have been linked to the appearance of AD-like neurodegeneration markers (Djelti et al., 2015; Xue-shan et al., 2016). Pharmacological modulation of cholesterol might therefore be a therapeutic target for the neurodegenerative events produced by HSV-1 and OS. Indeed, administration of the cholesterol-lowering drug 2-hydroxypropyl-beta-cyclodextrin (HP-β-cyclodextrin) is proposed as potential therapeutic tool in NPC1 and AD (Aqul et al., 2011; Yao et al., 2012). The neuroprotective effects of HP-β-cyclodextrin are mediated by reduced Aβ production and enhanced clearance mechanisms (Yao et al., 2012). Lovastatin—an inhibitor of cholesterol synthesis—also suppressed the aberrant tau phosphorylation induced by okadaic acid and FTDP-17 mutations in cultured rat primary neurons (Li et al., 2015). To test the hypothesis that cholesterol depletion might attenuate lysosomal impairment and the neurodegenerative events induced by HSV-1 and OS, the modulation of cholesterol levels in our cell models is required. Reduction of cholesterol levels will be accomplished with methyl-β-cyclodextrin (MβCD; a cholesterol-binding agent) or lovastatin and increased lysosomal cholesterol will be reached with U18666A (an inhibitor of endo-lysosomal cholesterol export). The optimisation of these agents in our cell models has already been initiated.

3. Role of LAMP2 in AD-like neurodegeneration induced by HSV-1 and OS

So far, the results obtained in this thesis are drawn from *in vitro* experiments with cell models mimicking SAD. In this way, microarray analyses pointed to the lysosomal pathway as important player in the neurodegenerative events in our infection cell model and identified a list of putative candidates that might mediate the HSV-1 and OS-induced damage. Here, LAMP2 was among the most strongly modulated ones. An important question is whether the candidates discovered in the cell models are involved in the "real" disease. The access of our group to case/control samples helped us to confirm some *in vitro* results with actual data from AD patients. Genetic association studies suggested the implication of *LAMP2* in SAD confirming the validity/outcome of our cell model experiments. Our results showed significant association for LAMP2 with males, with increased risk for APOE-ε4 carriers. These results will be replicated in an

additional sample of 10,000 cases/controls, available through our association to Dementia Genetics Spanish Consortium (DEGESCO).

These findings are interesting because they point to a potential molecular mechanism involved in the consistently reported gender difference on genetic susceptibility to AD. Since *LAMP2* is located on the X chromosome, it is tempting to speculate that the preferential association in men that we observe could be attributed to the fact that males are "hemizygous" for *LAMP2*. In this sense, a recent study reported the role of autophagy in some paradigmatic human diseases (cancer, neurodegenerative, autoimmune, cardiovascular) and the presence of 'cell sex' differences. In this review they provided evidence that the involvement of the autophagic pathway in neurodegenerative diseases is gender-dependent (Lista et al., 2011). Further, a study on neuronal cells exposed to nutrient starvation showed that neurons from males more readily undergo autophagy and die, whereas neurons from females mobilize fatty acids, accumulate triglycerides, form lipid droplets and survive longer, and suggested that autophagic response could be gender and tissue specific (Du et al., 2009). Although more data are needed to confirm our current genetic association results, the study of the molecular basis of gender differences in AD prevalence and clinical expression is undoubtedly of great interest since not only the prevalence (Genin et al., 2011), but also the clinical and neuropathological manifestations (Gallart-Palau et al., 2016; Lin et al., 2015) and response to treatments differ between men and women. The effect of gender on AD susceptibility is especially intriguing in the context of our project considering that HSV-1, like AD, appears to have a preference for the female gender (reviewed in Itzhaki, 2014).

To strengthen the hypothesis for a causal role of HSV-1, it would be of great value to know whether the study subjects have HSV-1 in their brains, especially in combination with their genetic background like *LAMP2* and *APOE* genotype. However, this observation can only be performed post-mortem, since there are no available tools for *in vivo* detection of the virus in the brain. Moreover, the mere presence of the virus would not demonstrate its pathogenicity, and several factors must be taken into account to determine it: the brain area where the virus is located, the state of infection (latent or lytic), the strain and genotype of the virus and the genotype of the host. In summary, proving a causal role for HSV-1 is a hard task, as occurs for virtually all the infectious agents claimed to be involved in chronic diseases. However, there are methods to check for HSV-1 infection both in the periphery (HSV-1 specific IgG and IgM antibodies in plasma/sera) and in CSF (viral DNA and IgG/IgM specific antibodies) (Letenneur et al., 2008; Lovheim et al., 2014) and although these detections do not demonstrate that HSV-1 has reached the CNS, they allow studying the correlation between the infection state and neurodegeneration signals in patients. We have started the study of these markers in a small number of the individuals from our case/control cohort, whose samples were obtained, and these preliminary data are in line with the higher plasma IgM levels in patients reported by Letenneur et al., 2008. In the near future, we plan to extend the

analysis to a larger number of samples, mainly through collaborations in the context of the DEGESCO consortium.

LAMP2 is known as one of the most abundant membrane proteins of the lysosome. Together with LAMP1 they constitute about half of all proteins of the lysosomal membrane, but little is known about their function (Endo et al., 2015; Eskelinen, 2006). Both are transmembrane proteins with a highly glycosylated luminal domain, a single transmembrane domain and a C-terminal cytoplasmic tail. The molecular mass of LAMP2 is about 45 kDa, however with the glycosylation it raises up to 120 kDa (Carlsson et al., 1988; Mane et al., 1989). Alternative splicing of *LAMP2* generates three isoforms, LAMP2A, -2B and -2C (Eskelinen et al., 2005). LAMP2A was identified as the receptor in the lysosomal membrane for substrate proteins of chaperone-mediated autophagy (CMA) (Kaushik et al., 2012). Mutations in *LAMP2* cause Danon disease, a X-linked disorder characterized by hypertrophic cardiomyopathy and mental retardation (Endo et al., 2015).

To further understand their functions, researchers created LAMP1 and LAMP2 single or double deficient cell and animal models. Interestingly, LAMP2 single deficiency is more severe than LAMP1 single deficiency and replicates the phenotype observed in Danon disease patients in mice, like accumulation of autophagic vesicles in heart and skeletal muscle (Saftig et al., 2001). More recently, the work with KO mice revealed that LAMP2 deficiency leads to impaired phagosomal maturation in neutrophils causing periodontitis (Beertsen et al., 2008). Actually, this clinical outcome is caused by deficient fusion between phagosomes and lysosomes in affected animals. Given the severe LAMP2 KO phenotype, it is not surprising that double deficient animals present embryonic lethality at day 15.5. Absence of both LAMPs prevent the recruitment of late endosomal/lysosomal markers (Huynh et al., 2007). Another study indicated a role of LAMP2 in fusion events between autophagosomes and lysosomes. In this context, LAMP2 is required for syntaxin-17 (STX17) expression by the autophagosomes and subsequent interaction with VAMP8 on lysosomes to mediate the fusion (Hubert et al., 2016). It is interesting to note that a role for LAMP2 in endo-lysosomal cholesterol transport has been suggested (Schneede et al., 2011). Probably, LAMP2 is required for cholesterol transport out late endosomes/lysosome and towards the ER for esterification. While MEFs deficient in LAMP2 showed accumulation of unesterified cholesterol in late endosomes/lysosomes, LAMP1-deficient MEFs did not (Eskelinen et al., 2004). A recent report demonstrated that LAMP2 is able to bind cholesterol directly and this capacity facilitates the cholesterol export from lysosomes (Li et al., 2016).

LAMP2 is localized on the X chromosome, and mutations in LAMP2 consequently affect male and females in a gender-dependent manner. The facts that AD prevalence and clinical outcome are also gender-dependent (Genin et al., 2011; Lin et al., 2015) and HSV-1 infection

seems to affect more likely to females (Itzhaki, 2014) support the hypothesis of a possible implication of this gene in HSV-1-induced AD-like neurodegenerative events. In relation with pathogens, LAMP proteins have been shown to be necessary for microbicidal activity of phagosomes and LAMP double deficient fibroblasts were unable to digest *Neisseria*-containing phagosomes (Binker et al., 2007). Recent reports revealed LAMP2 as a target by viral proteins of the human immunodeficiency virus (HIV) and influenza A virus causing impairment of the lysosomal activity (Fields et al., 2015; Ju et al., 2015).

In summary, our results show that LAMP2 expression is significantly upregulated in our cell model of infection and OS and *LAMP2* gene is associated with a higher risk for AD. In addition, LAMP2 is able to modulate lysosomal function through different mechanisms including the transport of cholesterol and the fusion between autophagosomes and lysosomes. These data highlight the importance of LAMP2 for proper lysosomal function and supports our decision to study this candidate in relation to HSV-1-induced lysosomal dysfunction and neurodegeneration.

To study whether LAMP2 is involved in the lysosomal dysfunction and AD-like neurodegenerative events induced by HSV-1 in our cell model, we generated LAMP2-deficient SK-N-MC cells. Although the commercial shRNAs used in this study were validated and should achieve a ~90% reduction in LAMP2 expression, we did not obtain any LAMP2-deficient cell lines with such efficient gene silencing (the strongest effect was a 67% reduction). Given the 90% reduction of LAMP2 protein levels in LAMP2-deficient N2a cells and the genetic deletion of LAMP2 in MEF cells derived from LAMP2 KO mice, we initiated the experiments in these two murine cell lines. As a first characterization step, the effect of LAMP2 deficiency on HSV-1 infection was evaluated and showed that the lack of LAMP2 reduces HSV-1 infection efficiency. In LAMP2-deficient cells, less viral DNA and proteins were observed, as well as less infectious particles suggesting that LAMP2 might affect HSV-1 viral cycle. Further experiments need to be done in order to confirm this hypothesis. As mentioned before, LAMPs have been targeted by viral proteins of several viruses, like HIV and influenza A virus (Fields et al., 2015; Ju et al., 2015). To our knowledge, no interactions between HSV proteins and LAMPs have been reported. The fact that LAMP2 deficiency causes a less effective infection in our cells, however, might suggest otherwise. To check if LAMP2 could be interacting directly with HSV-1 proteins, co-immunoprecipitation (Co-IP) experiments and in situ proximity ligation assays (PLAs) will be performed. Nevertheless, impairment of HSV-1 infection induced by LAMP2 deficiency could affect the neurodegenerative events induced by the virus.

Cholesterol, as a major component of plasma membranes, is necessary for herpesvirus entry into the cells (Bender et al., 2003; Rahn et al., 2011). The absence of LAMP2 could cause cholesterol alterations and might reduce the virus ability to enter the cells. Beyond entry, HSV-1 transcription and infectivity are also affected by cholesterol changes (Wudiri et al., 2014).

Pharmacological depletion of cholesterol by MβCD reduced plaque numbers in Vero cells (Wudiri et al., 2017). In line, LAMP2-deficient cells showed lower extracellular viral titer that might in part be caused by cholesterol alterations. To investigate this hypothesis, measurements of total and lysosomal cholesterol levels in LAMP2-deficient cells could provide further insight. Since the methods for cholesterol quantification and the partial purification of lysosomes are already standard protocol at our laboratory, these experiments will be initiated shortly. Additionally, levels and cellular distribution of cholesterol will be studied by microscopy experiments using filipin staining of the cells. The pharmacological modulation of cellular cholesterol levels will also be performed to see if the HSV-1-induced phenotype can be rescued by cholesterol depletion.

Then, the impact of HSV-1 and OS on LAMP2 expression was also checked. In wt MEF and N2a cells, OS increased LAMP2 protein levels in all conditions tested and HSV-1 infection also induced an increment of LAMP2 levels in wt MEF cells, reproducing the results obtained in SK-N-MC cells. However, HSV-1 infection provoked a reduction of LAMP2 expression in a dose-dependent manner in N2a cells. The HSV-1-induced decrease of LAMP2 levels in N2a cells is in contrast to the increase of lysosomal burden and LAMP2 levels in SK-N-MC cells provoked by the virus. Gene expression analysis also reported upregulation of LAMP2 by OS and HSV-1 in two independent methods (microarray and RT-qPCR). This discrepancy might be explained by the presence of cell-type specific effects.

The neurodegenerative effects of HSV-1 infection in SK-N-MC cells are well known by our group. To see if these effects can be reproduced in MEF and N2a cells and evaluate if a differential response in LAMP2-deficient cells takes place, we started analysing Aβ, tau phosphorylation and LC3-II levels in both murine cell lines. Preliminary results confirm that the HSV-1-induced neurodegeneration was also observed. HSV-1 infection provoked increased levels of phosphorylated tau, accumulation of intracellular Aβ42 and the autophagic marker LC3-II, and an inhibition of the secretion of Aβ40 and Aβ42. Moreover, HSV-1 also diminished the activity of lysosomal hydrolases. Thus, these cell models fully recapitulate the pathologic markers found in HSV-1 infected SK-N-MC cells, and are appropriate to assess the role of LAMP2 in the HSV-1-induced neurodegeneration.

Preliminary results showed no significant differences in wt and LAMP2-deficient MEF and N2a cells suggesting that LAMP2 is not implicated in the generation of the AD-like neurodegenerative events. However, it is too soon to reach any conclusions. Some of the experiments lack replicates to reach statistical power and those might reveal subtle differences not detected so far. Also, the experiments will be performed under different infection conditions. Lower viral dose and extended incubation times might reveal alterations that are not present in the current approach. The fact that LAMP2 deficiency causes a lower production of infectious particles

indicates that, if LAMP2 is implicated in HSV-1-mediated neurodegeneration, changes might be observed at later time points when a full replication cycle has been completed. Furthermore, only LAMP2-deficient cells have been analysed so far. The opposite approach—LAMP2 overexpression—might be useful to elucidate the role of LAMP2. Therefore, an additional SK-N-MC cell line overexpressing LAMP2 will be generated. HSV-1 infection efficiency, lysosomal alterations, and AD-like neurodegeneration markers will be studied in this model of LAMP2 overexpression.

4. Generation of patient-specific iPSCs

During the development of this thesis the generation of iPSCs was initiated. This model will be used to reproduce the results in a more physiological model. The discovery of defined factors that can reprogram somatic cells into iPSCs is a relatively recent development celebrating its 10 years anniversary. In 2006, Yamanaka's group published the combination of four factors sufficient for reprogramming mouse fibroblasts—OCT3/4, SOX2, cMYC, and KLF4 (Takahashi et al., 2006)—and only one year later they proved the concept valuable as well for human fibroblasts (Takahashi et al., 2007). The cocktail of these four factors is commonly known as the Yamanaka factors. The great potential of this method for modelling and investigating human disease, as well as drug screening was quickly noted. To date, hundreds of established cell lines from patients with familial and sporadic AD, Parkinson's disease, and many other diseases were published (summarised in Mungenast et al., 2016).

We started the generation of two individual iPSC lines from each subject—one SAD patient and one age-matched control. After the successful generation of fibroblasts from skin biopsies, those were reprogrammed by delivery of the Yamanaka factors with Sendai virus (SeV) vectors. Initially, the stepwise morphological changes were observed as expected and colonies emerged giving rise to individual iPSC lines. Before their characterization, each line was passaged more than 10 times to make sure the SeV vectors were eliminated from the cells. In this period of time, the cell lines derived from the control individual showed differentiated cells inside the colonies indicating a not fully reprogrammed state. The exogenous expression of the Yamanaka factors might have caused the initial iPSC-like phenotype. However, cell lines were positive for TRA1-60, a marker for pluripotency, which was not one of the initial transduced factors indicating that some of the cellular endogenous battery of pluripotent genes was temporally stimulated. The appearance of only partial reprogrammed colonies is quite common during the establishment of individual human iPSC lines. Literature states that age and source of the cell type strongly influence reprogrammability and that fibroblasts show a high background of non-iPSC colonies (Lowry et al., 2008). The reprogramming efficiency of the used method was estimated to vary between 0.01 and 1%. However, extraction of a skin biopsy is a non-invasive procedure for the

donor and was considered as the only feasible option within this thesis project. Further, many other factors are important for reprogramming efficiency and successful growing, like delivery method of the defined factors, passage skills, culture conditions, quality of feeder cells, etc. (discussed in Maherali et al., 2008). Since reprogramming efficiency in general is still very low, a new concept has evolved avoiding the pluripotent state and directly converting somatic cells into another cell lineage by chemical factors. This method is called direct reprogramming. In 2012 researchers successfully generated neuronal-like cells directly from human fibroblasts (Ladewig et al., 2012). Recently, two studies reported the direct conversion of fibroblasts into neurons obtained from AD (Hu et al., 2015) or Huntington's disease (Liu et al., 2014) patients. Direct reprogramming as alternative method should be taken into consideration.

However, the two patient-derived cell lines under characterization confirmed their pluripotent state in the experiments performed so far. Both—immunofluorescence and RT-qPCR—showed the expression of pluripotent markers. Further, the mRNA levels of markers characteristic for differentiation were negative confirming the pluripotency of these cell lines. Several tests still have to be performed before characterization is complete, but so far it seems like the generated iPSC lines are adequate for further investigations.

These cell lines will be used to characterize their response to HSV-1 infection and OS. We will evaluate if there are differences in the lysosomal alterations and AD-like neurodegenerative events induced by HSV-1 and OS between control- and patient-derived cells. These experiments will be performed either with iPSCs directly or after their differentiation into neurons.

CONCLUSIONS

The results obtained in the present thesis permit the following conclusions to be drawn:

1. Oxidative stress modulates the expression of a set of genes in a human neuronal cell line infected with HSV-1 (as a model of sporadic AD) or harbouring the APP Swedish mutation (as a model of familial AD). Functional enrichment analysis of these genes identified the impairment of the lysosomal pathway as a putative common pathogenic mechanism for sporadic and familial Alzheimer's disease.
2. The functional analysis of the lysosomal pathway in the sporadic AD cell model showed that several aspects of the lysosomal system were severely altered. HSV-1 and oxidative stress increased lysosomal burden and decreased the degradative activity of the lysosomal system. These results suggest that the lysosomal dysfunction observed could underlay the AD-like neurodegeneration induced by HSV-1 and oxidative stress.
3. The intracellular accumulation of cholesterol, likely in endo-lysosomal compartments, induced by HSV-1 and oxidative stress indicates that alterations of cholesterol homeostasis might be one of the mechanisms involved in the lysosomal dysfunction induced by HSV-1 and oxidative stress.
4. Genetic association studies identified common variants in the lysosomal-associated membrane protein 2 (*LAMP2*) gene as putative risk factors for sporadic AD pointing to LAMP2 as a suitable candidate to participate in the lysosomal alterations and the neurodegeneration events induced by HSV-1 and oxidative stress.
5. HSV-1 induced the appearance of the main AD-like neurodegenerative markers in wildtype and LAMP2-deficient murine embryonic fibroblasts and murine neuroblastoma N2a cells, including the phosphorylation of tau and the accumulation of intracellular Aβ. In addition, LAMP2 deficiency did not affect the neurodegenerative events induced by HSV-1, at least during the first infection viral cycle, but strongly reduced the efficiency of the infection.

CONCLUSIONES

El trabajo experimental realizado en esta tesis ha permitido obtener las siguientes conclusiones:

1. El estrés oxidativo modula la expresión de un conjunto de genes en células neuronales humanas infectadas con HSV-1 (como modelo de la EA esporádica) y en células portadoras de APP con la mutación "sueca" (como modelo de la EA familiar). El análisis bioinformático de enriquecimiento funcional de estos genes identificó la vía lisosomal como un posible mecanismo patogénico común en las formas familiar y esporádica de la enfermedad.

2. El estudio funcional de la vía lisosomal en el modelo celular de EA esporádica mostró que varios aspectos del sistema lisosomal están fuertemente alterados. La infección por HSV-1 y el estrés oxidativo aumentan los niveles lisosomales pero disminuyen la actividad degradativa de los lisosomas. Estos resultados sugieren que la disfunción lisosomal podría estar implicada en la neurodegeneración inducida por HSV-1 y el estrés oxidativo.

3. La acumulación intracelular de colesterol, probablemente en compartimentos endo-lisosomales, inducida por HSV-1 y el estrés oxidativo indica que la alteración de la homeostasis del colesterol podría constituir uno de los mecanismos implicados en la disfunción lisosomal inducida por estos dos factores.

4. Estudios de asociación genética señalan a variantes comunes en el gen de la proteína de membrana asociada al lisosoma 2 (*LAMP2*) como un posible factor de riesgo para la EA esporádica. Estos datos sugieren que LAMP2 podría ser un candidato idóneo para mediar la disfunción lisosomal y la neurodegeneración inducida por HSV-1 y el estrés oxidativo.

5. HSV-1 induce la aparición de los principales marcadores de neurodegeneración característicos del alzhéimer, incluyendo la fosforilación de tau y la acumulación intracelular de Aβ, en fibroblastos embrionarios de ratón y células de neuroblastoma murino N2a control y deficientes en LAMP2. Además, la deficiencia de LAMP2 no afecta a los eventos de neurodegeneración inducidos por HSV-1, al menos durante el primer ciclo de replicación viral, aunque sí reduce significativamente la eficiencia de infección.

REFERENCES

Aizenstein, H.J., R.D. Nebes, J.A. Saxton, J.C. Price, C.A. Mathis, N.D. Tsopelas, S.K. Ziolko, J.A. James, B.E. Snitz, P.R. Houck, W. Bi, A.D. Cohen, B.J. Lopresti, S.T. DeKosky, E.M. Halligan, and W.E. Klunk, *Frequent amyloid deposition without significant cognitive impairment among the elderly.* Arch Neurol, 2008. **65**(11): p. 1509-17.

Almeida, C.G., R.H. Takahashi, and G.K. Gouras, *Beta-amyloid accumulation impairs multivesicular body sorting by inhibiting the ubiquitin-proteasome system.* J Neurosci, 2006. **26**(16): p. 4277-88.

Alonso, A.C., I. Grundke-Iqbal, and K. Iqbal, *Alzheimer's disease hyperphosphorylated tau sequesters normal tau into tangles of filaments and disassembles microtubules.* Nat Med, 1996. **2**(7): p. 783-7.

Alonso, A.C., T. Zaidi, I. Grundke-Iqbal, and K. Iqbal, *Role of abnormally phosphorylated tau in the breakdown of microtubules in Alzheimer disease.* Proc Natl Acad Sci U S A, 1994. **91**(12): p. 5562-6.

Alonso, A.D., I. Grundke-Iqbal, H.S. Barra, and K. Iqbal, *Abnormal phosphorylation of tau and the mechanism of Alzheimer neurofibrillary degeneration: sequestration of microtubule-associated proteins 1 and 2 and the disassembly of microtubules by the abnormal tau.* Proc Natl Acad Sci U S A, 1997. **94**(1): p. 298-303.

Alonso, R., D. Pisa, A.I. Marina, E. Morato, A. Rabano, and L. Carrasco, *Fungal infection in patients with Alzheimer's disease.* J Alzheimers Dis, 2014. **41**(1): p. 301-11.

Alvarez, G., J. Aldudo, M. Alonso, S. Santana, and F. Valdivieso, *Herpes simplex virus type 1 induces nuclear accumulation of hyperphosphorylated tau in neuronal cells.* J Neurosci Res, 2012. **90**(5): p. 1020-9.

Andersen, J.K., *Oxidative stress in neurodegeneration: cause or consequence?* Nat Med, 2004. **10 Suppl**: p. S18-25.

Appelqvist, H., P. Waster, K. Kagedal, and K. Ollinger, *The lysosome: from waste bag to potential therapeutic target.* J Mol Cell Biol, 2013. **5**(4): p. 214-26.

Aqul, A., B. Liu, C.M. Ramirez, A.A. Pieper, S.J. Estill, D.K. Burns, B. Liu, J.J. Repa, S.D. Turley, and J.M. Dietschy, *Unesterified cholesterol accumulation in late endosomes/lysosomes causes neurodegeneration and is prevented by driving cholesterol export from this compartment.* J Neurosci, 2011. **31**(25): p. 9404-13.

Armstrong, A., N. Mattsson, H. Appelqvist, C. Janefjord, L. Sandin, L. Agholme, B. Olsson, S. Svensson, K. Blennow, H. Zetterberg, and K. Kagedal, *Lysosomal network proteins as potential novel CSF biomarkers for Alzheimer's disease.* Neuromolecular Med, 2014. **16**(1): p. 150-60.

Arriagada, P.V., J.H. Growdon, E.T. Hedley-Whyte, and B.T. Hyman, *Neurofibrillary tangles but not senile plaques parallel duration and severity of Alzheimer's disease.* Neurology, 1992. **42**(3 Pt 1): p. 631-9.

Aubert, M. and J.A. Blaho, *Modulation of apoptosis during herpes simplex virus infection in human cells.* Microbes Infect, 2001. **3**(10): p. 859-66.

Avila, J., *Tau aggregation into fibrillar polymers: taupathies.* FEBS Lett, 2000. **476**(1-2): p. 89-92.

Avila, J., J.J. Lucas, M. Perez, and F. Hernandez, *Role of tau protein in both physiological and pathological conditions.* Physiol Rev, 2004. **84**(2): p. 361-84.

Avrahami, L., D. Farfara, M. Shaham-Kol, R. Vassar, D. Frenkel, and H. Eldar-Finkelman, *Inhibition of glycogen synthase kinase-3 ameliorates beta-amyloid pathology and restores lysosomal acidification and mammalian target of rapamycin activity in the Alzheimer disease mouse model: in vivo and in vitro studies.* J Biol Chem, 2013. **288**(2): p. 1295-306.

Avrahami, L., D. Farfara, M. Shaham-Kol, R. Vassar, D. Frenkel, and H. Eldar-Finkelman, *Inhibition of Glycogen Synthase Kinase-3 Ameliorates β-Amyloid Pathology and Restores Lysosomal Acidification and Mammalian Target of Rapamycin Activity in the Alzheimer Disease Mouse Model: IN VIVO AND IN VITRO STUDIES.* The Journal of Biological Chemistry, 2013. **288**(2): p. 1295-1306.

Barrachina, M., T. Maes, C. Buesa, and I. Ferrer, *Lysosome-associated membrane protein 1 (LAMP-1) in Alzheimer's disease.* Neuropathol Appl Neurobiol, 2006. **32**(5): p. 505-16.

Beertsen, W., M. Willenborg, V. Everts, A. Zirogianni, R. Podschun, B. Schroder, E.L. Eskelinen, and P. Saftig, *Impaired phagosomal maturation in neutrophils leads to periodontitis in lysosomal-associated membrane protein-2 knockout mice.* J Immunol, 2008. **180**(1): p. 475-82.

Bender, F.C., J.C. Whitbeck, M. Ponce de Leon, H. Lou, R.J. Eisenberg, and G.H. Cohen, *Specific association of glycoprotein B with lipid rafts during herpes simplex virus entry.* J Virol, 2003. **77**(17): p. 9542-52.

Bertram, L., C.M. Lill, and R.E. Tanzi, *The genetics of Alzheimer disease: back to the future.* Neuron, 2010. **68**(2): p. 270-81.

Billings, L.M., S. Oddo, K.N. Green, J.L. McGaugh, and F.M. LaFerla, *Intraneuronal Abeta causes the onset of early Alzheimer's disease-related cognitive deficits in transgenic mice.* Neuron, 2005. **45**(5): p. 675-88.

Binker, M.G., L.I. Cosen-Binker, M.R. Terebiznik, G.V. Mallo, S.E. McCaw, E.L. Eskelinen, M. Willenborg, J.H. Brumell, P. Saftig, S. Grinstein, and S.D. Gray-Owen, *Arrested maturation of Neisseria-containing phagosomes in the absence of the lysosome-associated membrane proteins, LAMP-1 and LAMP-2.* Cell Microbiol, 2007. **9**(9): p. 2153-66.

Bjorkhem, I., *Crossing the barrier: oxysterols as cholesterol transporters and metabolic modulators in the brain.* J Intern Med, 2006. **260**(6): p. 493-508.

Bjorkhem, I., *Five decades with oxysterols.* Biochimie, 2013. **95**(3): p. 448-54.

Bowman, E.J., A. Siebers, and K. Altendorf, *Bafilomycins: a class of inhibitors of membrane ATPases from microorganisms, animal cells, and plant cells.* Proc Natl Acad Sci U S A, 1988. **85**(21): p. 7972-6.

Bradshaw, M.J. and A. Venkatesan, *Herpes Simplex Virus-1 Encephalitis in Adults: Pathophysiology, Diagnosis, and Management.* Neurotherapeutics, 2016. **13**(3): p. 493-508.

Braulke, T. and J.S. Bonifacino, *Sorting of lysosomal proteins.* Biochim Biophys Acta, 2009. **1793**(4): p. 605-14.

Brown, W.J., J. Goodhouse, and M.G. Farquhar, *Mannose-6-phosphate receptors for lysosomal enzymes cycle between the Golgi complex and endosomes.* J Cell Biol, 1986. **103**(4): p. 1235-47.

Bucci, C., P. Thomsen, P. Nicoziani, J. McCarthy, and B. van Deurs, *Rab7: a key to lysosome biogenesis.* Mol Biol Cell, 2000. **11**(2): p. 467-80.

Buee, L., T. Bussiere, V. Buee-Scherrer, A. Delacourte, and P.R. Hof, *Tau protein isoforms, phosphorylation and role in neurodegenerative disorders.* Brain Res Brain Res Rev, 2000. **33**(1): p. 95-130.

Burg, V.K., H.S. Grimm, T.L. Rothhaar, S. Grosgen, B. Hundsdorfer, V.J. Haupenthal, V.C. Zimmer, J. Mett, O. Weingartner, U. Laufs, L.M. Broersen, H. Tanila, T. Vanmierlo, D. Lutjohann, T. Hartmann, and M.O. Grimm, *Plant sterols the better cholesterol in Alzheimer's disease? A mechanistical study.* J Neurosci, 2013. **33**(41): p. 16072-87.

Burgos, J.S., C. Ramirez, I. Sastre, M.J. Bullido, and F. Valdivieso, *Involvement of apolipoprotein E in the hematogenous route of herpes simplex virus type 1 to the central nervous system.* J Virol, 2002. **76**(23): p. 12394-8.

Burgos, J.S., C. Ramirez, I. Sastre, M.J. Bullido, and F. Valdivieso, *ApoE4 is more efficient than E3 in brain access by herpes simplex virus type 1.* Neuroreport, 2003. **14**(14): p. 1825-7.

Burgos, J.S., C. Ramirez, I. Sastre, and F. Valdivieso, *Effect of apolipoprotein E on the cerebral load of latent herpes simplex virus type 1 DNA.* J Virol, 2006. **80**(11): p. 5383-7.

Butler, D., J. Hwang, C. Estick, A. Nishiyama, S.S. Kumar, C. Baveghems, H.B. Young-Oxendine, M.L. Wisniewski, A. Charalambides, and B.A. Bahr, *Protective effects of positive lysosomal modulation in Alzheimer's disease transgenic mouse models.* PLoS One, 2011. **6**(6): p. e20501.

Cai, Z., B. Zhao, and A. Ratka, *Oxidative stress and beta-amyloid protein in Alzheimer's disease.* Neuromolecular Med, 2011. **13**(4): p. 223-50.

Cappai, R. and K.J. Barnham, *Delineating the mechanism of Alzheimer's disease A beta peptide neurotoxicity.* Neurochem Res, 2008. **33**(3): p. 526-32.

Carlsson, S.R., J. Roth, F. Piller, and M. Fukuda, *Isolation and characterization of human lysosomal membrane glycoproteins, h-lamp-1 and h-lamp-2. Major sialoglycoproteins carrying polylactosaminoglycan.* J Biol Chem, 1988. **263**(35): p. 18911-9.

Carmona-Saez, P., M. Chagoyen, F. Tirado, J.M. Carazo, and A. Pascual-Montano, *GENECODIS: a web-based tool for finding significant concurrent annotations in gene lists.* Genome Biol, 2007. **8**(1): p. R3.

Carrascosa, A.L., J.F. Santaren, and E. Vinuela, *Production and titration of African swine fever virus in porcine alveolar macrophages.* J Virol Methods, 1982. **3**(6): p. 303-10.

Caspersen, C., N. Wang, J. Yao, A. Sosunov, X. Chen, J.W. Lustbader, H.W. Xu, D. Stern, G. McKhann, and S.D. Yan, *Mitochondrial Abeta: a potential focal point for neuronal metabolic dysfunction in Alzheimer's disease.* FASEB J, 2005. **19**(14): p. 2040-1.

Cataldo, A.M., J.L. Barnett, C. Pieroni, and R.A. Nixon, *Increased neuronal endocytosis and protease delivery to early endosomes in sporadic Alzheimer's disease: neuropathologic evidence for a mechanism of increased beta-amyloidogenesis.* J Neurosci, 1997. **17**(16): p. 6142-51.

Cataldo, A.M., C.M. Peterhoff, J.C. Troncoso, T. Gomez-Isla, B.T. Hyman, and R.A. Nixon, *Endocytic pathway abnormalities precede amyloid beta deposition in sporadic Alzheimer's disease and Down syndrome: differential effects of APOE genotype and presenilin mutations.* Am J Pathol, 2000. **157**(1): p. 277-86.

Cermak, S., M. Kosicek, A. Mladenovic-Djordjevic, K. Smiljanic, S. Kanazir, and S. Hecimovic, *Loss of Cathepsin B and L Leads to Lysosomal Dysfunction, NPC-Like Cholesterol Sequestration and Accumulation of the Key Alzheimer's Proteins.* PLoS One, 2016. **11**(11): p. e0167428.

Chen, X., L. Hui, and J.D. Geiger, *Role of LDL cholesterol and endolysosomes in amyloidogenesis and Alzheimer's disease.* J Neurol Neurophysiol, 2014. **5**(5).

Coen, K., R.S. Flannagan, S. Baron, L.R. Carraro-Lacroix, D. Wang, W. Vermeire, C. Michiels, S. Munck, V. Baert, S. Sugita, F. Wuytack, P.R. Hiesinger, S. Grinstein, and W. Annaert, *Lysosomal calcium homeostasis defects, not proton pump defects, cause endo-lysosomal dysfunction in PSEN-deficient cells.* J Cell Biol, 2012. **198**(1): p. 23-35.

Corder, E.H., A.M. Saunders, N.J. Risch, W.J. Strittmatter, D.E. Schmechel, P.C. Gaskell, Jr., J.B. Rimmler, P.A. Locke, P.M. Conneally, K.E. Schmader, and et al., *Protective effect of apolipoprotein E type 2 allele for late onset Alzheimer disease.* Nat Genet, 1994. **7**(2): p. 180-4.

Corder, E.H., A.M. Saunders, W.J. Strittmatter, D.E. Schmechel, P.C. Gaskell, G.W. Small, A.D. Roses, J.L. Haines, and M.A. Pericak-Vance, *Gene dose of apolipoprotein E type 4 allele and the risk of Alzheimer's disease in late onset families.* Science, 1993. **261**(5123): p. 921-3.

Cormont, M., I. Meton, M. Mari, P. Monzo, F. Keslair, C. Gaskin, T.E. McGraw, and Y. Le Marchand-Brustel, *CD2AP/CMS regulates endosome morphology and traffic to the degradative pathway through its interaction with Rab4 and c-Cbl.* Traffic, 2003. **4**(2): p. 97-112.

Crook, J.M., D. Hei, and G. Stacey, *The International Stem Cell Banking Initiative (ISCBI): raising standards to bank on.* In Vitro Cell Dev Biol Anim, 2010. **46**(3-4): p. 169-72.

Cruchaga, C., G. Haller, S. Chakraverty, K. Mayo, F.L. Vallania, R.D. Mitra, K. Faber, J. Williamson, T. Bird, R. Diaz-Arrastia, T.M. Foroud, B.F. Boeve, N.R. Graff-Radford, P. St Jean, M. Lawson, M.G. Ehm, R. Mayeux, A.M. Goate, and N.-L.N.F.S. Consortium, *Rare variants in APP, PSEN1 and PSEN2 increase risk for AD in late-onset Alzheimer's disease families.* PLoS One, 2012. **7**(2): p. e31039.

Cruchaga, C., C.M. Karch, S.C. Jin, B.A. Benitez, Y. Cai, R. Guerreiro, O. Harari, J. Norton, J. Budde, S. Bertelsen, A.T. Jeng, B. Cooper, T. Skorupa, D. Carrell, D. Levitch, S. Hsu, J. Choi, M. Ryten, U.K.B.E. Consortium, J. Hardy, M. Ryten, D. Trabzuni, M.E. Weale, A. Ramasamy, C. Smith, C. Sassi, J. Bras, J.R. Gibbs, D.G. Hernandez, M.K. Lupton, J. Powell, P. Forabosco, P.G. Ridge, C.D. Corcoran, J.T. Tschanz, M.C. Norton, R.G. Munger, C. Schmutz, M. Leary, F.Y. Demirci, M.N. Bamne, X. Wang, O.L. Lopez, M. Ganguli, C. Medway, J. Turton, J. Lord, A. Braae, I. Barber, K. Brown, U.K.C. Alzheimer's Research, P. Passmore, D. Craig, J. Johnston, B. McGuinness, S. Todd, R. Heun, H. Kolsch, P.G. Kehoe, N.M. Hooper, E.R. Vardy, D.M. Mann, S. Pickering-Brown, K. Brown, N. Kalsheker, J. Lowe, K. Morgan, A. David Smith, G. Wilcock, D. Warden, C. Holmes, P. Pastor, O. Lorenzo-Betancor, Z. Brkanac, E. Scott, E. Topol, K. Morgan, E. Rogaeva, A.B. Singleton, J. Hardy, M.I. Kamboh, P. St George-Hyslop, N. Cairns, J.C. Morris, J.S. Kauwe and A.M. Goate, *Rare coding variants in the phospholipase D3 gene confer risk for Alzheimer's disease.* Nature, 2014. **505**(7484): p. 550-4.

De Strooper, B., *Proteases and proteolysis in Alzheimer disease: a multifactorial view on the disease process.* Physiol Rev, 2010. **90**(2): p. 465-94.

De Strooper, B. and W. Annaert, *Proteolytic processing and cell biological functions of the amyloid precursor protein.* J Cell Sci, 2000. **113 (Pt 11)**: p. 1857-70.

Delobel, P., S. Flament, M. Hamdane, C. Mailliot, A.V. Sambo, S. Begard, N. Sergeant, A. Delacourte, J.P. Vilain, and L. Buee, *Abnormal Tau phosphorylation of the Alzheimer-type also occurs during mitosis.* J Neurochem, 2002. **83**(2): p. 412-20.

Djelti, F., J. Braudeau, E. Hudry, M. Dhenain, J. Varin, I. Bieche, C. Marquer, F. Chali, S. Ayciriex, N. Auzeil, S. Alves, D. Langui, M.C. Potier, O. Laprevote, M. Vidaud, C. Duyckaerts, R. Miles, P. Aubourg, and N. Cartier, *CYP46A1 inhibition, brain cholesterol accumulation and neurodegeneration pave the way for Alzheimer's disease.* Brain, 2015. **138**(Pt 8): p. 2383-98.

Dobrowolski, R., P. Vick, D. Ploper, I. Gumper, H. Snitkin, D.D. Sabatini, and E.M. De Robertis, *Presenilin deficiency or lysosomal inhibition enhances Wnt signaling through relocalization of GSK3 to the late-endosomal compartment.* Cell Rep, 2012. **2**(5): p. 1316-28.

Du, L., R.W. Hickey, H. Bayir, S.C. Watkins, V.A. Tyurin, F. Guo, P.M. Kochanek, L.W. Jenkins, J. Ren, G. Gibson, C.T. Chu, V.E. Kagan, and R.S. Clark, *Starving neurons show sex difference in autophagy.* J Biol Chem, 2009. **284**(4): p. 2383-96.

Emiliani, C., L. Urbanelli, L. Racanicchi, A. Orlacchio, G. Pelicci, S. Sorbi, G. Bernardi, and A. Orlacchio, *Up-regulation of glycohydrolases in Alzheimer's Disease fibroblasts correlates with Ras activation.* J Biol Chem, 2003. **278**(40): p. 38453-60.

Endo, Y., A. Furuta, and I. Nishino, *Danon disease: a phenotypic expression of LAMP-2 deficiency.* Acta Neuropathol, 2015. **129**(3): p. 391-8.

Eskelinen, E.L., *Roles of LAMP-1 and LAMP-2 in lysosome biogenesis and autophagy.* Mol Aspects Med, 2006. **27**(5-6): p. 495-502.

Eskelinen, E.L., A.M. Cuervo, M.R. Taylor, I. Nishino, J.S. Blum, J.F. Dice, I.V. Sandoval, J. Lippincott-Schwartz, J.T. August, and P. Saftig, *Unifying nomenclature for the isoforms of the lysosomal membrane protein LAMP-2.* Traffic, 2005. **6**(11): p. 1058-61.

Eskelinen, E.L., C.K. Schmidt, S. Neu, M. Willenborg, G. Fuertes, N. Salvador, Y. Tanaka, R. Lullmann-Rauch, D. Hartmann, J. Heeren, K. von Figura, E. Knecht, and P. Saftig, *Disturbed cholesterol traffic but normal proteolytic function in LAMP-1/LAMP-2 double-deficient fibroblasts.* Mol Biol Cell, 2004. **15**(7): p. 3132-45.

Eskelinen, E.L., Y. Tanaka, and P. Saftig, *At the acidic edge: emerging functions for lysosomal membrane proteins.* Trends Cell Biol, 2003. **13**(3): p. 137-45.

Fatokun, A.A., T.W. Stone, and R.A. Smith, *Hydrogen peroxide mediates damage by xanthine and xanthine oxidase in cerebellar granule neuronal cultures.* Neurosci Lett, 2007. **416**(1): p. 34-8.

Fields, B.N., D.M. Knipe, and P.M. Howley, *Fields virology*. 3rd ed. 1996, Philadelphia: Lippincott - Raven Press.

Fields, J., W. Dumaop, S. Eleuteri, S. Campos, E. Serger, M. Trejo, K. Kosberg, A. Adame, B. Spencer, E. Rockenstein, J.J. He, and E. Masliah, *HIV-1 Tat alters neuronal autophagy by modulating autophagosome fusion to the lysosome: implications for HIV-associated neurocognitive disorders.* J Neurosci, 2015. **35**(5): p. 1921-38.

Filocamo, M. and A. Morrone, *Lysosomal storage disorders: molecular basis and laboratory testing.* Hum Genomics, 2011. **5**(3): p. 156-69.

Fraldi, A., F. Annunziata, A. Lombardi, H.J. Kaiser, D.L. Medina, C. Spampanato, A.O. Fedele, R. Polishchuk, N.C. Sorrentino, K. Simons, and A. Ballabio, *Lysosomal fusion and SNARE function are impaired by cholesterol accumulation in lysosomal storage disorders.* EMBO J, 2010. **29**(21): p. 3607-20.

Friedman, J.E., J.B. Zabriskie, C. Plank, D. Ablashi, J. Whitman, B. Shahan, R. Edgell, M. Shieh, O. Rapalino, R. Zimmerman, and D. Sheng, *A randomized clinical trial of valacyclovir in multiple sclerosis.* Mult Scler, 2005. **11**(3): p. 286-95.

Furuchi, T., K. Aikawa, H. Arai, and K. Inoue, *Bafilomycin A1, a specific inhibitor of vacuolar-type H(+)-ATPase, blocks lysosomal cholesterol trafficking in macrophages.* J Biol Chem, 1993. **268**(36): p. 27345-8.

Gabbita, S.P., M.A. Lovell, and W.R. Markesbery, *Increased nuclear DNA oxidation in the brain in Alzheimer's disease.* J Neurochem, 1998. **71**(5): p. 2034-40.

Gallart-Palau, X., B.S. Lee, S.S. Adav, J. Qian, A. Serra, J.E. Park, M.K. Lai, C.P. Chen, R.N. Kalaria, and S.K. Sze, *Gender differences in white matter pathology and mitochondrial dysfunction in Alzheimer's disease with cerebrovascular disease.* Mol Brain, 2016. **9**: p. 27.

Genin, E., D. Hannequin, D. Wallon, K. Sleegers, M. Hiltunen, O. Combarros, M.J. Bullido, S. Engelborghs, P. De Deyn, C. Berr, F. Pasquier, B. Dubois, G. Tognoni, N. Fievet, N. Brouwers, K. Bettens, B. Arosio, E. Coto, M. Del Zompo, I. Mateo, J. Epelbaum, A. Frank-Garcia, S. Helisalmi, E. Porcellini, A. Pilotto, P. Forti, R. Ferri, E. Scarpini, G. Siciliano, V. Solfrizzi, S. Sorbi, G. Spalletta, F. Valdivieso, S. Vepsalainen, V. Alvarez, P. Bosco, M. Mancuso, F. Panza, B. Nacmias, P. Bossu, O. Hanon, P. Piccardi, G. Annoni, D.

Seripa, D. Galimberti, F. Licastro, H. Soininen, J.F. Dartigues, M.I. Kamboh, C. Van Broeckhoven, J.C. Lambert, P. Amouyel and D. Campion, *APOE and Alzheimer disease: a major gene with semi-dominant inheritance.* Mol Psychiatry, 2011. **16**(9): p. 903-7.

Gerard, H.C., U. Dreses-Werringloer, K.S. Wildt, S. Deka, C. Oszust, B.J. Balin, W.H. Frey, 2nd, E.Z. Bordayo, J.A. Whittum-Hudson, and A.P. Hudson, *Chlamydophila (Chlamydia) pneumoniae in the Alzheimer's brain.* FEMS Immunol Med Microbiol, 2006. **48**(3): p. 355-66.

Ghosh, P., N.M. Dahms, and S. Kornfeld, *Mannose 6-phosphate receptors: new twists in the tale.* Nat Rev Mol Cell Biol, 2003. **4**(3): p. 202-12.

Ghribi, O., B. Larsen, M. Schrag, and M.M. Herman, *High cholesterol content in neurons increases BACE, beta-amyloid, and phosphorylated tau levels in rabbit hippocampus.* Exp Neurol, 2006. **200**(2): p. 460-7.

Giannakopoulos, P., F.R. Herrmann, T. Bussiere, C. Bouras, E. Kovari, D.P. Perl, J.H. Morrison, G. Gold, and P.R. Hof, *Tangle and neuron numbers, but not amyloid load, predict cognitive status in Alzheimer's disease.* Neurology, 2003. **60**(9): p. 1495-500.

Gibson, G.E. and H.M. Huang, *Oxidative stress in Alzheimer's disease.* Neurobiol Aging, 2005. **26**(5): p. 575-8.

Ginsberg, S.D., E.J. Mufson, S.E. Counts, J. Wuu, M.J. Alldred, R.A. Nixon, and S. Che, *Regional selectivity of rab5 and rab7 protein upregulation in mild cognitive impairment and Alzheimer's disease.* J Alzheimers Dis, 2010. **22**(2): p. 631-9.

Glabe, C.G., *Structural classification of toxic amyloid oligomers.* J Biol Chem, 2008. **283**(44): p. 29639-43.

Goedert, M., *Tau protein and the neurofibrillary pathology of Alzheimer's disease.* Trends Neurosci, 1993. **16**(11): p. 460-5.

Goedert, M., M.G. Spillantini, M.C. Potier, J. Ulrich, and R.A. Crowther, *Cloning and sequencing of the cDNA encoding an isoform of microtubule-associated protein tau containing four tandem repeats: differential expression of tau protein mRNAs in human brain.* EMBO J, 1989. **8**(2): p. 393-9.

Gong, C.X., T. Lidsky, J. Wegiel, L. Zuck, I. Grundke-Iqbal, and K. Iqbal, *Phosphorylation of microtubule-associated protein tau is regulated by protein phosphatase 2A in mammalian brain. Implications for neurofibrillary degeneration in Alzheimer's disease.* J Biol Chem, 2000. **275**(8): p. 5535-44.

Gouras, G.K., J. Tsai, J. Naslund, B. Vincent, M. Edgar, F. Checler, J.P. Greenfield, V. Haroutunian, J.D. Buxbaum, H. Xu, P. Greengard, and N.R. Relkin, *Intraneuronal Abeta42 accumulation in human brain.* Am J Pathol, 2000. **156**(1): p. 15-20.

Gowrishankar, S., P. Yuan, Y. Wu, M. Schrag, S. Paradise, J. Grutzendler, P. De Camilli, and S.M. Ferguson, *Massive accumulation of luminal protease-deficient axonal lysosomes at Alzheimer's disease amyloid plaques.* Proc Natl Acad Sci U S A, 2015. **112**(28): p. E3699-708.

Grimm, M.O., V.C. Zimmer, J. Lehmann, H.S. Grimm, and T. Hartmann, *The impact of cholesterol, DHA, and sphingolipids on Alzheimer's disease.* Biomed Res Int, 2013. **2013**: p. 814390.

Grundke-Iqbal, I., K. Iqbal, M. Quinlan, Y.C. Tung, M.S. Zaidi, and H.M. Wisniewski, *Microtubule-associated protein tau. A component of Alzheimer paired helical filaments.* J Biol Chem, 1986. **261**(13): p. 6084-9.

Guerreiro, R., A. Wojtas, J. Bras, M. Carrasquillo, E. Rogaeva, E. Majounie, C. Cruchaga, C. Sassi, J.S. Kauwe, S. Younkin, L. Hazrati, J. Collinge, J. Pocock, T. Lashley, J. Williams, J.C.

Lambert, P. Amouyel, A. Goate, R. Rademakers, K. Morgan, J. Powell, P. St George-Hyslop, A. Singleton, J. Hardy, and G. Alzheimer Genetic Analysis, *TREM2 variants in Alzheimer's disease.* N Engl J Med, 2013. **368**(2): p. 117-27.

Hajjar, D.P., K.B. Pomerantz, D.J. Falcone, B.B. Weksler, and A.J. Grant, *Herpes simplex virus infection in human arterial cells. Implications in arteriosclerosis.* J Clin Invest, 1987. **80**(5): p. 1317-21.

Hanger, D.P., B.H. Anderton, and W. Noble, *Tau phosphorylation: the therapeutic challenge for neurodegenerative disease.* Trends Mol Med, 2009. **15**(3): p. 112-9.

Hansen, M.B., S.E. Nielsen, and K. Berg, *Re-examination and further development of a precise and rapid dye method for measuring cell growth/cell kill.* J Immunol Methods, 1989. **119**(2): p. 203-10.

Hardy, J., *The amyloid hypothesis for Alzheimer's disease: a critical reappraisal.* J Neurochem, 2009. **110**(4): p. 1129-34.

Harold, D., R. Abraham, P. Hollingworth, R. Sims, A. Gerrish, M.L. Hamshere, J.S. Pahwa, V. Moskvina, K. Dowzell, A. Williams, N. Jones, C. Thomas, A. Stretton, A.R. Morgan, S. Lovestone, J. Powell, P. Proitsi, M.K. Lupton, C. Brayne, D.C. Rubinsztein, M. Gill, B. Lawlor, A. Lynch, K. Morgan, K.S. Brown, P.A. Passmore, D. Craig, B. McGuinness, S. Todd, C. Holmes, D. Mann, A.D. Smith, S. Love, P.G. Kehoe, J. Hardy, S. Mead, N. Fox, M. Rossor, J. Collinge, W. Maier, F. Jessen, B. Schurmann, R. Heun, H. van den Bussche, I. Heuser, J. Kornhuber, J. Wiltfang, M. Dichgans, L. Frolich, H. Hampel, M. Hull, D. Rujescu, A.M. Goate, J.S. Kauwe, C. Cruchaga, P. Nowotny, J.C. Morris, K. Mayo, K. Sleegers, K. Bettens, S. Engelborghs, P.P. De Deyn, C. Van Broeckhoven, G. Livingston, N.J. Bass, H. Gurling, A. McQuillin, R. Gwilliam, P. Deloukas, A. Al-Chalabi, C.E. Shaw, M. Tsolaki, A.B. Singleton, R. Guerreiro, T.W. Muhleisen, M.M. Nothen, S. Moebus, K.H. Jockel, N. Klopp, H.E. Wichmann, M.M. Carrasquillo, V.S. Pankratz, S.G. Younkin, P.A. Holmans, M. O'Donovan, M.J. Owen and J. Williams, *Genome-wide association study identifies variants at CLU and PICALM associated with Alzheimer's disease.* Nat Genet, 2009. **41**(10): p. 1088-93.

Harris, S.A. and E.A. Harris, *Herpes Simplex Virus Type 1 and Other Pathogens are Key Causative Factors in Sporadic Alzheimer's Disease.* J Alzheimers Dis, 2015. **48**(2): p. 319-53.

Henriksen, L., M.V. Grandal, S.L.J. Knudsen, B. van Deurs, and L.M. Grøvdal, *Internalization Mechanisms of the Epidermal Growth Factor Receptor after Activation with Different Ligands.* PLOS ONE, 2013. **8**(3): p. e58148.

Hsu, H.Y., A.C. Nicholson, K.B. Pomerantz, R.J. Kaner, and D.P. Hajjar, *Altered cholesterol trafficking in herpesvirus-infected arterial cells. Evidence for viral protein kinase-mediated cholesterol accumulation.* J Biol Chem, 1995. **270**(33): p. 19630-7.

Hu, W., B. Qiu, W. Guan, Q. Wang, M. Wang, W. Li, L. Gao, L. Shen, Y. Huang, G. Xie, H. Zhao, Y. Jin, B. Tang, Y. Yu, J. Zhao, and G. Pei, *Direct Conversion of Normal and Alzheimer's Disease Human Fibroblasts into Neuronal Cells by Small Molecules.* Cell Stem Cell, 2015. **17**(2): p. 204-12.

Hubert, V., A. Peschel, B. Langer, M. Groger, A. Rees, and R. Kain, *LAMP-2 is required for incorporating syntaxin-17 into autophagosomes and for their fusion with lysosomes.* Biol Open, 2016. **5**(10): p. 1516-1529.

Hung, S.Y., W.P. Huang, H.C. Liou, and W.M. Fu, *Autophagy protects neuron from Abeta-induced cytotoxicity.* Autophagy, 2009. **5**(4): p. 502-10.

Huotari, J. and A. Helenius, *Endosome maturation.* EMBO J, 2011. **30**(17): p. 3481-500.

Huynh, K.K., E.L. Eskelinen, C.C. Scott, A. Malevanets, P. Saftig, and S. Grinstein, *LAMP proteins are required for fusion of lysosomes with phagosomes.* EMBO J, 2007. **26**(2): p. 313-24.

International Genomics of Alzheimer's Disease, C., *Convergent genetic and expression data implicate immunity in Alzheimer's disease.* Alzheimers Dement, 2015. **11**(6): p. 658-71.

Iqbal, K., F. Liu, C.X. Gong, C. Alonso Adel, and I. Grundke-Iqbal, *Mechanisms of tau-induced neurodegeneration.* Acta Neuropathol, 2009. **118**(1): p. 53-69.

Itzhaki, R.F., *Herpes simplex virus type 1 and Alzheimer's disease: increasing evidence for a major role of the virus.* Front Aging Neurosci, 2014. **6**: p. 202.

Itzhaki, R.F., S.L. Cosby, and M.A. Wozniak, *Herpes simplex virus type 1 and Alzheimer's disease: the autophagy connection.* J Neurovirol, 2008. **14**(1): p. 1-4.

Itzhaki, R.F., R. Lathe, B.J. Balin, M.J. Ball, E.L. Bearer, H. Braak, M.J. Bullido, C. Carter, M. Clerici, S.L. Cosby, K. Del Tredici, H. Field, T. Fulop, C. Grassi, W.S. Griffin, J. Haas, A.P. Hudson, A.R. Kamer, D.B. Kell, F. Licastro, L. Letenneur, H. Lovheim, R. Mancuso, J. Miklossy, C. Otth, A.T. Palamara, G. Perry, C. Preston, E. Pretorius, T. Strandberg, N. Tabet, S.D. Taylor-Robinson, and J.A. Whittum-Hudson, *Microbes and Alzheimer's Disease.* J Alzheimers Dis, 2016. **51**(4): p. 979-84.

Itzhaki, R.F., R. Lathe, B.J. Balin, M.J. Ball, E.L. Bearer, H. Braak, M.J. Bullido, C. Carter, M. Clerici, S.L. Cosby, K. Del Tredici, H. Field, T. Fulop, C. Grassi, W.S.T. Griffin, J. Haas, A.P. Hudson, A.R. Kamer, D.B. Kell, F. Licastro, L. Letenneur, H. Lövheim, R. Mancuso, J. Miklossy, C. Otth, A.T. Palamara, G. Perry, C. Preston, E. Pretorius, T. Strandberg, N. Tabet, S.D. Taylor-Robinson, and J.A. Whittum-Hudson, *Microbes and Alzheimers Disease.* J Alzheimers Dis, 2016. **51**(4): p. 979-984.

Itzhaki, R.F., W.R. Lin, D. Shang, G.K. Wilcock, B. Faragher, and G.A. Jamieson, *Herpes simplex virus type 1 in brain and risk of Alzheimer's disease.* Lancet, 1997. **349**(9047): p. 241-4.

Itzhaki, R.F. and M.A. Wozniak, *Could antivirals be used to treat Alzheimer's disease?* Future Microbiol, 2012. **7**(3): p. 307-9.

Jamieson, G.A., N.J. Maitland, G.K. Wilcock, J. Craske, and R.F. Itzhaki, *Latent herpes simplex virus type 1 in normal and Alzheimer's disease brains.* J Med Virol, 1991. **33**(4): p. 224-7.

Jerome, K.R., R. Fox, Z. Chen, P. Sarkar, and L. Corey, *Inhibition of apoptosis by primary isolates of herpes simplex virus.* Arch Virol, 2001. **146**(11): p. 2219-25.

Jick, H., G.L. Zornberg, S.S. Jick, S. Seshadri, and D.A. Drachman, *Statins and the risk of dementia.* Lancet, 2000. **356**(9242): p. 1627-31.

Johansson, A.C., H. Appelqvist, C. Nilsson, K. Kagedal, K. Roberg, and K. Ollinger, *Regulation of apoptosis-associated lysosomal membrane permeabilization.* Apoptosis, 2010. **15**(5): p. 527-40.

Jones, L., D. Harold, and J. Williams, *Genetic evidence for the involvement of lipid metabolism in Alzheimer's disease.* Biochim Biophys Acta, 2010. **1801**(8): p. 754-61.

Jorm, A.F. and D. Jolley, *The incidence of dementia: a meta-analysis.* Neurology, 1998. **51**(3): p. 728-33.

Ju, X., Y. Yan, Q. Liu, N. Li, M. Sheng, L. Zhang, X. Li, Z. Liang, F. Huang, K. Liu, Y. Zhao, Y. Zhang, Z. Zou, J. Du, Y. Zhong, H. Zhou, P. Yang, H. Lu, M. Tian, D. Li, J. Zhang, N. Jin, and C. Jiang, *Neuraminidase of Influenza A Virus Binds Lysosome-Associated Membrane Proteins Directly and Induces Lysosome Rupture.* J Virol, 2015. **89**(20): p. 10347-58.

Kang, J., H.G. Lemaire, A. Unterbeck, J.M. Salbaum, C.L. Masters, K.H. Grzeschik, G. Multhaup, K. Beyreuther, and B. Muller-Hill, *The precursor of Alzheimer's disease amyloid A4 protein resembles a cell-surface receptor.* Nature, 1987. **325**(6106): p. 733-6.

Karch, C.M. and A.M. Goate, *Alzheimer's disease risk genes and mechanisms of disease pathogenesis.* Biol Psychiatry, 2015. **77**(1): p. 43-51.

Kaushik, S. and A.M. Cuervo, *Chaperone-mediated autophagy: a unique way to enter the lysosome world.* Trends Cell Biol, 2012. **22**(8): p. 407-17.

Kawahara, M. and Y. Kuroda, *Molecular mechanism of neurodegeneration induced by Alzheimer's beta-amyloid protein: channel formation and disruption of calcium homeostasis.* Brain Res Bull, 2000. **53**(4): p. 389-97.

Kayed, R., Y. Sokolov, B. Edmonds, T.M. McIntire, S.C. Milton, J.E. Hall, and C.G. Glabe, *Permeabilization of lipid bilayers is a common conformation-dependent activity of soluble amyloid oligomers in protein misfolding diseases.* J Biol Chem, 2004. **279**(45): p. 46363-6.

Kennedy, P.G., J. Rovnak, H. Badani, and R.J. Cohrs, *A comparison of herpes simplex virus type 1 and varicella-zoster virus latency and reactivation.* J Gen Virol, 2015. **96**(Pt 7): p. 1581-602.

Kitaguchi, N., Y. Takahashi, Y. Tokushima, S. Shiojiri, and H. Ito, *Novel precursor of Alzheimer's disease amyloid protein shows protease inhibitory activity.* Nature, 1988. **331**(6156): p. 530-2.

Klionsky, D.J., K. Abdelmohsen, A. Abe, M.J. Abedin, H. Abeliovich, A. Acevedo Arozena, H. Adachi, C.M. Adams, P.D. Adams, K. Adeli, P.J. Adhihetty, S.G. Adler, G. Agam, R. Agarwal, M.K. Aghi, M. Agnello, P. Agostinis, P.V. Aguilar, J. Aguirre-Ghiso, E.M. Airoldi, S. Ait-Si-Ali, T. Akematsu, E.T. Akporiaye, M. Al-Rubeai, G.M. Albaiceta, C. Albanese, D. Albani, M.L. Albert, J. Aldudo, H. Algul, M. Alirezaei, I. Alloza, A. Almasan, M. Almonte-Beceril, E.S. Alnemri, C. Alonso, N. Altan-Bonnet, D.C. Altieri, S. Alvarez, L. Alvarez-Erviti, S. Alves, G. Amadoro, A. Amano, C. Amantini, S. Ambrosio, I. Amelio, A.O. Amer, M. Amessou, A. Amon, Z. An, F.A. Anania, S.U. Andersen, U.P. Andley, C.K. Andreadi, N. Andrieu-Abadie, A. Anel, D.K. Ann, S. Anoopkumar-Dukie, M. Antonioli, H. Aoki, N. Apostolova, S. Aquila, K. Aquilano, K. Araki, E. Arama, A. Aranda, J. Araya, A. Arcaro, E. Arias, H. Arimoto, A.R. Ariosa, J.L. Armstrong, T. Arnould, I. Arsov, K. Asanuma, V. Askanas, E. Asselin, R. Atarashi, S.S. Atherton, J.D. Atkin, L.D. Attardi, P. Auberger, G. Auburger, L. Aurelian, R. Autelli, L. Avagliano, M.L. Avantaggiati, L. Avrahami, S. Awale, N. Azad, T. Bachetti, J.M. Backer, D.H. Bae, J.S. Bae, O.N. Bae, S.H. Bae, E.H. Baehrecke, S.H. Baek, S. Baghdiguian, A. Bagniewska-Zadworna et al., *Guidelines for the use and interpretation of assays for monitoring autophagy (3rd edition).* Autophagy, 2016. **12**(1): p. 1-222.

Koike, M., H. Nakanishi, P. Saftig, J. Ezaki, K. Isahara, Y. Ohsawa, W. Schulz-Schaeffer, T. Watanabe, S. Waguri, S. Kametaka, M. Shibata, K. Yamamoto, E. Kominami, C. Peters, K. von Figura, and Y. Uchiyama, *Cathepsin D deficiency induces lysosomal storage with ceroid lipofuscin in mouse CNS neurons.* J Neurosci, 2000. **20**(18): p. 6898-906.

Kok, E., S. Haikonen, T. Luoto, H. Huhtala, S. Goebeler, H. Haapasalo, and P.J. Karhunen, *Apolipoprotein E-dependent accumulation of Alzheimer disease-related lesions begins in middle age.* Ann Neurol, 2009. **65**(6): p. 650-7.

Komatsu, M., T. Ueno, S. Waguri, Y. Uchiyama, E. Kominami, and K. Tanaka, *Constitutive autophagy: vital role in clearance of unfavorable proteins in neurons.* Cell Death Differ, 2007. **14**(5): p. 887-94.

Koprowski, H., Y.M. Zheng, E. Heber-Katz, N. Fraser, L. Rorke, Z.F. Fu, C. Hanlon, and B. Dietzschold, *In vivo expression of inducible nitric oxide synthase in experimentally induced neurologic diseases.* Proc Natl Acad Sci U S A, 1993. **90**(7): p. 3024-7.

Kountouras, J., E. Gavalas, C. Zavos, C. Stergiopoulos, D. Chatzopoulos, N. Kapetanakis, and D. Gisakis, *Alzheimer's disease and Helicobacter pylori infection: Defective immune regulation and apoptosis as proposed common links.* Med Hypotheses, 2007. **68**(2): p. 378-88.

Koyuncu, O.O., I.B. Hogue, and L.W. Enquist, *Virus infections in the nervous system.* Cell Host Microbe, 2013. **13**(4): p. 379-93.

Kristen, H., S. Santana, I. Sastre, M. Recuero, M.J. Bullido, and J. Aldudo, *Herpes simplex virus type 2 infection induces AD-like neurodegeneration markers in human neuroblastoma cells.* Neurobiol Aging, 2015. **36**(10): p. 2737-47.

Ladewig, J., J. Mertens, J. Kesavan, J. Doerr, D. Poppe, F. Glaue, S. Herms, P. Wernet, G. Kogler, F.J. Muller, P. Koch, and O. Brustle, *Small molecules enable highly efficient neuronal conversion of human fibroblasts.* Nat Methods, 2012. **9**(6): p. 575-8.

LaFerla, F.M., K.N. Green, and S. Oddo, *Intracellular amyloid-beta in Alzheimer's disease.* Nat Rev Neurosci, 2007. **8**(7): p. 499-509.

Lambert, J.C., S. Heath, G. Even, D. Campion, K. Sleegers, M. Hiltunen, O. Combarros, D. Zelenika, M.J. Bullido, B. Tavernier, L. Letenneur, K. Bettens, C. Berr, F. Pasquier, N. Fievet, P. Barberger-Gateau, S. Engelborghs, P. De Deyn, I. Mateo, A. Franck, S. Helisalmi, E. Porcellini, O. Hanon, I. European Alzheimer's Disease Initiative, M.M. de Pancorbo, C. Lendon, C. Dufouil, C. Jaillard, T. Leveillard, V. Alvarez, P. Bosco, M. Mancuso, F. Panza, B. Nacmias, P. Bossu, P. Piccardi, G. Annoni, D. Seripa, D. Galimberti, D. Hannequin, F. Licastro, H. Soininen, K. Ritchie, H. Blanche, J.F. Dartigues, C. Tzourio, I. Gut, C. Van Broeckhoven, A. Alperovitch, M. Lathrop and P. Amouyel, *Genome-wide association study identifies variants at CLU and CR1 associated with Alzheimer's disease.* Nat Genet, 2009. **41**(10): p. 1094-9.

Lambert, J.C., C.A. Ibrahim-Verbaas, D. Harold, A.C. Naj, R. Sims, C. Bellenguez, A.L. DeStafano, J.C. Bis, G.W. Beecham, B. Grenier-Boley, G. Russo, T.A. Thorton-Wells, N. Jones, A.V. Smith, V. Chouraki, C. Thomas, M.A. Ikram, D. Zelenika, B.N. Vardarajan, Y. Kamatani, C.F. Lin, A. Gerrish, H. Schmidt, B. Kunkle, M.L. Dunstan, A. Ruiz, M.T. Bihoreau, S.H. Choi, C. Reitz, F. Pasquier, C. Cruchaga, D. Craig, N. Amin, C. Berr, O.L. Lopez, P.L. De Jager, V. Deramecourt, J.A. Johnston, D. Evans, S. Lovestone, L. Letenneur, F.J. Moron, D.C. Rubinsztein, G. Eiriksdottir, K. Sleegers, A.M. Goate, N. Fievet, M.W. Huentelman, M. Gill, K. Brown, M.I. Kamboh, L. Keller, P. Barberger-Gateau, B. McGuiness, E.B. Larson, R. Green, A.J. Myers, C. Dufouil, S. Todd, D. Wallon, S. Love, E. Rogaeva, J. Gallacher, P. St George-Hyslop, J. Clarimon, A. Lleo, A. Bayer, D.W. Tsuang, L. Yu, M. Tsolaki, P. Bossu, G. Spalletta, P. Proitsi, J. Collinge, S. Sorbi, F. Sanchez-Garcia, N.C. Fox, J. Hardy, M.C. Deniz Naranjo, P. Bosco, R. Clarke, C. Brayne, D. Galimberti, M. Mancuso, F. Matthews, I. European Alzheimer's Disease, Genetic, D. Environmental Risk in Alzheimer's, C. Alzheimer's Disease Genetic, H. Cohorts for, E. Aging Research in Genomic, S. Moebus, P. Mecocci, M. Del Zompo, W. Maier, H. Hampel, A. Pilotto, M. Bullido, F. Panza, P. Caffarra et al., *Meta-analysis of 74,046 individuals identifies 11 new susceptibility loci for Alzheimer's disease.* Nat Genet, 2013. **45**(12): p. 1452-8.

Lambert, J.C., D. Zelenika, M. Hiltunen, V. Chouraki, O. Combarros, M.J. Bullido, G. Tognoni, N. Fievet, A. Boland, B. Arosio, E. Coto, M. Del Zompo, I. Mateo, A. Frank-Garcia, S. Helisalmi, E. Porcellini, A. Pilotto, P. Forti, R. Ferri, M. Delepine, E. Scarpini, G. Siciliano, V. Solfrizzi, S. Sorbi, G. Spalletta, G. Ravaglia, F. Valdivieso, V. Alvarez, P. Bosco, M. Mancuso, F. Panza, B. Nacmias, P. Bossu, P. Piccardi, G. Annoni, D. Seripa, D. Galimberti, F. Licastro, M. Lathrop, H. Soininen, and P. Amouyel, *Evidence of the association of BIN1 and PICALM with the AD risk in contrasting European populations.* Neurobiol Aging, 2011. **32**(4): p. 756 e11-5.

LeBlanc, A.C., R. Xue, and P. Gambetti, *Amyloid precursor protein metabolism in primary cell cultures of neurons, astrocytes, and microglia.* J Neurochem, 1996. **66**(6): p. 2300-10.

Lee, J.H., W.H. Yu, A. Kumar, S. Lee, P.S. Mohan, C.M. Peterhoff, D.M. Wolfe, M. Martinez-Vicente, A.C. Massey, G. Sovak, Y. Uchiyama, D. Westaway, A.M. Cuervo, and R.A. Nixon, *Lysosomal proteolysis and autophagy require presenilin 1 and are disrupted by Alzheimer-related PS1 mutations.* Cell, 2010. **141**(7): p. 1146-58.

Leow, S.M., S.X. Chua, G. Venkatachalam, L. Shen, L. Luo, and M.V. Clement, *Sub-lethal oxidative stress induces lysosome biogenesis via a lysosomal membrane permeabilization-cathepsin-caspase 3-transcription factor EB-dependent pathway.* Oncotarget, 2017. **8**(10): p. 16170-16189.

Letenneur, L., K. Peres, H. Fleury, I. Garrigue, P. Barberger-Gateau, C. Helmer, J.M. Orgogozo, S. Gauthier, and J.F. Dartigues, *Seropositivity to herpes simplex virus antibodies and risk of Alzheimer's disease: a population-based cohort study.* PLoS One, 2008. **3**(11): p. e3637.

Lewis, J., D.W. Dickson, W.L. Lin, L. Chisholm, A. Corral, G. Jones, S.H. Yen, N. Sahara, L. Skipper, D. Yager, C. Eckman, J. Hardy, M. Hutton, and E. McGowan, *Enhanced neurofibrillary degeneration in transgenic mice expressing mutant tau and APP.* Science, 2001. **293**(5534): p. 1487-91.

Li, J. and S.R. Pfeffer, *Lysosomal membrane glycoproteins bind cholesterol and contribute to lysosomal cholesterol export.* Elife, 2016. **5**.

Li, M. and J.C. Izpisua Belmonte, *Looking to the future following 10 years of induced pluripotent stem cell technologies.* Nat Protoc, 2016. **11**(9): p. 1579-85.

Li, R., D.E. Xu, and T. Ma, *Lovastatin suppresses the aberrant tau phosphorylation from FTDP-17 mutation and okadaic acid-induction in rat primary neurons.* Neuroscience, 2015. **294**: p. 14-20.

Li, W.W., J. Li, and J.K. Bao, *Microautophagy: lesser-known self-eating.* Cell Mol Life Sci, 2012. **69**(7): p. 1125-36.

Licastro, F., I. Carbone, M. Ianni, and E. Porcellini, *Gene signature in Alzheimer's disease and environmental factors: the virus chronicle.* J Alzheimers Dis, 2011. **27**(4): p. 809-17.

Lin, K.A., K.R. Choudhury, B.G. Rathakrishnan, D.M. Marks, J.R. Petrella, P.M. Doraiswamy, and I. Alzheimer's Disease Neuroimaging, *Marked gender differences in progression of mild cognitive impairment over 8 years.* Alzheimers Dement (N Y), 2015. **1**(2): p. 103-110.

Lin, W.R., M.A. Wozniak, R.J. Cooper, G.K. Wilcock, and R.F. Itzhaki, *Herpesviruses in brain and Alzheimer's disease.* J Pathol, 2002. **197**(3): p. 395-402.

Lista, P., E. Straface, S. Brunelleschi, F. Franconi, and W. Malorni, *On the role of autophagy in human diseases: a gender perspective.* J Cell Mol Med, 2011. **15**(7): p. 1443-57.

Liu, Y., Y. Xue, S. Ridley, D. Zhang, K. Rezvani, X.D. Fu, and H. Wang, *Direct reprogramming of Huntington's disease patient fibroblasts into neuron-like cells leads to abnormal neurite outgrowth, increased cell death, and aggregate formation.* PLoS One, 2014. **9**(10): p. e109621.

Lloyd-Evans, E., A.J. Morgan, X. He, D.A. Smith, E. Elliot-Smith, D.J. Sillence, G.C. Churchill, E.H. Schuchman, A. Galione, and F.M. Platt, *Niemann-Pick disease type C1 is a sphingosine storage disease that causes deregulation of lysosomal calcium.* Nat Med, 2008. **14**(11): p. 1247-55.

Lovheim, H., J. Gilthorpe, R. Adolfsson, L.G. Nilsson, and F. Elgh, *Reactivated herpes simplex infection increases the risk of Alzheimer's disease.* Alzheimers Dement, 2014.

Lowry, W.E., L. Richter, R. Yachechko, A.D. Pyle, J. Tchieu, R. Sridharan, A.T. Clark, and K. Plath, *Generation of human induced pluripotent stem cells from dermal fibroblasts.* Proc Natl Acad Sci U S A, 2008. **105**(8): p. 2883-8.

Lubke, T., P. Lobel, and D.E. Sleat, *Proteomics of the lysosome.* Biochim Biophys Acta, 2009. **1793**(4): p. 625-35.

Lund, K.A., L.K. Opresko, C. Starbuck, B.J. Walsh, and H.S. Wiley, *Quantitative analysis of the endocytic system involved in hormone-induced receptor internalization.* J Biol Chem, 1990. **265**(26): p. 15713-23.

Lustbader, J.W., M. Cirilli, C. Lin, H.W. Xu, K. Takuma, N. Wang, C. Caspersen, X. Chen, S. Pollak, M. Chaney, F. Trinchese, S. Liu, F. Gunn-Moore, L.F. Lue, D.G. Walker, P. Kuppusamy, Z.L. Zewier, O. Arancio, D. Stern, S.S. Yan, and H. Wu, *ABAD directly links Abeta to mitochondrial toxicity in Alzheimer's disease.* Science, 2004. **304**(5669): p. 448-52.

Madshus, I.H. and E. Stang, *Internalization and intracellular sorting of the EGF receptor: a model for understanding the mechanisms of receptor trafficking.* J Cell Sci, 2009. **122**(Pt 19): p. 3433-9.

Maetzel, D., S. Sarkar, H. Wang, L. Abi-Mosleh, P. Xu, Albert W. Cheng, Q. Gao, M. Mitalipova, and R. Jaenisch, *Genetic and Chemical Correction of Cholesterol Accumulation and Impaired Autophagy in Hepatic and Neural Cells Derived from Niemann-Pick Type C Patient-Specific iPS Cells.* Stem Cell Reports, 2014. **2**(6): p. 866-880.

Magini, A., A. Polchi, A. Tozzi, B. Tancini, M. Tantucci, L. Urbanelli, T. Borsello, P. Calabresi, and C. Emiliani, *Abnormal cortical lysosomal beta-hexosaminidase and beta-galactosidase activity at post-synaptic sites during Alzheimer's disease progression.* Int J Biochem Cell Biol, 2015. **58**: p. 62-70.

Maherali, N. and K. Hochedlinger, *Guidelines and techniques for the generation of induced pluripotent stem cells.* Cell Stem Cell, 2008. **3**(6): p. 595-605.

Mahley, R.W. and S.C. Rall, Jr., *Apolipoprotein E: far more than a lipid transport protein.* Annu Rev Genomics Hum Genet, 2000. **1**: p. 507-37.

Malnar, M., S. Hecimovic, N. Mattsson, and H. Zetterberg, *Bidirectional links between Alzheimer's disease and Niemann-Pick type C disease.* Neurobiol Dis, 2014. **72 Pt A**: p. 37-47.

Mane, S.M., L. Marzella, D.F. Bainton, V.K. Holt, Y. Cha, J.E. Hildreth, and J.T. August, *Purification and characterization of human lysosomal membrane glycoproteins.* Arch Biochem Biophys, 1989. **268**(1): p. 360-78.

Markesbery, W.R. and J.M. Carney, *Oxidative alterations in Alzheimer's disease.* Brain Pathol, 1999. **9**(1): p. 133-46.

Marques, C.P., M.C. Cheeran, J.M. Palmquist, S. Hu, and J.R. Lokensgard, *Microglia are the major cellular source of inducible nitric oxide synthase during experimental herpes encephalitis.* J Neurovirol, 2008. **14**(3): p. 229-38.

Maxfield, F.R. and T.E. McGraw, *Endocytic recycling.* Nat Rev Mol Cell Biol, 2004. **5**(2): p. 121-32.

McKhann, G., D. Drachman, M. Folstein, R. Katzman, D. Price, and E.M. Stadlan, *Clinical diagnosis of Alzheimer's disease: report of the NINCDS-ADRDA Work Group under the auspices of Department of Health and Human Services Task Force on Alzheimer's Disease.* Neurology, 1984. **34**(7): p. 939-44.

Meyding-Lamade, U., J. Haas, W. Lamade, K. Stingele, R. Kehm, A. Fath, K. Heinrich, B. Storch Hagenlocher, and B. Wildemann, *Herpes simplex virus encephalitis: long-term comparative study of viral load and the expression of immunologic nitric oxide synthase in mouse brain tissue.* Neurosci Lett, 1998. **244**(1): p. 9-12.

Miklossy, J., *Alzheimer's disease - a neurospirochetosis. Analysis of the evidence following Koch's and Hill's criteria.* J Neuroinflammation, 2011. **8**: p. 90.

Miklossy, J., *Emerging roles of pathogens in Alzheimer disease.* Expert Rev Mol Med, 2011. **13**: p. e30.

Milatovic, D., Y. Zhang, S.J. Olson, K.S. Montine, L.J. Roberts, 2nd, J.D. Morrow, T.J. Montine, T.S. Dermody, and T. Valyi-Nagy, *Herpes simplex virus type 1 encephalitis is associated*

with elevated levels of F2-isoprostanes and F4-neuroprostanes. J Neurovirol, 2002. **8**(4): p. 295-305.

Moreau, K., A. Fleming, S. Imarisio, A. Lopez Ramirez, J.L. Mercer, M. Jimenez-Sanchez, C.F. Bento, C. Puri, E. Zavodszky, F. Siddiqi, C.P. Lavau, M. Betton, C.J. O'Kane, D.S. Wechsler, and D.C. Rubinsztein, *PICALM modulates autophagy activity and tau accumulation.* Nat Commun, 2014. **5**: p. 4998.

Morris, M., S. Maeda, K. Vossel, and L. Mucke, *The many faces of tau.* Neuron, 2011. **70**(3): p. 410-26.

Mu, F.T., J.M. Callaghan, O. Steele-Mortimer, H. Stenmark, R.G. Parton, P.L. Campbell, J. McCluskey, J.P. Yeo, E.P. Tock, and B.H. Toh, *EEA1, an early endosome-associated protein. EEA1 is a conserved alpha-helical peripheral membrane protein flanked by cysteine "fingers" and contains a calmodulin-binding IQ motif.* J Biol Chem, 1995. **270**(22): p. 13503-11.

Mueller-Steiner, S., Y. Zhou, H. Arai, E.D. Roberson, B. Sun, J. Chen, X. Wang, G. Yu, L. Esposito, L. Mucke, and L. Gan, *Antiamyloidogenic and neuroprotective functions of cathepsin B: implications for Alzheimer's disease.* Neuron, 2006. **51**(6): p. 703-14.

Mullan, M., F. Crawford, K. Axelman, H. Houlden, L. Lilius, B. Winblad, and L. Lannfelt, *A pathogenic mutation for probable Alzheimer's disease in the APP gene at the N-terminus of beta-amyloid.* Nat Genet, 1992. **1**(5): p. 345-7.

Muller, U.C., T. Deller, and M. Korte, *Not just amyloid: physiological functions of the amyloid precursor protein family.* Nat Rev Neurosci, 2017. **18**(5): p. 281-298.

Mungenast, A.E., S. Siegert, and L.H. Tsai, *Modeling Alzheimer's disease with human induced pluripotent stem (iPS) cells.* Mol Cell Neurosci, 2016. **73**: p. 13-31.

Nakamura, S. and T. Yoshimori, *New insights into autophagosome-lysosome fusion.* J Cell Sci, 2017. **130**(7): p. 1209-1216.

Neefjes, J. and R. van der Kant, *Stuck in traffic: an emerging theme in diseases of the nervous system.* Trends Neurosci, 2014. **37**(2): p. 66-76.

Niazy, N., S. Temme, D. Bocuk, C. Giesen, A. Konig, N. Temme, A. Ziegfeld, T.F. Gregers, O. Bakke, T. Lang, A.M. Eis-Hubinger, and N. Koch, *Misdirection of endosomal trafficking mediated by herpes simplex virus-encoded glycoprotein B.* FASEB J, 2017. **31**(4): p. 1650-1667.

Nicoll, M.P., J.T. Proenca, and S. Efstathiou, *The molecular basis of herpes simplex virus latency.* FEMS Microbiol Rev, 2012. **36**(3): p. 684-705.

Nixon, R.A., *Endosome function and dysfunction in Alzheimer's disease and other neurodegenerative diseases.* Neurobiol Aging, 2005. **26**(3): p. 373-82.

Nixon, R.A., *Autophagy in neurodegenerative disease: friend, foe or turncoat?* Trends Neurosci, 2006. **29**(9): p. 528-35.

Nixon, R.A. and D.S. Yang, *Autophagy failure in Alzheimer's disease--locating the primary defect.* Neurobiol Dis, 2011. **43**(1): p. 38-45.

Nixon, R.A., D.S. Yang, and J.H. Lee, *Neurodegenerative lysosomal disorders: a continuum from development to late age.* Autophagy, 2008. **4**(5): p. 590-9.

Nogales-Cadenas, R., P. Carmona-Saez, M. Vazquez, C. Vicente, X. Yang, F. Tirado, J.M. Carazo, and A. Pascual-Montano, *GeneCodis: interpreting gene lists through enrichment analysis and integration of diverse biological information.* Nucleic Acids Res, 2009. **37**(Web Server issue): p. W317-22.

Nunomura, A., R.J. Castellani, X. Zhu, P.I. Moreira, G. Perry, and M.A. Smith, *Involvement of oxidative stress in Alzheimer disease.* J Neuropathol Exp Neurol, 2006. **65**(7): p. 631-41.

Nunomura, A., G. Perry, M.A. Pappolla, R. Wade, K. Hirai, S. Chiba, and M.A. Smith, *RNA oxidation is a prominent feature of vulnerable neurons in Alzheimer's disease.* J Neurosci, 1999. **19**(6): p. 1959-64.

Oddo, S., A. Caccamo, J.D. Shepherd, M.P. Murphy, T.E. Golde, R. Kayed, R. Metherate, M.P. Mattson, Y. Akbari, and F.M. LaFerla, *Triple-transgenic model of Alzheimer's disease with plaques and tangles: intracellular Abeta and synaptic dysfunction.* Neuron, 2003. **39**(3): p. 409-21.

Ohkuma, S. and B. Poole, *Fluorescence probe measurement of the intralysosomal pH in living cells and the perturbation of pH by various agents.* Proc Natl Acad Sci U S A, 1978. **75**(7): p. 3327-31.

Ohnuki, M., K. Takahashi, and S. Yamanaka, *Generation and characterization of human induced pluripotent stem cells.* Curr Protoc Stem Cell Biol, 2009. **Chapter 4**: p. Unit 4A 2.

Owen, D.J., C.M. Crump, and S.C. Graham, *Tegument Assembly and Secondary Envelopment of Alphaherpesviruses.* Viruses, 2015. **7**(9): p. 5084-114.

Palu, G., M.A. Biasolo, G. Sartor, L. Masotti, E. Papini, M. Floreani, and P. Palatini, *Effects of herpes simplex virus type 1 infection on the plasma membrane and related functions of HeLa S3 cells.* J Gen Virol, 1994. **75 (Pt 12)**: p. 3337-44.

Pani, A., S. Dessi, G. Diaz, P. La Colla, C. Abete, C. Mulas, F. Angius, M.D. Cannas, C.D. Orru, P.L. Cocco, A. Mandas, P. Putzu, A. Laurenzana, C. Cellai, A.M. Costanza, A. Bavazzano, A. Mocali, and F. Paoletti, *Altered cholesterol ester cycle in skin fibroblasts from patients with Alzheimer's disease.* J Alzheimers Dis, 2009. **18**(4): p. 829-41.

Pani, A., A. Mandas, G. Diaz, C. Abete, P.L. Cocco, F. Angius, A. Brundu, N. Mucaka, M.E. Pais, A. Saba, L. Barberini, C. Zaru, M. Palmas, P.F. Putzu, A. Mocali, F. Paoletti, P. La Colla, and S. Dessi, *Accumulation of neutral lipids in peripheral blood mononuclear cells as a distinctive trait of Alzheimer patients and asymptomatic subjects at risk of disease.* BMC Med, 2009. **7**: p. 66.

Pappolla, M.A., R.A. Omar, K.S. Kim, and N.K. Robakis, *Immunohistochemical evidence of oxidative [corrected] stress in Alzheimer's disease.* Am J Pathol, 1992. **140**(3): p. 621-8.

Peric, A. and W. Annaert, *Early etiology of Alzheimer's disease: tipping the balance toward autophagy or endosomal dysfunction?* Acta Neuropathol, 2015. **129**(3): p. 363-81.

Persson, T., B.O. Popescu, and A. Cedazo-Minguez, *Oxidative stress in Alzheimer's disease: why did antioxidant therapy fail?* Oxid Med Cell Longev, 2014. **2014**: p. 427318.

Piper, R.C. and D.J. Katzmann, *Biogenesis and function of multivesicular bodies.* Annu Rev Cell Dev Biol, 2007. **23**: p. 519-47.

Pisa, D., R. Alonso, A. Rabano, I. Rodal, and L. Carrasco, *Different Brain Regions are Infected with Fungi in Alzheimer's Disease.* Sci Rep, 2015. **5**: p. 15015.

Pitto, M., F. Raimondo, C. Zoia, L. Brighina, C. Ferrarese, and M. Masserini, *Enhanced GM1 ganglioside catabolism in cultured fibroblasts from Alzheimer patients.* Neurobiol Aging, 2005. **26**(6): p. 833-8.

Platt, F.M., B. Boland, and A.C. van der Spoel, *The cell biology of disease: lysosomal storage disorders: the cellular impact of lysosomal dysfunction.* J Cell Biol, 2012. **199**(5): p. 723-34.

Polito, V.A., H. Li, H. Martini-Stoica, B. Wang, L. Yang, Y. Xu, D.B. Swartzlander, M. Palmieri, A. di Ronza, V.M. Lee, M. Sardiello, A. Ballabio, and H. Zheng, *Selective clearance of aberrant tau proteins and rescue of neurotoxicity by transcription factor EB.* EMBO Mol Med, 2014. **6**(9): p. 1142-60.

Porcellini, E., I. Carbone, M. Ianni, and F. Licastro, *Alzheimer's disease gene signature says: beware of brain viral infections.* Immun Ageing, 2010. **7**: p. 16.

Porter, K., J. Nallathambi, Y. Lin, and P.B. Liton, *Lysosomal basification and decreased autophagic flux in oxidatively stressed trabecular meshwork cells: Implications for glaucoma pathogenesis.* Autophagy, 2013. **9**(4): p. 581-594.

Rahn, E., P. Petermann, M.J. Hsu, F.J. Rixon, and D. Knebel-Morsdorf, *Entry pathways of herpes simplex virus type 1 into human keratinocytes are dynamin- and cholesterol-dependent.* PLoS One, 2011. **6**(10): p. e25464.

Rappaport, J., R.L. Manthe, M. Solomon, C. Garnacho, and S. Muro, *A Comparative Study on the Alterations of Endocytic Pathways in Multiple Lysosomal Storage Disorders.* Mol Pharm, 2016. **13**(2): p. 357-68.

Recuero, M., V.A. Munive, I. Sastre, J. Aldudo, F. Valdivieso, and M.J. Bullido, *A free radical-generating system regulates AbetaPP metabolism/processing: involvement of the ubiquitin/proteasome and autophagy/lysosome pathways.* J Alzheimers Dis, 2013. **34**(3): p. 637-47.

Recuero, M., T. Munoz, J. Aldudo, M. Subias, M.J. Bullido, and F. Valdivieso, *A free radical-generating system regulates APP metabolism/processing.* FEBS Lett, 2010. **584**(22): p. 4611-8.

Recuero, M., M.C. Vicente, A. Martinez-Garcia, M.C. Ramos, P. Carmona-Saez, I. Sastre, J. Aldudo, E. Vilella, A. Frank, M.J. Bullido, and F. Valdivieso, *A free radical-generating system induces the cholesterol biosynthesis pathway: a role in Alzheimer's disease.* Aging Cell, 2009. **8**(2): p. 128-39.

Repnik, U., V. Stoka, V. Turk, and B. Turk, *Lysosomes and lysosomal cathepsins in cell death.* Biochim Biophys Acta, 2012. **1824**(1): p. 22-33.

Robinton, D.A. and G.Q. Daley, *The promise of induced pluripotent stem cells in research and therapy.* Nature, 2012. **481**(7381): p. 295-305.

Rodriguez-Rodriguez, E., J.L. Vazquez-Higuera, P. Sanchez-Juan, I. Mateo, A. Pozueta, A. Martinez-Garcia, A. Frank, F. Valdivieso, J. Berciano, M.J. Bullido, and O. Combarros, *Epistasis between intracellular cholesterol trafficking-related genes (NPC1 and ABCA1) and Alzheimer's disease risk.* J Alzheimers Dis, 2010. **21**(2): p. 619-25.

Rogaeva, E., *The solved and unsolved mysteries of the genetics of early-onset Alzheimer's disease.* Neuromolecular Med, 2002. **2**(1): p. 1-10.

Rohrer, J. and R. Kornfeld, *Lysosomal hydrolase mannose 6-phosphate uncovering enzyme resides in the trans-Golgi network.* Mol Biol Cell, 2001. **12**(6): p. 1623-31.

Rothaug, M., S. Stroobants, M. Schweizer, J. Peters, F. Zunke, M. Allerding, R. D'Hooge, P. Saftig, and J. Blanz, *LAMP-2 deficiency leads to hippocampal dysfunction but normal clearance of neuronal substrates of chaperone-mediated autophagy in a mouse model for Danon disease.* Acta Neuropathol Commun, 2015. **3**: p. 6.

Rowe, A.M., A.J. St Leger, S. Jeon, D.K. Dhaliwal, J.E. Knickelbein, and R.L. Hendricks, *Herpes keratitis.* Prog Retin Eye Res, 2013. **32**: p. 88-101.

Saftig, P. and J. Klumperman, *Lysosome biogenesis and lysosomal membrane proteins: trafficking meets function.* Nat Rev Mol Cell Biol, 2009. **10**(9): p. 623-35.

Saftig, P., Y. Tanaka, R. Lullmann-Rauch, and K. von Figura, *Disease model: LAMP-2 enlightens Danon disease.* Trends Mol Med, 2001. **7**(1): p. 37-9.

Santana, S., M.J. Bullido, M. Recuero, F. Valdivieso, and J. Aldudo, *Herpes simplex virus type I induces an incomplete autophagic response in human neuroblastoma cells.* J Alzheimers Dis, 2012. **30**(4): p. 815-31.

Santana, S., M. Recuero, M.J. Bullido, F. Valdivieso, and J. Aldudo, *Herpes simplex virus type I induces the accumulation of intracellular beta-amyloid in autophagic compartments and the inhibition of the non-amyloidogenic pathway in human neuroblastoma cells.* Neurobiol Aging, 2012. **33**(2): p. 430 e19-33.

Santana, S., I. Sastre, M. Recuero, M.J. Bullido, and J. Aldudo, *Oxidative stress enhances neurodegeneration markers induced by herpes simplex virus type 1 infection in human neuroblastoma cells.* PLoS One, 2013. **8**(10): p. e75842.

Scherf, N., M. Herberg, K. Thierbach, T. Zerjatke, T. Kalkan, P. Humphreys, A. Smith, I. Glauche, and I. Roeder, *Imaging, quantification and visualization of spatio-temporal patterning in mESC colonies under different culture conditions.* Bioinformatics, 2012. **28**(18): p. i556-i561.

Schmechel, D.E., D. Goldgaber, D.S. Burkhart, J.R. Gilbert, D.C. Gajdusek, and A.D. Roses, *Cellular localization of messenger RNA encoding amyloid-beta-protein in normal tissue and in Alzheimer disease.* Alzheimer Dis Assoc Disord, 1988. **2**(2): p. 96-111.

Schneede, A., C.K. Schmidt, M. Holtta-Vuori, J. Heeren, M. Willenborg, J. Blanz, M. Domanskyy, B. Breiden, S. Brodesser, J. Landgrebe, K. Sandhoff, E. Ikonen, P. Saftig, and E.L. Eskelinen, *Role for LAMP-2 in endosomal cholesterol transport.* J Cell Mol Med, 2011. **15**(2): p. 280-95.

Schultz, M.L., L. Tecedor, M. Chang, and B.L. Davidson, *Clarifying lysosomal storage diseases.* Trends Neurosci, 2011. **34**(8): p. 401-10.

Selkoe, D.J. and J. Hardy, *The amyloid hypothesis of Alzheimer's disease at 25 years.* EMBO Mol Med, 2016. **8**(6): p. 595-608.

Settembre, C., A. Fraldi, D.L. Medina, and A. Ballabio, *Signals from the lysosome: a control centre for cellular clearance and energy metabolism.* Nat Rev Mol Cell Biol, 2013. **14**(5): p. 283-96.

Shearman, M.S., C.I. Ragan, and L.L. Iversen, *Inhibition of PC12 cell redox activity is a specific, early indicator of the mechanism of beta-amyloid-mediated cell death.* Proc Natl Acad Sci U S A, 1994. **91**(4): p. 1470-4.

Shulman, R.G., D.L. Rothman, K.L. Behar, and F. Hyder, *Energetic basis of brain activity: implications for neuroimaging.* Trends Neurosci, 2004. **27**(8): p. 489-95.

Siest, G., T. Pillot, A. Régis-Bailly, B. Leininger-Muller, J. Steinmetz, M.M. Galteau, and S. Visvikis, *Apolipoprotein E: an important gene and protein to follow in laboratory medicine.* Clinical Chemistry, 1995. **41**(8): p. 1068.

Siintola, E., S. Partanen, P. Stromme, A. Haapanen, M. Haltia, J. Maehlen, A.E. Lehesjoki, and J. Tyynela, *Cathepsin D deficiency underlies congenital human neuronal ceroid-lipofuscinosis.* Brain, 2006. **129**(Pt 6): p. 1438-45.

Smith, M.A., C.A. Rottkamp, A. Nunomura, A.K. Raina, and G. Perry, *Oxidative stress in Alzheimer's disease.* Biochim Biophys Acta, 2000. **1502**(1): p. 139-44.

Smyth, G.K., *Linear models and empirical bayes methods for assessing differential expression in microarray experiments.* Stat Appl Genet Mol Biol, 2004. **3**: p. Article3.

Snyder, E.M., Y. Nong, C.G. Almeida, S. Paul, T. Moran, E.Y. Choi, A.C. Nairn, M.W. Salter, P.J. Lombroso, G.K. Gouras, and P. Greengard, *Regulation of NMDA receptor trafficking by amyloid-beta.* Nat Neurosci, 2005. **8**(8): p. 1051-8.

Sobo, K., I. Le Blanc, P.P. Luyet, M. Fivaz, C. Ferguson, R.G. Parton, J. Gruenberg, and F.G. van der Goot, *Late endosomal cholesterol accumulation leads to impaired intra-endosomal trafficking.* PLoS One, 2007. **2**(9): p. e851.

Sotthibundhu, A., A.M. Sykes, B. Fox, C.K. Underwood, W. Thangnipon, and E.J. Coulson, *Beta-amyloid(1-42) induces neuronal death through the p75 neurotrophin receptor.* J Neurosci, 2008. **28**(15): p. 3941-6.

Steiner, I., P.G. Kennedy, and A.R. Pachner, *The neurotropic herpes viruses: herpes simplex and varicella-zoster.* Lancet Neurol, 2007. **6**(11): p. 1015-28.

Steinman, R.M., I.S. Mellman, W.A. Muller, and Z.A. Cohn, *Endocytosis and the recycling of plasma membrane.* J Cell Biol, 1983. **96**(1): p. 1-27.

Su, B., X. Wang, A. Nunomura, P.I. Moreira, H.G. Lee, G. Perry, M.A. Smith, and X. Zhu, *Oxidative stress signaling in Alzheimer's disease.* Curr Alzheimer Res, 2008. **5**(6): p. 525-32.

Suga, M., H. Kii, K. Niikura, Y. Kiyota, and M.K. Furue, *Development of a Monitoring Method for Nonlabeled Human Pluripotent Stem Cell Growth by Time-Lapse Image Analysis.* Stem Cells Transl Med, 2015. **4**(7): p. 720-30.

Sun, B., Y. Zhou, B. Halabisky, I. Lo, S.H. Cho, S. Mueller-Steiner, N. Devidze, X. Wang, A. Grubb, and L. Gan, *Cystatin C-cathepsin B axis regulates amyloid beta levels and associated neuronal deficits in an animal model of Alzheimer's disease.* Neuron, 2008. **60**(2): p. 247-57.

Tabas-Madrid, D., R. Nogales-Cadenas, and A. Pascual-Montano, *GeneCodis3: a non-redundant and modular enrichment analysis tool for functional genomics.* Nucleic Acids Res, 2012.

Takahashi, K., K. Tanabe, M. Ohnuki, M. Narita, T. Ichisaka, K. Tomoda, and S. Yamanaka, *Induction of pluripotent stem cells from adult human fibroblasts by defined factors.* Cell, 2007. **131**(5): p. 861-72.

Takahashi, K. and S. Yamanaka, *Induction of pluripotent stem cells from mouse embryonic and adult fibroblast cultures by defined factors.* Cell, 2006. **126**(4): p. 663-76.

Takahashi, R.H., T.A. Milner, F. Li, E.E. Nam, M.A. Edgar, H. Yamaguchi, M.F. Beal, H. Xu, P. Greengard, and G.K. Gouras, *Intraneuronal Alzheimer abeta42 accumulates in multivesicular bodies and is associated with synaptic pathology.* Am J Pathol, 2002. **161**(5): p. 1869-79.

Takashima, A., K. Noguchi, K. Sato, T. Hoshino, and K. Imahori, *Tau protein kinase I is essential for amyloid beta-protein-induced neurotoxicity.* Proc Natl Acad Sci U S A, 1993. **90**(16): p. 7789-93.

Tanaka, S., S. Nakamura, K. Ueda, M. Kameyama, S. Shiojiri, Y. Takahashi, N. Kitaguchi, and H. Ito, *Three types of amyloid protein precursor mRNA in human brain: their differential expression in Alzheimer's disease.* Biochem Biophys Res Commun, 1988. **157**(2): p. 472-9.

Tang, C.H., J.W. Lee, M.G. Galvez, L. Robillard, S.E. Mole, and H.A. Chapman, *Murine cathepsin F deficiency causes neuronal lipofuscinosis and late-onset neurological disease.* Mol Cell Biol, 2006. **26**(6): p. 2309-16.

Toei, M., R. Saum, and M. Forgac, *Regulation and isoform function of the V-ATPases.* Biochemistry, 2010. **49**(23): p. 4715-23.

Tokunaga, K., N. Saitoh, I.G. Goldberg, C. Sakamoto, Y. Yasuda, Y. Yoshida, S. Yamanaka, and M. Nakao, *Computational image analysis of colony and nuclear morphology to evaluate human induced pluripotent stem cells.* Sci Rep, 2014. **4**: p. 6996.

Tomic, J.L., A. Pensalfini, E. Head, and C.G. Glabe, *Soluble fibrillar oligomer levels are elevated in Alzheimer's disease brain and correlate with cognitive dysfunction.* Neurobiol Dis, 2009. **35**(3): p. 352-8.

Tonnies, E. and E. Trushina, *Oxidative Stress, Synaptic Dysfunction, and Alzheimer's Disease.* J Alzheimers Dis, 2017. **57**(4): p. 1105-1121.

Torres, M., S. Jimenez, R. Sanchez-Varo, V. Navarro, L. Trujillo-Estrada, E. Sanchez-Mejias, I. Carmona, J.C. Davila, M. Vizuete, A. Gutierrez, and J. Vitorica, *Defective lysosomal proteolysis and axonal transport are early pathogenic events that worsen with age leading to increased APP metabolism and synaptic Abeta in transgenic APP/PS1 hippocampus.* Mol Neurodegener, 2012. **7**: p. 59.

Trojanowski, J.Q. and V.M. Lee, *Phosphorylation of paired helical filament tau in Alzheimer's disease neurofibrillary lesions: focusing on phosphatases.* FASEB J, 1995. **9**(15): p. 1570-6.

Turk, V., V. Stoka, O. Vasiljeva, M. Renko, T. Sun, B. Turk, and D. Turk, *Cysteine cathepsins: from structure, function and regulation to new frontiers.* Biochim Biophys Acta, 2012. **1824**(1): p. 68-88.

Valyi-Nagy, T. and T.S. Dermody, *Role of oxidative damage in the pathogenesis of viral infections of the nervous system.* Histol Histopathol, 2005. **20**(3): p. 957-67.

Valyi-Nagy, T., S.J. Olson, K. Valyi-Nagy, T.J. Montine, and T.S. Dermody, *Herpes simplex virus type 1 latency in the murine nervous system is associated with oxidative damage to neurons.* Virology, 2000. **278**(2): p. 309-21.

van Weering, D.H., J.P. Medema, A. van Puijenbroek, B.M. Burgering, P.D. Baas, and J.L. Bos, *Ret receptor tyrosine kinase activates extracellular signal-regulated kinase 2 in SK-N-MC cells.* Oncogene, 1995. **11**(11): p. 2207-14.

Vina, J. and A. Lloret, *Why women have more Alzheimer's disease than men: gender and mitochondrial toxicity of amyloid-beta peptide.* J Alzheimers Dis, 2010. **20 Suppl 2**: p. S527-33.

Vogelsberg-Ragaglia, V., T. Schuck, J.Q. Trojanowski, and V.M. Lee, *PP2A mRNA expression is quantitatively decreased in Alzheimer's disease hippocampus.* Exp Neurol, 2001. **168**(2): p. 402-12.

Wakao, S., M. Kitada, Y. Kuroda, F. Ogura, T. Murakami, A. Niwa, and M. Dezawa, *Morphologic and gene expression criteria for identifying human induced pluripotent stem cells.* PLoS One, 2012. **7**(12): p. e48677.

Walkley, S.U. and M.T. Vanier, *Secondary lipid accumulation in lysosomal disease.* Biochim Biophys Acta, 2009. **1793**(4): p. 726-36.

Wang, J.Z. and F. Liu, *Microtubule-associated protein tau in development, degeneration and protection of neurons.* Prog Neurobiol, 2008. **85**(2): p. 148-75.

Weingarten, M.D., A.H. Lockwood, S.Y. Hwo, and M.W. Kirschner, *A protein factor essential for microtubule assembly.* Proc Natl Acad Sci U S A, 1975. **72**(5): p. 1858-62.

Whyte, L.S., A.A. Lau, K.M. Hemsley, J.J. Hopwood, and T.J. Sargeant, *Endo-lysosomal and autophagic dysfunction: a driving factor in Alzheimer's disease?* J Neurochem, 2017. **140**(5): p. 703-717.

Wiley, H.S., *Anomalous binding of epidermal growth factor to A431 cells is due to the effect of high receptor densities and a saturable endocytic system.* J Cell Biol, 1988. **107**(2): p. 801-10.

Williams, T.I., B.C. Lynn, W.R. Markesbery, and M.A. Lovell, *Increased levels of 4-hydroxynonenal and acrolein, neurotoxic markers of lipid peroxidation, in the brain in Mild Cognitive Impairment and early Alzheimer's disease.* Neurobiol Aging, 2006. **27**(8): p. 1094-9.

Wolfe, D.M., J.H. Lee, A. Kumar, S. Lee, S.J. Orenstein, and R.A. Nixon, *Autophagy failure in Alzheimer's disease and the role of defective lysosomal acidification.* Eur J Neurosci, 2013. **37**(12): p. 1949-61.

Wozniak, M.A., A.L. Frost, and R.F. Itzhaki, *Alzheimer's disease-specific tau phosphorylation is induced by herpes simplex virus type 1.* J Alzheimers Dis, 2009. **16**(2): p. 341-50.

Wozniak, M.A., A.L. Frost, C.M. Preston, and R.F. Itzhaki, *Antivirals reduce the formation of key Alzheimer's disease molecules in cell cultures acutely infected with herpes simplex virus type 1.* PLoS One, 2011. **6**(10): p. e25152.

Wozniak, M.A., R.F. Itzhaki, S.J. Shipley, and C.B. Dobson, *Herpes simplex virus infection causes cellular beta-amyloid accumulation and secretase upregulation.* Neurosci Lett, 2007. **429**(2-3): p. 95-100.

Wozniak, M.A., A.P. Mee, and R.F. Itzhaki, *Herpes simplex virus type 1 DNA is located within Alzheimer's disease amyloid plaques.* J Pathol, 2009. **217**(1): p. 131-8.

Wozniak, M.A., S.J. Shipley, M. Combrinck, G.K. Wilcock, and R.F. Itzhaki, *Productive herpes simplex virus in brain of elderly normal subjects and Alzheimer's disease patients.* J Med Virol, 2005. **75**(2): p. 300-6.

Wudiri, G.A. and A.V. Nicola, *Cellular cholesterol facilitates the post-entry replication cycle of herpes simplex virus 1.* J Virol, 2017.

Wudiri, G.A., S.M. Pritchard, H. Li, J. Liu, H.C. Aguilar, S.D. Gilk, and A.V. Nicola, *Molecular requirement for sterols in herpes simplex virus entry and infectivity.* J Virol, 2014. **88**(23): p. 13918-22.

Xiao, Q., P. Yan, X. Ma, H. Liu, R. Perez, A. Zhu, E. Gonzales, D.L. Tripoli, L. Czerniewski, A. Ballabio, J.R. Cirrito, A. Diwan, and J.M. Lee, *Neuronal-Targeted TFEB Accelerates Lysosomal Degradation of APP, Reducing Abeta Generation and Amyloid Plaque Pathogenesis.* J Neurosci, 2015. **35**(35): p. 12137-51.

Xue-shan, Z., P. Juan, W. Qi, R. Zhong, P. Li-hong, T. Zhi-han, J. Zhi-sheng, W. Gui-xue, and L. Lu-shan, *Imbalanced cholesterol metabolism in Alzheimer's disease.* Clin Chim Acta, 2016. **456**: p. 107-14.

Yamamoto, A., Y. Tagawa, T. Yoshimori, Y. Moriyama, R. Masaki, and Y. Tashiro, *Bafilomycin A1 prevents maturation of autophagic vacuoles by inhibiting fusion between autophagosomes and lysosomes in rat hepatoma cell line, H-4-II-E cells.* Cell Struct Funct, 1998. **23**(1): p. 33-42.

Yamamoto, N., E. Matsubara, S. Maeda, H. Minagawa, A. Takashima, W. Maruyama, M. Michikawa, and K. Yanagisawa, *A ganglioside-induced toxic soluble Abeta assembly. Its enhanced formation from Abeta bearing the Arctic mutation.* J Biol Chem, 2007. **282**(4): p. 2646-55.

Yang, D.S., P. Stavrides, P.S. Mohan, S. Kaushik, A. Kumar, M. Ohno, S.D. Schmidt, D. Wesson, U. Bandyopadhyay, Y. Jiang, M. Pawlik, C.M. Peterhoff, A.J. Yang, D.A. Wilson, P. St George-Hyslop, D. Westaway, P.M. Mathews, E. Levy, A.M. Cuervo, and R.A. Nixon, *Reversal of autophagy dysfunction in the TgCRND8 mouse model of Alzheimer's disease ameliorates amyloid pathologies and memory deficits.* Brain, 2011. **134**(Pt 1): p. 258-77.

Yang, D.S., P. Stavrides, M. Saito, A. Kumar, J.A. Rodriguez-Navarro, M. Pawlik, C. Huo, S.U. Walkley, M. Saito, A.M. Cuervo, and R.A. Nixon, *Defective macroautophagic turnover of brain lipids in the TgCRND8 Alzheimer mouse model: prevention by correcting lysosomal proteolytic deficits.* Brain, 2014. **137**(Pt 12): p. 3300-18.

Yao, J., D. Ho, N.Y. Calingasan, N.H. Pipalia, M.T. Lin, and M.F. Beal, *Neuroprotection by cyclodextrin in cell and mouse models of Alzheimer disease.* J Exp Med, 2012. **209**(13): p. 2501-13.

Yatin, S.M., M. Aksenova, M. Aksenov, W.R. Markesbery, T. Aulick, and D.A. Butterfield, *Temporal relations among amyloid beta-peptide-induced free-radical oxidative stress,*

neuronal toxicity, and neuronal defensive responses. J Mol Neurosci, 1998. **11**(3): p. 183-97.

Yin, Z., C. Pascual, and D.J. Klionsky, *Autophagy: machinery and regulation.* Microb Cell, 2016. **3**(12): p. 588-596.

Yoshimori, T., A. Yamamoto, Y. Moriyama, M. Futai, and Y. Tashiro, *Bafilomycin A1, a specific inhibitor of vacuolar-type H(+)-ATPase, inhibits acidification and protein degradation in lysosomes of cultured cells.* J Biol Chem, 1991. **266**(26): p. 17707-12.

Yu, W.H., A.M. Cuervo, A. Kumar, C.M. Peterhoff, S.D. Schmidt, J.H. Lee, P.S. Mohan, M. Mercken, M.R. Farmery, L.O. Tjernberg, Y. Jiang, K. Duff, Y. Uchiyama, J. Naslund, P.M. Mathews, A.M. Cataldo, and R.A. Nixon, *Macroautophagy--a novel Beta-amyloid peptide-generating pathway activated in Alzheimer's disease.* J Cell Biol, 2005. **171**(1): p. 87-98.

Yu, W.H., A. Kumar, C. Peterhoff, L. Shapiro Kulnane, Y. Uchiyama, B.T. Lamb, A.M. Cuervo, and R.A. Nixon, *Autophagic vacuoles are enriched in amyloid precursor protein-secretase activities: implications for beta-amyloid peptide over-production and localization in Alzheimer's disease.* Int J Biochem Cell Biol, 2004. **36**(12): p. 2531-40.

Zambrano, A., L. Solis, N. Salvadores, M. Cortes, R. Lerchundi, and C. Otth, *Neuronal cytoskeletal dynamic modification and neurodegeneration induced by infection with herpes simplex virus type 1.* J Alzheimers Dis, 2008. **14**(3): p. 259-69.

Zandi, P.P., D.L. Sparks, A.S. Khachaturian, J. Tschanz, M. Norton, M. Steinberg, K.A. Welsh-Bohmer, J.C. Breitner, and i. Cache County Study, *Do statins reduce risk of incident dementia and Alzheimer disease? The Cache County Study.* Arch Gen Psychiatry, 2005. **62**(2): p. 217-24.

Zemlan, F.P., O.J. Thienhaus, and H.B. Bosmann, *Superoxide dismutase activity in Alzheimer's disease: possible mechanism for paired helical filament formation.* Brain Res, 1989. **476**(1): p. 160-2.

Zhang, Y.W., R. Thompson, H. Zhang, and H. Xu, *APP processing in Alzheimer's disease.* Mol Brain, 2011. **4**: p. 3.

Zheng, W.H., S. Bastianetto, F. Mennicken, W. Ma, and S. Kar, *Amyloid beta peptide induces tau phosphorylation and loss of cholinergic neurons in rat primary septal cultures.* Neuroscience, 2002. **115**(1): p. 201-11.

ANNEX I

GENES REGULATED BY OXIDATIVE STRESS IN CELLS INFECTED WITH HSV-1 OR CARRYING THE APP_{swe} MUTATION

Gene Symbol	Gene Description	Genbank Accession	N probes	Fold change	q-value (%)
ABTB1	Homo sapiens ankyrin repeat and BTB (POZ) domain containing 1 (ABTB1), transcript variant 2	NM_172027	2	2.2815	0.0270
ACSL4	Homo sapiens acyl-CoA synthetase long-chain family member 4 (ACSL4), transcript variant 1	NM_004458	1	1.8919	0.0028
ANG	Homo sapiens angiogenin, ribonuclease, RNase A family, 5 (ANG), transcript variant 1	NM_001145	1	2.1334	0.0463
ARHGEF9	Homo sapiens Cdc42 guanine nucleotide exchange factor (GEF) 9 (ARHGEF9), transcript variant 1	NM_015185	1	1.7690	0.0010
ATP6AP1	Homo sapiens ATPase, H+ transporting, lysosomal accessory protein 1 (ATP6AP1)	NM_001183	1	1.3882	0.0278
BNIP3L	Homo sapiens BCL2/adenovirus E1B 19kDa interacting protein 3-like (BNIP3L)	NM_004331	2	1.8344	0.0113
BRI3	Homo sapiens brain protein I3 (BRI3), transcript variant 1	NM_015379	1	1.4088	0.0316
BTG1	Homo sapiens B-cell translocation gene 1, anti-proliferative (BTG1)	NM_001731	1	1.6624	0.0157
C4orf21	Homo sapiens chromosome 4 open reading frame 21 (C4orf21)	NM_018392	1	1.6315	0.0130
C5orf41	Homo sapiens chromosome 5 open reading frame 41 (C5orf41), transcript variant 1	NM_153607	1	1.5886	0.0228
C6orf1	Homo sapiens chromosome 6 open reading frame 1 (C6orf1), transcript variant 1	NM_178508	2	1.9415	0.0005
CEACAM19	Homo sapiens carcinoembryonic antigen-related cell adhesion molecule 19 (CEACAM19), transcript variant 2	NM_020219	1	1.7605	0.0424
COL6A1	Homo sapiens collagen, type VI, alpha 1 (COL6A1)	NM_001848	1	1.6844	0.0068
CPAMD8	Homo sapiens C3 and PZP-like, alpha-2-macroglobulin domain containing 8 (CPAMD8)	NM_015692	1	2.5021	0.0008
CTSF	Homo sapiens cathepsin F (CTSF)	NM_003793	1	1.4361	0.0238
DFNB59	Homo sapiens deafness, autosomal recessive 59 (DFNB59)	NM_001042702	1	1.8164	0.0091

Gene Symbol	Gene Description	Genbank Accession	N probes	Fold change	q-value (%)
DHRS3	Homo sapiens dehydrogenase/reductase (SDR family) member 3 (DHRS3)	NM_004753	1	1.7435	0.0266
DHX58	Homo sapiens DEXH (Asp-Glu-X-His) box polypeptide 58 (DHX58)	NM_024119	1	1.7268	0.0043
DKFZP564C152	Homo sapiens mRNA; cDNA DKFZp564C152 (from clone DKFZp564C152)	AL049980	1	1.6484	0.0183
DKKL1	Homo sapiens dickkopf-like 1 (soggy) (DKKL1)	NM_014419	1	2.0490	0.0458
EMP3	Homo sapiens epithelial membrane protein 3 (EMP3)	NM_001425	1	1.5822	0.0067
FADS2	Homo sapiens fatty acid desaturase 2 (FADS2)	NM_004265	2	1.8574	0.0027
FAP	Homo sapiens fibroblast activation protein, alpha (FAP)	NM_004460	1	1.8710	0.0016
FLRT1	Homo sapiens fibronectin leucine rich transmembrane protein 1 (FLRT1)	NM_013280	1	1.4575	0.0168
FZD5	Homo sapiens frizzled homolog 5 (Drosophila) (FZD5)	NM_003468	2	1.5974	0.0236
IFI27L1	Homo sapiens interferon, alpha-inducible protein 27-like 1 (IFI27L1), transcript variant 2	NM_206949	2	1.3042	0.0415
IFITM1	Homo sapiens interferon induced transmembrane protein 1 (9-27) (IFITM1)	NM_003641	1	1.5528	0.0109
KCNAB2	Homo sapiens potassium voltage-gated channel, shaker-related subfamily, beta member 2 (KCNAB2), transcript variant 1	NM_003636	2	1.1626	0.0006
KLF15	Homo sapiens Kruppel-like factor 15 (KLF15)	NM_014079	1	0.2340	0.00005
KLF6	Homo sapiens Kruppel-like factor 6 (KLF6), transcript variant A	NM_001300	3	0.9652	0.0048
LAMP2	Homo sapiens lysosomal-associated membrane protein 2 (LAMP2), transcript variant A	NM_002294	3	1.6598	0.0043
LINC-PINT	#NV	#NV	1	2.1352	0.0195
LIPA	Homo sapiens lipase A, lysosomal acid, cholesterol esterase (LIPA), transcript variant 2	NM_000235	1	2.0291	0.0002
LIPH	lipase, member H	BM768581	2	0.8470	0.0222
LOC389831	Homo sapiens cDNA: FLJ23285 fis, clone HEP09071.	AK026938	2	1.4535	0.0137
LOC643783	PREDICTED: Homo sapiens hypothetical LOC643783 (LOC643783)	XM_931798	1	0.5023	0.0109
LUM	Homo sapiens lumican (LUM)	NM_002345	2	0.8265	0.0199

Gene Symbol	Gene Description	Genbank Accession	N probes	Fold change	q-value (%)
MAFF	Homo sapiens v-maf musculoaponeurotic fibrosarcoma oncogene homolog F (avian) (MAFF), transcript variant 1	NM_012323	1	1.9401	0.0195
METTL7A	Homo sapiens methyltransferase like 7A (METTL7A)	NM_014033	1	1.4724	0.0495
MFGE8	Homo sapiens milk fat globule-EGF factor 8 protein (MFGE8), transcript variant 1	NM_005928	2	0.8212	0.0012
MPZL1	Homo sapiens myelin protein zero-like 1 (MPZL1), transcript variant 1	NM_003953	2	0.7148	0.0034
MYL5	Homo sapiens myosin, light chain 5, regulatory (MYL5)	NM_002477	1	1.9158	0.0028
NINL	Homo sapiens ninein-like (NINL)	NM_025176	1	1.3474	0.0311
NIPAL3	Homo sapiens NIPA-like domain containing 3 (NIPAL3)	NM_020448	3	1.7355	0.0166
NPC1	Homo sapiens Niemann-Pick disease, type C1 (NPC1)	NM_000271	1	1.8179	0.0042
NUDT14	Homo sapiens nudix (nucleoside diphosphate linked moiety X)-type motif 14 (NUDT14)	NM_177533	2	1.6996	0.0122
ORAI3	Homo sapiens ORAI calcium release-activated calcium modulator 3 (ORAI3)	NM_152288	1	2.1279	0.0161
OSTM1	Homo sapiens osteopetrosis associated transmembrane protein 1 (OSTM1)	NM_014028	2	0.6789	0.0141
PBXIP1	Homo sapiens pre-B-cell leukemia homeobox interacting protein 1 (PBXIP1)	NM_020524	1	1.9004	0.0053
PDE1A	Homo sapiens phosphodiesterase 1A, calmodulin-dependent (PDE1A), transcript variant 2	NM_001003683	2	0.2410	0.0080
SCN4B	Homo sapiens sodium channel, voltage-gated, type IV, beta (SCN4B), transcript variant 1	NM_174934	1	1.6820	0.0118
SLC22A18	Homo sapiens solute carrier family 22, member 18 (SLC22A18), transcript variant 2	NM_183233	1	1.8687	0.0045
SLC25A1	Homo sapiens solute carrier family 25 (mitochondrial carrier; citrate transporter), member 1 (SLC25A1), nuclear gene encoding mitochondrial protein	NM_005984	1	2.0476	0.0007
SLC8A2	Homo sapiens solute carrier family 8 (sodium/calcium exchanger), member 2 (SLC8A2)	NM_015063	1	2.5470	0.0191

Gene Symbol	Gene Description	Genbank Accession	N probes	Fold change	q-value (%)
STXBP1	Homo sapiens syntaxin binding protein 1 (STXBP1), transcript variant 2	NM_001032221	2	2.2706	0.0054
TMEM173	Homo sapiens transmembrane protein 173 (TMEM173), nuclear gene encoding mitochondrial protein	NM_198282	1	1.6504	0.0157
TMEM41B	Homo sapiens transmembrane protein 41B (TMEM41B), transcript variant 1	NM_015012	2	1.4958	0.0195
TMEM60	Homo sapiens transmembrane protein 60 (TMEM60)	NM_032936	1	1.4869	0.0053
TMEM80	Homo sapiens transmembrane protein 80 (TMEM80), transcript variant 2	NM_001042463	1	1.3786	0.0209
TP53INP1	Homo sapiens tumor protein p53 inducible nuclear protein 1 (TP53INP1), transcript variant 1	NM_033285	1	2.2619	0.0100
TXNDC16	Homo sapiens thioredoxin domain containing 16 (TXNDC16), transcript variant 1	NM_020784	1	1.6440	0.0263
UGT3A2	Homo sapiens UDP glycosyltransferase 3 family, polypeptide A2 (UGT3A2), transcript variant 1	NM_174914	1	1.9942	0.0016
ULBP2	Homo sapiens UL16 binding protein 2 (ULBP2)	NM_025217	3	1.1315	0.0221
VASN	Homo sapiens vasorin (VASN)	NM_138440	1	1.5488	0.0084
VEGFB	Homo sapiens vascular endothelial growth factor B (VEGFB)	NM_003377	2	1.4669	0.0213
WNT6	Homo sapiens wingless-type MMTV integration site family, member 6 (WNT6)	NM_006522	1	1.7378	0.0083
ZBTB1	Homo sapiens zinc finger and BTB domain containing 1 (ZBTB1), transcript variant 2	NM_014950	2	0.7973	0.0030
ZDHHC23	Homo sapiens zinc finger, DHHC-type containing 23 (ZDHHC23)	NM_173570	1	1.3578	0.0470

Genes modulated by oxidative stress in SK-N-MC cells infected with HSV-1 or stably expressing the Swedish APP mutation, but not in their corresponding control cells, at 24 h of X-XOD treatment. Gene expression was analyzed in human genome Agilent microarrays as detailed in Methods. Gene official symbol, description and mRNA GenBank accession code are shown. N is the number of probes in the array for each gene. Gene expression fold change is calculated for cells infected with HSV-1 and treated with X-XOD for 24 h with respect to infected non treated cells. Significance of the difference (q-value, expressed in %) was calculated with the FDR method as detailed in Methods.

FUNCTIONAL ANNOTATION OF THE GENES REGULATED BY OXIDATIVE STRESS IN CELLS INFECTED WITH HSV-1 OR CARRYING THE APP_{swe} MUTATION

Item Code	Item Name	NG	Hyp*	Genes
Kegg:04142	Lysosome	5	6.58E-05	CTSF, NPC1, LIPA, LAMP2, ATP6AP1
GO:0002576	platelet degranulation (BP)	3	0.00446234	VEGFB, STXBP1, LAMP2
GO:0007596, GO:0030168	blood coagulation (BP),platelet activation (BP)	4	0.00503844	VEGFB, PDE1A, LAMP2, SLC8A2
GO:0006629	lipid metabolic process (BP)	4	0.00548076	FADS2, LIPA, ACSL4, LIPH
GO:0007596	blood coagulation (BP)	5	0.0066467	VEGFB, MAFF, PDE1A, LAMP2, SLC8A2
GO:0006811	ion transport (BP)	5	0.00915111	SLC22A18, SCN4B, KCNAB2, ATP6AP1, SLC8A2
GO:0001525	angiogenesis (BP)	3	0.00969942	ANG, MFGE8, FZD5
GO:0008152	metabolic process (BP)	4	0.0097892	ANG, UGT3A2, METTL7A, FAP
GO:0055085	transmembrane transport (BP)	5	0.0130151	SLC25A1, SLC22A18, KCNAB2, ARHGEF9, SLC8A2
Kegg:04510	Focal adhesion	3	0.0134567	VEGFB, MYL5, COL6A1
GO:0008285	negative regulation of cell proliferation (BP)	3	0.0327046	EMP3, BTG1, IFITM1
GO:0045944	positive regulation of transcription from RNA polymerase II promoter (BP)	4	0.0330006	KLF6, KLF15, TMEM173, FZD5
GO:0006915	apoptotic process (BP)	4	0.0336196	ARHGEF9, TMEM173, FZD5, TP53INP1
GO:0045087	innate immune response (BP)	3	0.0338013	TMEM173, DHX58, IFITM1
GO:0055085, GO:0006811	transmembrane transport (BP),ion transport (BP)	3	0.035035	SLC22A18, KCNAB2, SLC8A2
Kegg:05200	Pathways in cancer	3	0.0352861	VEGFB, WNT6, FZD5
GO:0007268	synaptic transmission (BP)	3	0.041329	KCNAB2, STXBP1, ARHGEF9

The input list (the 68 genes of interest) was compared with the annotated human genome (34208 items) to identify KEGG Pathways, Gene Ontology Cellular Functions or Gene Ontology Molecular Functions over or underrepresented in the input list, using the GeneCodis annotation tool (http://genecodis.cnb.csic.es). The resultant items with a corrected p-value<0.05 and the symbol of the annotated genes are shown. NG = Number of annotated genes in the input list; Hyp* = Corrected hypergeometric p-value.